

**UNIVERSITY OF NAPLES FEDERICO II**

**Doctorate School in Molecular Medicine**

**Doctorate Program in  
Genetics and Molecular Medicine  
Coordinator: Prof. Lucio Nitsch  
XXVII Cycle**

**Role of extracellular matrix and  
mitochondria-related genes in determining  
cardiac defects in Down syndrome**

**RITA CICATIELLO**



**NAPLES 2015**

## TABLE OF CONTENTS

LIST OF PUBLICATIONS.....	3
ABSTRACT .....	4
1. INTRODUCTION.....	5
1.1 The Down syndrome .....	5
1.2 DS is a major cause of congenital heart defects .....	6
1.2.1 Down Syndrome Congenital Heart Disease Critical Region .....	6
1.2.2 CHDs in mouse models of DS.....	7
1.3 Atrioventricular valve development during cardiogenesis.....	9
1.4 Hsa21 genes are overexpressed in DS .....	11
1.5 Mitochondrial dysfunction is associated to DS .....	14
1.5.1 Structure and function of mitochondria .....	18
1.5.2 Molecular basis of mitochondrial dysfunction in DS .....	21
1.6 Pharmacological approaches for improving DS phenotype .....	24
1.7 Drugs affecting the <i>PGC-1<math>\alpha</math></i> pathway.....	27
1.8 A novel approach to assess mitochondrial respiration: XF <sup>e</sup> Analyzer.....	29
2. AIMS OF THE STUDY.....	32
3. MATERIALS AND METHODS.....	34
4. RESULTS .....	41
4.1 Meta-analysis of public expression dataset.....	41
4.2 OCR is decreased in DS-HFFs.....	49
4.3 DS-HFFs show a very fragmented mitochondrial network.....	49
4.5 <i>NR1P1</i> siRNA transfection decreases NRIP1 in the nucleus of DS-HFFs .....	51
4.6 <i>NR1P1</i> silencing improves mitochondrial function in DS-HFFs .....	52
4.7 Drug testing in DS-HFFs cultures .....	58
4.7.1 Metformin counteracts mitochondrial dysfunction in DS-HFFs .....	58
4.7.2 Pioglitazone counteracts mitochondrial dysfunction in DS-HFFs.....	63
5. DISCUSSION .....	68
6. CONCLUSIONS.....	78
7. FUTURE PERSPECTIVES.....	79
ACKNOWLEDGEMENTS.....	80
REFERENCES .....	81
APPENDIX 1 .....	93

## LIST OF PUBLICATIONS

1) Izzo A, Manco R, Bonfiglio F, Cali G, de Cristofaro T, Patergnani S, **Cicatiello R**, Scrima R, Pinton P, Conti A, Nitsch L. NRIP1/RIP140 siRNA-mediated attenuation counteracts mitochondrial dysfunction in Down syndrome. *Hum Mol Genet* 2014; 23:4406-19.

2) Izzo A, Genesio R, Ronga V, Nocera V, Marullo L, **Cicatiello R**, Sglavo G, Paladini D, Conti A, Nitsch L. “40Mb duplication in chromosome band 5p13.1p15.33 with 800kb terminal deletion in a foetus with mild phenotypic features.” *Eur J Med Genet* 2012; 55:140-4.

## ABSTRACT

Mitochondrial dysfunction, which is consistently observed in Down syndrome (DS), is suspected to worsen mental retardation and congenital cardiopathies in DS subjects, as well as to determine other phenotypic abnormalities, such as Alzheimer's disease, type 2 diabetes, obesity, and hypertrophic cardiopathy.

As the heart is one of the main targets of DS, we have analyzed gene expression of DS fetal hearts demonstrating a global downregulation of nuclear encoded mitochondrial genes (NEMGs) together with the upregulation of clusters of extracellular matrix proteins (ECMs). A mitochondrial dysfunction was found associated with NEMG downregulation in DS fetal fibroblasts (DS-HFFs).

Based on these previous results, this doctorate thesis was aimed:

- to identify Hsa21 genes responsible for either NEMG downregulation or ECM upregulation;
- to develop strategies to counteract the negative effects triggered by NEMG dysregulation in DS;
- to investigate how NEMG downregulation or ECM upregulation might affect cardiac phenotype.

Performing a meta-analysis on public expression data we identified two genes mapping to chromosome 21 (Hsa21), namely *NRIP1/RIP140* (nuclear receptor interacting protein 1) and *RUNX1* (Runt related transcription factor 1), as good candidates for NEMG downregulation and ECM upregulation, respectively. These genes are overexpressed in DS cells and in heart tissue.

*NRIP1* negatively regulates *PGC-1 $\alpha$* , a master regulator of the mitochondrial function. We attenuated by siRNA *NRIP1* expression in a cell model of DS demonstrating an inverse correlation between *NRIP1* and *PGC-1 $\alpha$*  expression, together with an improvement of mitochondrial function in silenced cells. We therefore developed a strategy to correct mitochondrial alterations in DS by pharmacologically stimulating the activity of the *NRIP1* targets *PGC-1 $\alpha$*  and PPARs. To this aim we supplemented cultures of DS-HFFs with drugs affecting *PGC-1 $\alpha$* , namely Metformin and Pioglitazone, to evaluate their modulatory impact on mitochondrial function.

We found both strategies effective in rescuing mitochondrial function in terms of oxygen consumption, ATP production and mitochondrial biogenesis.

# 1. INTRODUCTION

## 1.1 The Down syndrome

Down Syndrome (DS) is caused by a complete or partial trisomy of chromosome 21 (TS21) (Fig. 1). It occurs with an incidence of 1/700 newborns and it is characterized by a complex phenotype in which over 80 features occur with various degrees of expression and frequency (Epstein et al. 1991). Constant clinical features in DS subjects are: mental retardation, short stature and muscular hypotonia. Congenital cardiac defects (CHDs) are observed in ~ 50% of cases.

The life expectancy of DS subjects is less than 50-60 years. Starting from the age of 40 years DS subjects may suffer from Alzheimer's Disease (AD) (Cork, 1990). In addition diabetes, obesity and cardiac hypertrophy are important complications.

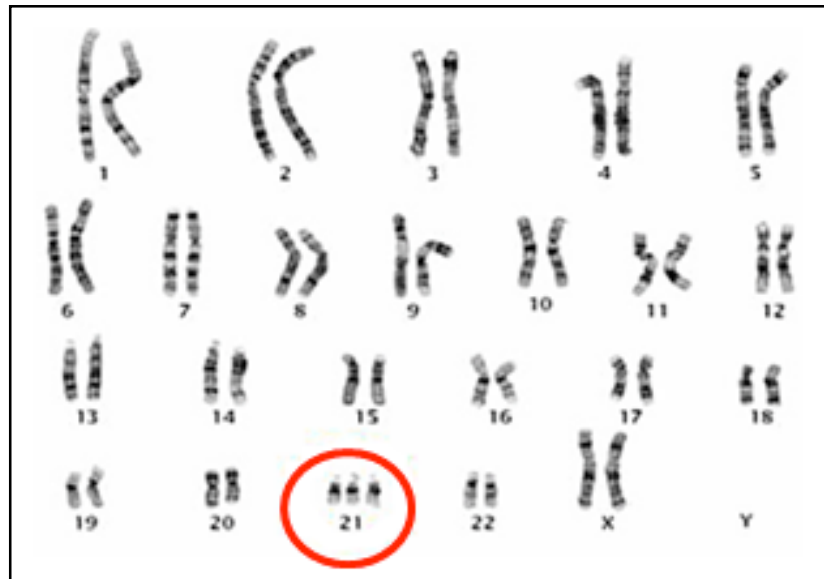


Fig. 1 DS karyotype. The presence of three copies of chromosome 21 causes DS.

## 1.2 DS is a major cause of congenital heart defects

DS is known to be a major cause of CHDs and the most frequent cause of atrioventricular septal defects (AVSDs) (Barlow et al. 2001). The most common CHDs in DS subjects are: atrioventricular canal defect (AVCD), ventricular septal defect (VSD) and tetralogy of Fallot (TOF) (Park et al. 1977). Most of them derive from the abnormal development of the endocardial cushions (Ferencz et al. 1989; Park et al. 1977). Defects of the outflow tract are also frequent. The high CHD incidence in DS suggests that the overexpression of genes mapping on Hsa21 alters the normal development of the heart either directly or influencing the expression of genes mapping to other chromosomes.

### 1.2.1 Down Syndrome Congenital Heart Disease Critical Region

Despite a large amount of studies, the molecular alterations that cause the DS phenotype are still elusive. Several attempts to identify the Hsa21 genes that contribute to the DS phenotype have led to identify a *Down Syndrome Critical Region* (DSCR) which spans approximately 5.4 Mb in band 21q22.3 (Fig. 2) (Korenberg et al. 1994; Delabar et al. 1993; McCormick et al. 1989; Rahmani et al. 1989). The DSCR hypothesis predicts that a gene, or some genes, in this region are sufficient to produce the specific DS features when present in three copies. Testing this hypothesis in mice Olson et al. (2004) found that trisomy of DSCR alone is necessary but not sufficient for brain DS phenotypes in trisomic mice. These results suggest that the origins of trisomic phenotypes are even more complicated than formerly assumed and that they probably involve multiple gene interactions (Olson et al. 2007).

Similar efforts have been made to identify a critical region for *Down Syndrome Congenital Heart Disease* (DS-CHD) by studying subjects with partial Hsa21 trisomies (Fig. 2) (Korenberg et al. 1990) and mouse models (Fig. 3) (Liu et al. 2014; Liu et al. 2011; Barlow et al. 2001), with conflicting results.

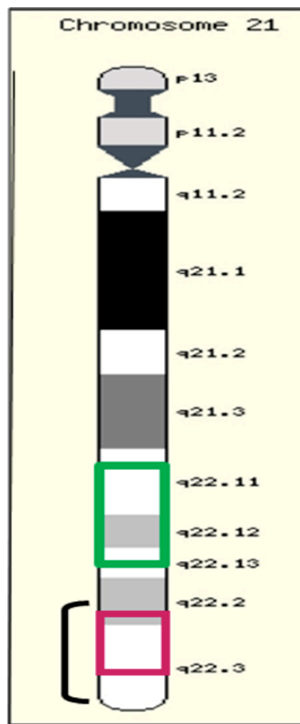


**Fig. 2 DSCR (dark)** (Korenberg et al. 1990); **DS-CHD (red)** (Liu et al. 2011; Barlow et al. 2001); **new DS-CHD (green)** (Liu et al.2011).

### 1.2.2 CHDs in mouse models of DS

Hsa21 presents high sequence omology of about 30 Mb with mouse chromosome 16, including part of DSCR. Other syntenic regions are localized on murine chromosomes 10 and 17. Many mouse models have been generated carrying three copies of Hsa21 syntenic regions of different sizes. Ts65Dn is the most widely used model from this group (Reeves et al. 1995). It is trisomic for ~13.4 Mb of the Hsa21 syntenic region on Mmu16, which contains approximately 99 orthologs of Hsa21 genes and exhibits some phenotypic features comparable to DS. Less than 8% of Ts65Dn mice develop septal defects, which increase their post-natal mortality (Moore, 2006). Unfortunately this mouse model is also trisomic for 5.8 Mb region on Mmu17, which is not syntenic to Hsa21 and may contribute to the cardiovascular phenotype (Liu et al. 2011).

In another mouse model, Dp(16)1Yu/+, the trisomic region spans from 21q11 band to 21q22.3 band thus including part of DS-CHD region. These transgenic mice develop congenital cardiopathy, atrioventricular septal defects including Tetralogy of Fallot and atrioventricular canal defect, with a similar percentage to that found in DS individuals (Li et al. 2007).

*Liu et al.* (2011), using a model derived from the Dp(16), identified a 5.4 Mb genomic region associated to congenital heart defects similar to that observed in DS-CHD. This region spans from Tiam1 and Kcnj6 and includes 52 Hsa21

orthologs genes and one miRNA. More recently the authors further narrowed the region to 3.7 Mb (Liu et al. 2014). This region spans from *Ifnar1* and *Kcnj6* and includes 35 Hsa21 orthologs genes (**Fig. 3, model 8**). The CHD frequency was lower than that observed in human DS subjects.

Some models have been designed, carrying the entire Hsa21 or fragments of it (O’Doherty et al. 2005, Shinohara et al. 2001). The Tc1 model was obtained introducing into the mouse genome Hsa21 traits with only two small deletions including about 8% of Hsa21 genes. This mouse model shows craniofacial anomalies and cardiac alterations, typical of DS. The morphogenetic defects include ventricular and atrioventricular septal defect, that are due to an incomplete fusion of endocardial cushions (Dunlevy et al. 2010). The main problem of this model is that Hsa21 sequences are frequently lost during cell divisions producing a mosaic condition.

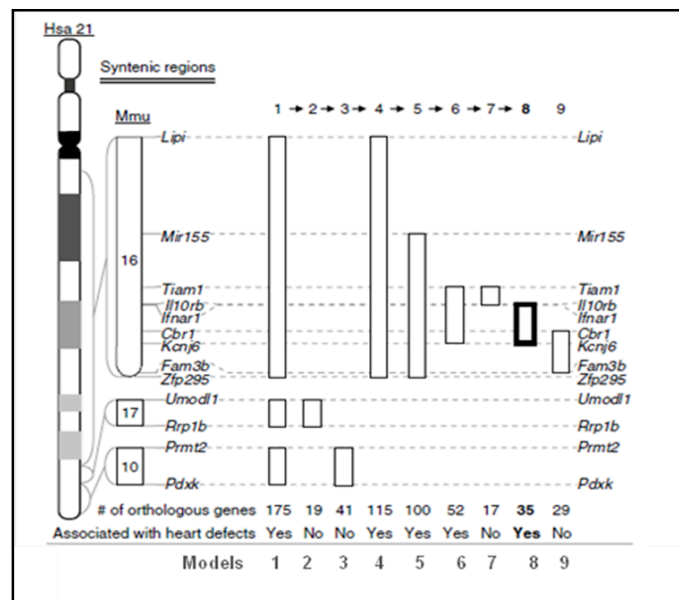


**Fig. 3 Synteny of different mouse models with Hsa21.** Mouse models: 1, Dp(10)1Yey/+; Dp(16)1Yey/+; Dp(17)1Yey/+. 2, Dp(17)1Yey/+. 3, Dp(10)1Yey/+. 4, Dp(16)1Yey/+. 5, Ts65Dn. 6, Dp(16)2Yey/+. 7, Dp(16)3Yey/+. 8, Dp(16)4Yey/+. 9, Ts1Rhr (Liu et al. 2014)

### 1.3 Atrioventricular valve development during cardiogenesis

In the vertebrate embryo, the heart is the first organ to become functional; its development starts at gastrulation with the formation of precardiac mesoderm (**Fig. 4**). Cells composing this middle embryonic germ layer then migrate anterolaterally to establish bilateral primary heart fields. The two heart fields eventually combine to form the cardiac crescent and, as the mesodermal cells differentiate into myocardial and endocardial progenitors, the primary heart tube (Abu-Issa and Kirby, 2007). The two poles of the linear tube soon receive contributions from a second cardiogenic population; this population of cells is termed the Second Heart Field (SHF) and its addition leads to pronounced elongation of the linear tube (Zaffran and Kelly, 2012; Snarr et al. 2007).

The primary heart tube has an outer myocardial layer and an inner endocardial layer of cells separated by the cardiac jelly (**Fig. 5**) (Armstrong and Bischoff, 2004). Cardiac jelly is composed primarily of proteoglycan glycosaminoglycans of which hyaluronan and chondroitin sulfates are the major components (Person et al. 2005).

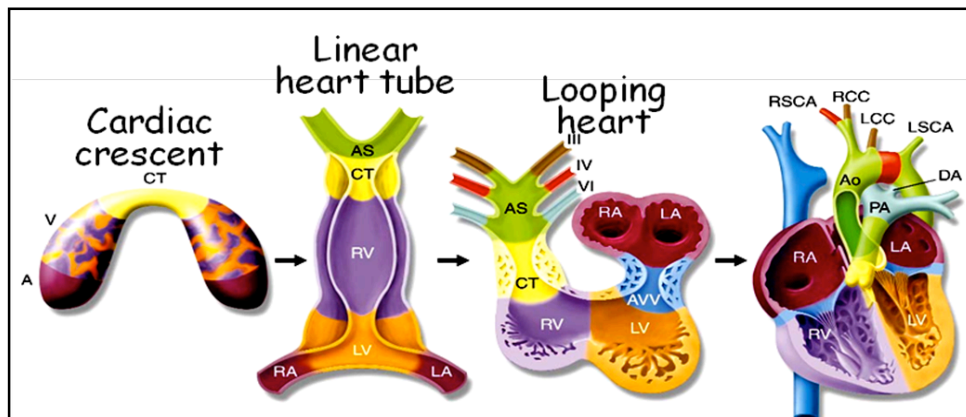


**Fig. 4 Schematic representation of cardiogenesis.** In the early steps of heart development, the precardiac mesodermal cells form two endothelial tubes, which join to form a primitive cardiac tube. As the cardiac tube extends, the primitive heart forms a loop. During the looping heart, atrioventricular valves and atrial and ventricular septa form. At last the heart with 4 chambers forms.

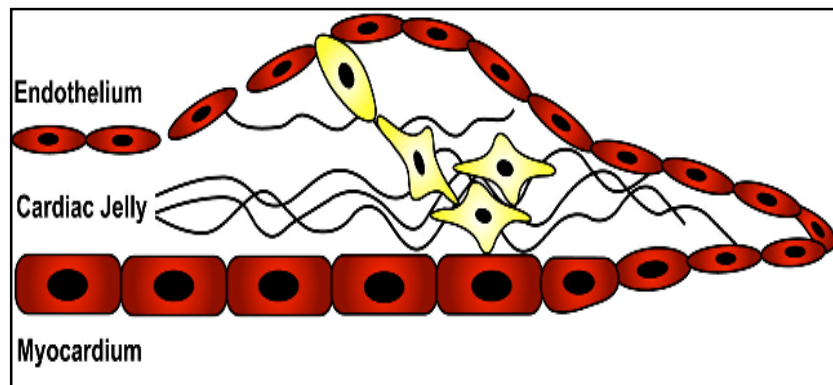


**Fig. 5 Schematic representation of the cardiac jelly.** In the cardiac primitive tube, the cardiac jelly, an acellular and extracellular matrix-rich space, separates the outer myocardial layer and the inner endocardial layer of cells.

After the heart tube begins rightward looping, the myocardium of specific regions of the primary heart tube, the atrioventricular (AV) junction and the ventricular outflow tract (OFT) upregulate secretion of ECM, which causes the cardiac jelly to swell into the lumen of the heart tube, forming primordial structures termed “endocardial cushions” (Combs and Yutzey, 2009; Person et al. 2005). Stimulated by local signals, a subset of AV and OFT endocardial cells lose cell–cell contact, resulting in their delamination into the cardiac jelly and their adoption of a migratory, mesenchymal-like phenotype. This phenotype is retained during the population of cardiac jelly of the AV and OFT cushions. The process whereby subsets of AV and OFT endocardial cells transform into a mesenchymal phenotype has been called an endocardial-to-mesenchymal transition (EMT), which determines the anatomical placement where the valves will form within the primary heart tube. This EMT results in the mesenchymalization of the two major endocardial cushions of the AV canal: the superior (ventral) endocardial cushion that is associated with the inner curvature of the looped heart and the inferior (dorsal) endocardial cushion that forms along its outer curvature. The two major cushions then expand and eventually fuse, separating the heart into left and right AV orifices (Fig. 6). Following development of the major endocardial cushions, the lateral cushions appear later as lateral swellings of mesenchyme at the junction between the atria and ventricles (de Lange et al. 2004; Wessels et al. 1996). Each of the four cushions plays an important role in AV valvuloseptal development; the superior and inferior AV cushions contribute to the aortic leaflet of the mitral valve and the septal leaflet of the tricuspid valve. The lateral cushions also make significant contributions to the AV valves; the right lateral cushion contributes to the anterosuperior and inferior leaflets of the tricuspid while the left lateral cushion is involved in formation of the mural leaflet of the mitral valve (Snarr et al. 2008).

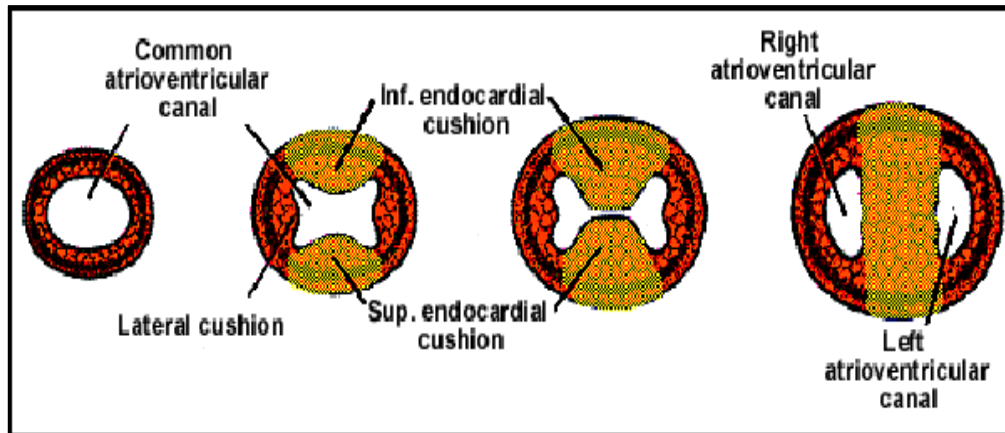


Fig. 6 Schematic representation of the atrioventricular canal from endocardial cushions

## 1.4 Hsa21 genes are overexpressed in DS

High-throughput technologies measuring thousands of transcripts in human DS cells (Conti et al. 2007; FitzPatrick et al. 2002) and in tissues from mouse models of DS (Dauphinot et al. 2005; Amano et al. 2004; Lyle et al. 2004; Kahlem et al. 2004) reported a global overexpression of triplicated genes in a dosage-dependent manner. Interestingly, these studies indicated that only a subset of Hsa21 genes is consistently overexpressed in comparison to euploid controls, and that the increase in expression may differ from the expected  $\sim 1.5$  fold (Conti et al. 2007; Mao et al. 2005; FitzPatrick et al. 2002). Also, the set of overexpressed Hsa21 genes differs across the trisomic cell types (Li et al. 2006). These findings indicate that other factors (e. g. developmental stage, tissue specific differences) also affect gene expression (Sommer and Henrique Silva 2008). Hsa21 gene expression may be regulated by dosage compensation or other mechanisms such that only a subset of those genes is expressed at the expected 50% increased levels in agreement with the above hypothesis.

It was hypothesized that, since Hsa21 encodes a number of transcription factors, coregulators and factors performing post-translational modification, including phosphorylation, dephosphorylation and sumoylation, the altered levels of these factors may contribute to the DS phenotype by perturbation of downstream gene expression (Gardiner et al. 2006).

The immediate conclusion of all these studies is that Hsa21 trisomy causes an overexpression of Hsa21 genes as a primary dosage effect. This produces, as secondary effect, the dysregulation of genes mapping on different chromosomes and as final effect the DS phenotype (**Fig. 7**).

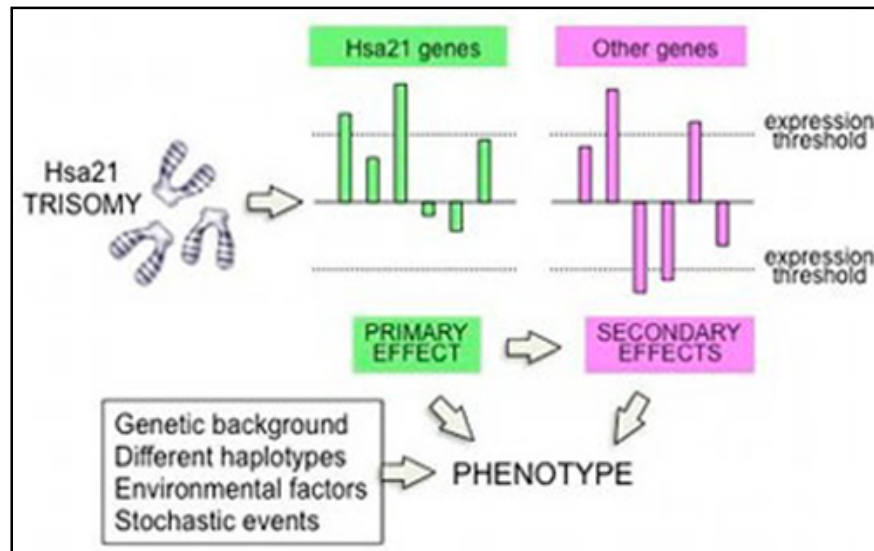


**Fig. 7 Primary and secondary effects of TS21.** Three copies of Hsa21 may cause a 50% increase in the expression of trisomic genes as primary dosage effect. The dysregulation of Hsa21 genes may cause alteration of disomic gene expression as secondary effects. Both primary and secondary effects will finally result in developmental defects and phenotypic alterations.

As the heart is one of the main DS targets, a gene expression profiling of fetal heart tissue by microarray technology was performed in 2007 (Conti et al. 2007). This study analyzed 15 fetal hearts at 18-22 weeks of gestation divided into 3 groups: 5 DS with CHDs, 5 without CHDs and 5 euploid samples. The analysis demonstrated that Hsa21 genes were globally upregulated by ~1.5 fold and 441 genes, mapping to other chromosomes, were significantly dysregulated in trisomic heart samples (**Fig. 8**). Functional class scoring and gene set enrichment analyses of the differentially expressed genes, revealed a high prevalence of genes encoding mitochondrial enzymes (**NEMGs**) among downregulated genes, and genes encoding extracellular matrix (**ECM**) proteins among the overexpressed genes (**Tab. S1 and S2, appendix 1**). Indeed, 65 out of 600 NEMGs mainly involved in all the respiratory complexes and mitochondrial functions were downregulated and 40 out of 700 ECM genes were upregulated (**Fig. 9**).

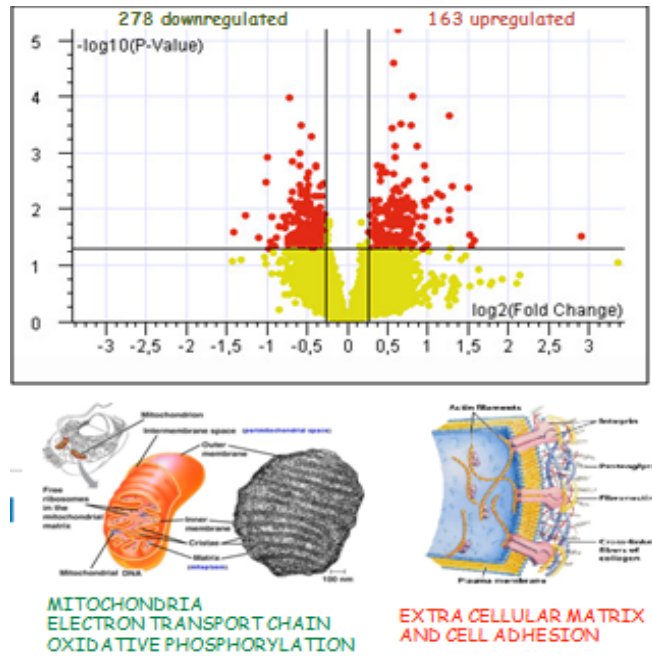


**Fig. 8** Volcano plot of differentially expressed genes between trisomic and non-trisomic hearts (Conti et al. 2007).

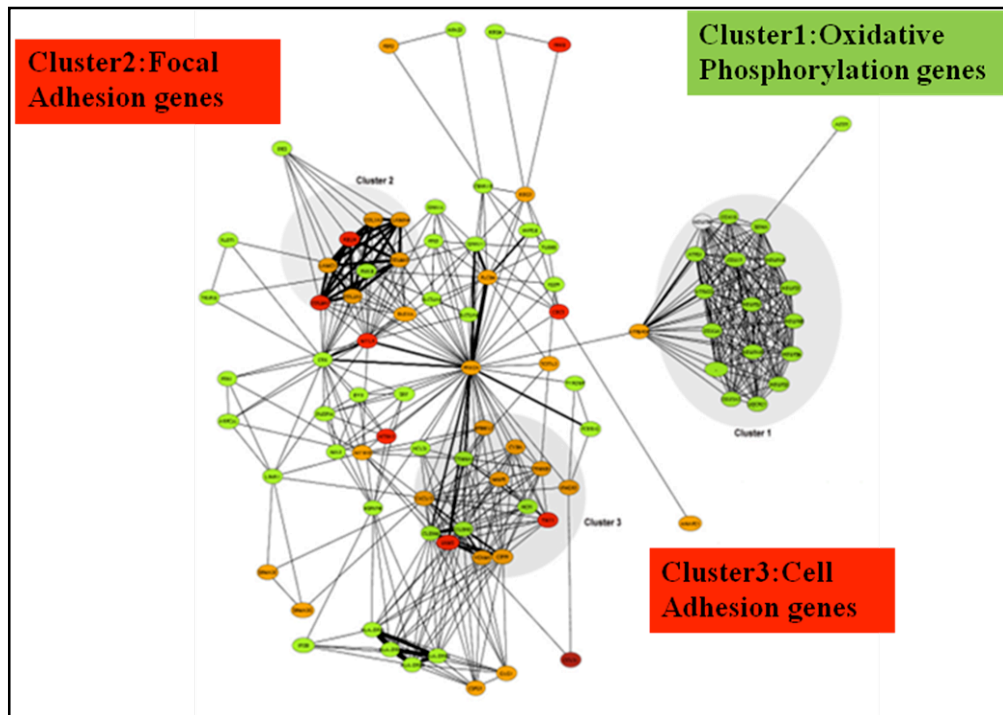


**Fig. 9 Genes and gene pathways affected by Hsa21 trisomy.** Pathway analysis was performed with **Pathway Miner** software on the 473 genes dysregulated in trisomic samples. The most affected pathways are: Oxidative Phosphorylation (**cluster 1**), containing 16 genes downregulated in trisomic samples, Focal Adhesion (**cluster 2**), containing at least 7 genes upregulated in trisomic samples, and a network of Cell Adhesion genes (**cluster 2**), upregulated in trisomic samples. Upregulated genes in clusters 2 and 3 are mostly ECM genes. Green indicates downregulated genes (darker green = more downregulated); red indicates upregulated genes (darker red = more upregulated) (Conti et al. 2007).

## 1.5 Mitochondrial dysfunction is associated to DS

TS21 has been associated to mitochondrial dysfunction in several DS cell types (Busciglio et al. 1995; Roat et al. 2007) and in mouse models (Shukkur et al. 2006; Shuchman et al. 2000), suggesting that a mitochondrial dysfunction affects the DS phenotype. Data from functional studies suggest that TS21 alters the mitochondrial function (Gardiner, 2003). DS has been associated to oxidative stress, increase of ROS production, altered intracellular calcium homeostasis, increase of apoptosis, decrease of protein level of complexes I, III and V in cerebellar and brain regions (Bambrick et al. 2008). Complex I was also deficient in mouse models of trisomy of chromosome 16. Impaired mitochondrial function, indicated by reduced mitochondrial redox activity and membrane potential, has been observed in DS astrocytes and in primary cultures of DS fibroblasts (Arbuzova et al. 2002; Busciglio et al. 2002). Deregulation of  $\text{Ca}^{2+}$  homeostasis and  $\text{Ca}^{2+}$  mediated signaling has been described in cells derived from DS patients and in mouse models of DS

(Yamato et al. 2009; Caviedes et al. 2006) since mitochondria function as a  $\text{Ca}^{2+}$  buffer. It has also been reported that the brain of the DS mouse model Ts1Cje has decreased mitochondrial membrane potential and ATP production (Shukkur et al. 2006). Recently it has been reported that both fetal and adult fibroblasts with TS21 show a drastic reduction in catalytic efficiency for the proteins involved in ATP production, such as increased levels of *ANT* (adenine nucleotide translocator), *AK* (adenylate kinase) and a drastic reduction in the catalytic efficiency respiratory chain complex I, which contributes to ROS overproduction in DS mitochondria (Valenti et al. 2010). These events were correlated with changes in the cAMP/PKA signaling pathway, which is known to affect the abundance of the transcriptional coactivator *PGC-1 $\alpha$ /PPARGC-1 $\alpha$*  (*peroxisome proliferator activated receptor gamma coactivator 1 $\alpha$* ) (Valenti et al. 2011). A decrease in basal levels of cAMP has been reported also in the hippocampus of the mouse model of DS, Ts65Dn, due to the altered basal activity of adenylate cyclase (Siarey et al. 2006).

Even though these results are indicative of widespread mitochondrial dysfunction in DS, few studies investigate the basis of mitochondrial dysfunction at the transcriptional level. Furthermore, no hypotheses have been formulated about the mechanisms by which trisomy of Hsa21 genes might induce such a dysfunction.

Mitochondrial function was investigated also in human fetal fibroblasts with TS21 (**DS-HFFs**), in our laboratory (Piccoli et al. 2013). Oxygen consumption rate (**OCR**) was decreased in trisomic fibroblasts (**Fig. 10A**). Electron microscopy of trisomic fibroblasts revealed that a significant number of mitochondria had an abnormal morphology, showing an increased size, irregular shape, evident breaks, mainly of inner membranes. In addition, the mitochondria showed alterations in the pattern of cristae where some were broadened and arranged concentrically or oriented parallel to the long axis of the organelle (longitudinal cristae) (**Fig. 10B**). Finally confocal microscopy analysis of ROS production, showed a significative increase of ROS in fibroblasts with Ts21 (**Fig. 10C**). Beside the upregulation of Hsa21 genes and the downregulation of NEMGs, a significant mitochondrial dysfunction was found that was more severe in fibroblasts from cardiopathic trisomic fetuses (**CDS-HFFs**) when compared with controls.

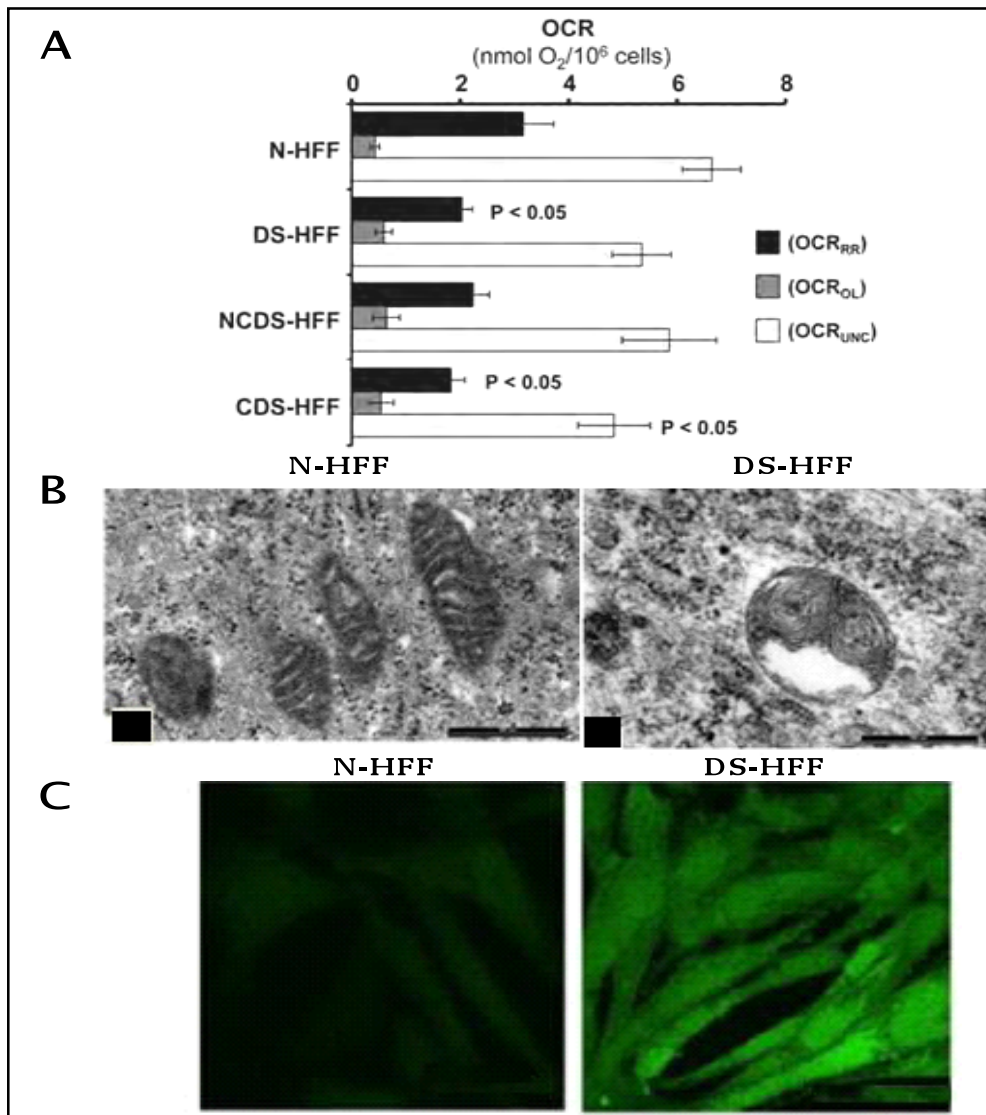


**Fig. 10 Mitochondrial function analysis in fibroblasts.** **A)** OCRs normalized to cell number were assessed by high-resolution oxymetry in intact cells. A comparative analysis between five different euploid (**N-HFFs**) and eight different trisomic (**DS-HFFs**) samples is shown; a distinction of the DS-HFFs between non-cardiopathic (**NCDS-HFFs**, n = 4) and cardiopathic (**CDS-HFFs**, n = 4) fetuses-derived fibroblasts is also reported. The endogenous OCR were measured under resting conditions (OCR<sub>RR</sub>), in the presence of oligomycin (OCR<sub>OL</sub>) and in the uncoupled state in the presence of FCCP (OCR<sub>UNC</sub>). **B)** Electron micrographs of normal mitochondria in N-HFF and morphologically abnormal mitochondria in DS-HFF (mitochondria with concentric cristae) **C)** Confocal microscopy analysis of ROS production in DS live fibroblasts. Representative LSCM imaging of the DCF-related fluorescence of euploid (N-HFFs) and DS (NCDS-HFFs and CDS-HFFs) fibroblasts (Piccoli et al. 2013).

One possible interpretation of these results is that a more pronounced pro oxidative state could induce a more severe cardiac phenotype, a concept that could be extended to other phenotypic traits. This study, together with the

previously cited one (Conti et al. 2007), suggests that the dysregulation of NEMGs is probably the basis of mitochondrial dysfunction in DS.

Mitochondrial alterations and oxidative stress are common features, also of neurodegenerative diseases, such as Alzheimer's Disease (AD), Parkinson's Disease and Huntington's Disease. Development of the DS brain is associated with decreased neuronal number and abnormal neuronal differentiation, indeed adults showed that DS cortical neurons, as well as fibroblasts with DS, exhibit a three to four fold increase in intracellular ROS, that causes neuronal apoptosis (Busciglio et al. 1995) (**Fig. 11**). In addition both DS neurons and astrocytes showed an abnormal pattern of protein processing as for amyloid  $\beta$  precursor protein (*APP*), consistent with chronic energy deficits (Busciglio et al. 2002). In DS astrocytes and neuronal cultures there is also a substantial alteration of the mitochondrial morphology, which exhibits increased fragmentation (Helguera et al. 2012) and a reduced mitochondrial redox activity and membrane potential (Arbuzova et al. 2002; Busciglio et al. 2002).

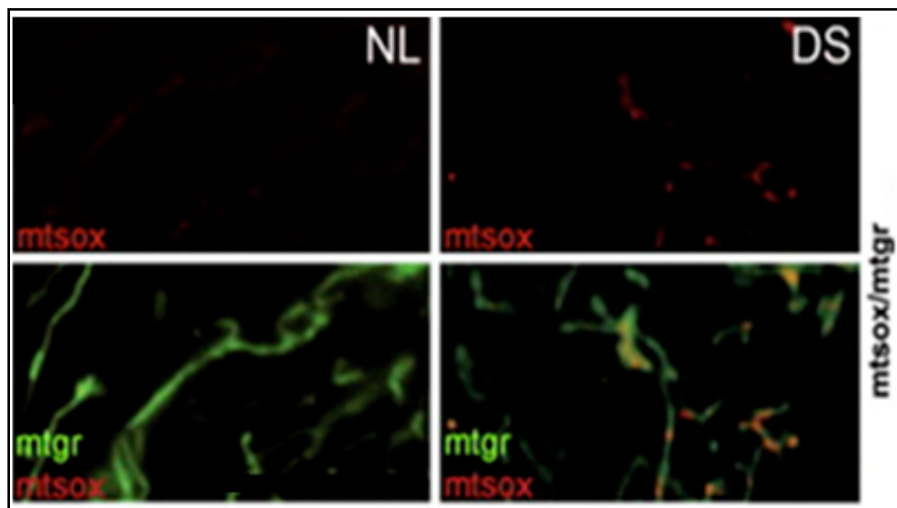


**Fig. 11** NL and DS astrocytes labeled with MitoTracker Green and MitoSOX. Simultaneous staining allows the visualization of superoxide production (mtsox, red) in live-cell mitochondria (mtgr, green) (Busciglio et al. 1995).

Proteomic approach demonstrated a significant reduction of mitochondrial respiratory enzymes in different brain regions from patients with DS and AD (Kim et al. 2000).

Further evidence for mitochondrial dysfunction was found in brain of the Ts1Cje (Sago et al. 1998), mouse model for DS, that shows decreased ATP levels, a decreased in mitochondrial membrane potential and an increased oxidative stress (Shukkur et al. 2006).

The identification of a molecular basis responsible for the deficiency of the OXPHOS in DS cells could provide an explanation for some clinical

characteristics of the syndrome. Indeed, genetic defects involving nuclear or mitochondrial OXPHOS enzymes are characteristic of clinical manifestations, including developmental delay, hypotonia, ophthalmoplegia, muscle weakness and cardiomyopathy, clinical signs present, although with variable severity in subjects affected by DS (Epstein, 1995). Although all these data are indicative of widespread mitochondrial dysfunction, the cause of this aspect of the disease is still unclear and remains to be investigated whether and how the alterations in the pathways/biomolecules of mitochondrial energy metabolism are involved in the pathogenesis of the syndrome.

#### 1.5.1 Structure and function of mitochondria

Mitochondria are intracellular organelles present in the cytoplasm of all eukaryotic cells. The overall volume of mitochondria is high in tissues and organs with high metabolic activity such as brain, retina, skeletal muscle, heart, kidney, and endocrine glands. The overall volume of mitochondria further increases in cells with enhanced energy demands, as in hyperactive skeletal muscle or in cardiac myocyte hypertrophy. Mitochondria are variable in size from 0.5 to 10  $\mu\text{m}$ , with an average diameter approximately of 1  $\mu\text{m}$ . The shape and number of these organelles are regulated by fission and fusion processes, which vary depending on the function of the cell and tissue. Mitochondria are surrounded by outer and inner membranes that are consistent with their symbiotic origin. The outer membrane is smooth and permeable to molecule of molecular mass up to approximately 5 KDa, whereas the inner envelope is highly folded and structured in cristae and offers the major permeability barrier to ions and molecules that traverse to the inner mitochondrial compartment by active transport. The two envelopes enclose an intermembrane space and an area inside the inner membrane, called matrix, where the basic mitochondrial macromolecular syntheses (DNA replication, transcription, and translation) take place. As the result of mitochondrial endosymbiotic origin, the organelles have its own genetic system with several bacteria-like features including a compact double stranded circular DNA genome of 16,5 Kb (**mtDNA**), which is self-replicating and maternally inherited (**Fig. 12**). Only 13 mitochondrial genes encode proteins, all of which are involved in electron transport and oxidative phosphorylation (Douglas, 2005).



inhibited by potassium cyanide (**KCN**); finally, there is the ATP synthase enzyme.

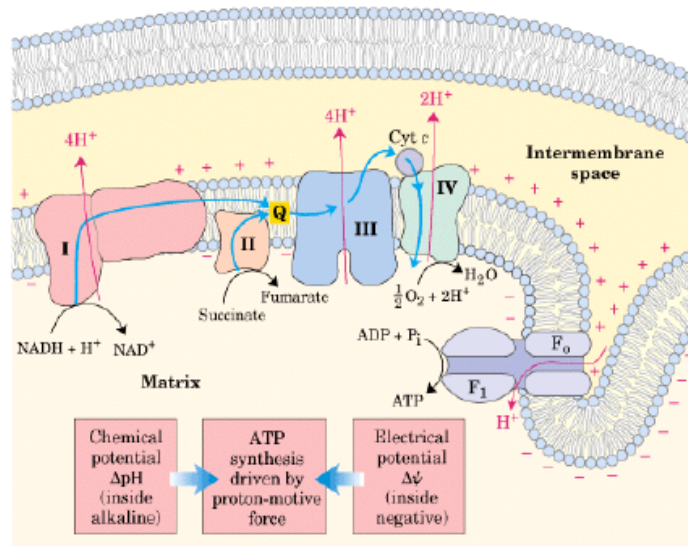


**Fig. 13 The OXPHOS process.** Schematic representation of the complexes activity during the OXPHOS. The transition of the electrons is accompanied by a translocation of protons across the mitochondrial membrane. This phenomenon produces a chemical gradient ( $\Phi$ ) and an electrical gradient ( $\Delta\psi$ ).

In addition to ATP synthesis, mitochondria also play central role in cellular  $\text{Ca}^{2+}$  homeostasis (Gunter et al. 2004), through its accumulation and release, as a result of physiologic stimuli. An important role in calcium signaling is covered by calcineurin/*NFAT* signaling pathway. *NFAT* is a  $\text{Ca}^{2+}$ /calcineurin (CaN) dependent transcription factor that has been implicated in the development and function of various organ systems, including the immune, endocrine, and cardiovascular systems (Crabtree and Olson, 2002). *NFAT* is exquisitely sensitive to the duration of the  $\text{Ca}^{2+}$  signal, which is explained by its activating mechanisms. In resting cells, phosphorylated *NFAT* resides in the cytosol. It is dephosphorylated by CaN in response to an increase in  $[\text{Ca}^{2+}]_i$ , resulting in unmasking of its nuclear localization signal (NLS) and its import into the nucleus.

The mitochondria are the major site for the production of ROS due to the highly propensity for aberrant release of free electrons. Increased production of ROS damages cell membranes through lipid peroxidation and further accelerates the high mutation rate of mtDNA. ROS are a variety of molecules and free radicals (chemical species with one unpaired electron) derived from molecular oxygen with the ability to react with reduced compounds. They comprise superoxide ( $\text{O}^{2-\bullet}$ ), hydrogen peroxide ( $\text{H}_2\text{O}_2$ ), and the highly reactive hydroxyl radical ( $\bullet\text{OH}$ ), although cells can also form minor amounts of singlet

oxygen. The initial product of the electron transport chain is  $O^{2-\bullet}$ , which is quickly transformed into  $H_2O_2$  by the enzyme superoxide dismutase (SOD).  $H_2O_2$  can be reduced to water by catalase or glutathione peroxidase or can be converted into  $\bullet OH$  in presence of reduced transition metals (reduced copper or iron). The main source of  $O^{2-\bullet}$  are respiratory complexes I and III located at the inner mitochondrial membrane (Camello-Almaraz et al. 2006; Chen et al. 2003).

### 1.5.2 Molecular basis of mitochondrial dysfunction in DS

The limited coding capacity of mtDNA necessitates that nuclear genes specify most proteins of the respiratory apparatus. Indeed most of the OXPHOS subunits are encoded by the nuclear genome. Some NEMGs act exclusively within the mitochondria to regulate the control of mitochondrial transcription and translation, others govern the expression of nuclear genes required for mitochondrial metabolism and organelle biogenesis. With only 13 OXPHOS polypeptides encoded by mtDNA, most of the OXPHOS subunits (at least 70) are encoded by the nuclear genome. The transcriptional regulatory network controlling the expression of nuclear and mitochondrial genes includes nuclear respiratory factors *NRF1* and *NRF2* and mitochondrial transcription factor A (*TFAM* or *mtTFA*). *NRF1* transcriptionally controls many genes involved in mitochondrial function and biogenesis, genes involved in assembly of the respiratory apparatus, constituents of the mtDNA transcription and replication machinery, mitochondrial and cytosolic enzymes of the heme biosynthetic pathway (Huo and Scarpulla, 2001). It is interesting to note that *NRF1* was found downregulated in DS fetal hearts.

*TFAM* binds to the mtDNA at multiple sites and functions in both mtDNA maintenance and transcription initiation (Scarpulla et al. 2011).

*NRF1* is a binding partner for the transcriptional coactivator *PGC-1 $\alpha$*  that coactivates numerous transcription factors, including nuclear receptors such as *PPAR $\gamma$*  and *PPAR $\alpha$* , and *ERR $\alpha$*  (estrogen receptor  $\alpha$ ), exerting the final effect to promote mitochondrial biogenesis and to regulate mitochondrial respiratory capacity (Scarpulla et al. 2012; Scarpulla et al. 2011; Leone et al. 2005) (**Fig. 14**). *PPAR $\alpha$*  (peroxisome proliferator activated receptor  $\alpha$ ) was the first NR (nuclear receptor) shown to be involved in the transcriptional control of mitochondrial metabolism. It is known to coordinately regulate nuclear genes encoding mitochondrial FAO enzymes. *PPAR $\alpha$*  is a member of a family of related NRs including the ubiquitously expressed *PPAR $\beta$*  (also known as *PPAR $\delta$* ) and *PPAR $\gamma$* , an adipose enriched transcription factor involved in adipocyte differentiation and the target of the insulin sensitizing thiazolidinediones.

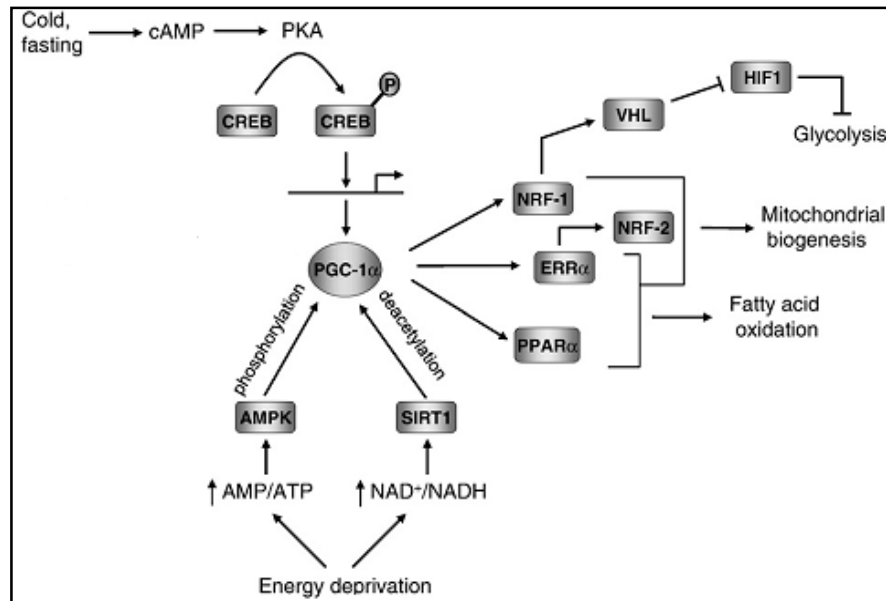


**Fig. 14 Regulatory network governing mitochondrial functions orchestrated by *PGC-1α*.** Interactions among some key participants in the transcriptional network regulating mitochondrial biogenesis are depicted schematically. The diagram summarizes the regulation of *PGC-1α* by transcriptional and post-transcriptional pathways and its interactions with some of its target transcription factors involved in metabolic regulation. Potential suppression of glycolysis through *NRF1* control of *VHL* expression and negative is also shown (Scarpulla et al. 2011).

*PGC-1α* function has been investigated in several specialized cell types and transgenic mouse models, demonstrating its role in the regulation of mitochondrial oxidative metabolism. Forced overexpression studies conducted in cultured adipocyte lines (Puigserver et al. 1998), cardiac myocytes (Lehman et al. 2000) and in conditional, tissue specific, transgenic mice (Russell et al. 2004), have shown that *PGC-1α* is capable of driving virtually all aspects of mitochondrial biogenesis, including activation of respiratory chain and FAO genes, increased mitochondrial number, and augmentation of mitochondrial respiratory capacity. Indeed *PGC-1α* knockout mice manifest a reduction of mitochondrial number and of respiratory capacity in skeletal muscle (Leone et al. 2005).

*PGC-1α* transcription and activity are positively regulated by  $\text{Ca}^{2+}$  signaling. Interestingly *PGC-1α* was found hypoexpressed both at the transcriptional and protein level in trisomic human heart and fibroblasts with TS21 (Fig. 15) (Piccoli et al. 2013; Conti et al. 2007).

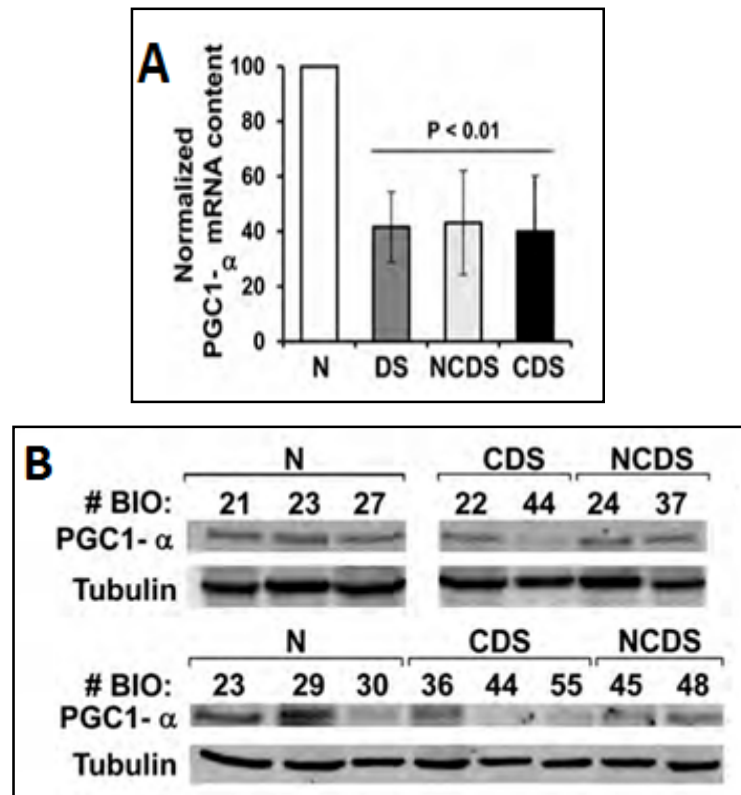


**Fig. 15 Expression analysis of the *PGC-1α*.** **A)** Expression analysis of the *PGC-1α* by qRT-PCR. The values, means + SEM, of the DS samples are normalized to that of the euploid fibroblasts. **B)** Analysis of the *PGC-1α* protein. Western blotting of *PGC-1α* on total cellular protein extracts from euploid and DS samples. To compare different electrophoretic runs, the densitometric value (normalized to tubulin) of the euploid sample BIO-23 was taken as an internal reference (Piccoli et al. 2013).

*PGC-1α* is activated via post-transcriptional phosphorylation by *AMPK* or by deacetylation via *SIRT1* in response to nutrient deprivation (Jager et al. 2007). Induction or activation of the coactivator can enhance mitochondrial biogenesis and oxidative function through the coactivation of multiple transcription factors involved in respiratory gene expression. *PGC-1α* activation may also promote an antioxidant environment by coactivating *ERRα* to induce *SIRT3*, a mitochondrial sirtuin that has been implicated in ROS detoxification. In addition, *AMPK* promotes autophagy through direct phosphorylation of *ULK1* or via suppression of the *TORC1* kinase complex.

Hsa21 genes that regulate mitochondrial biogenesis and function have been identified. The kinase *DYRK1A* and *DSCR1/RCAN1* (Bushdid et al. 2003) were considered to be involved in mitochondrial dysfunction in DS. *RCAN1* and *DYRK1A* genes are localized on Hsa21 and their overexpression, through the downregulation of NFATc genes (Fig. 16), might result in the depression of *PGC-1α* expression. Indeed in human DS fetal fibroblasts (DS-HFFs) and DS

hearts, *NFATc3* and *NFATc4* were significantly downregulated while *DYRK1A* and *DSCR1/RCAN1*, involved in regulating the levels of NFATc phosphorylation, were upregulated (Piccoli et al. 2013; Conti et al. 2007). *DYRK1A* and *DSCR1/RCAN1* play key roles in the calcineurin/NFAT pathway, which affects mitochondrial activity and morphology during heart development (Arron et al. 2006). Moreover *DSCR1/RCAN1* regulates mitochondrial function, increases susceptibility to oxidative stress in mammalian cells (Peiris et al. 2014), and modulates *NRF2* (O'Leary et al. 2004), a NEMG transcription factor.

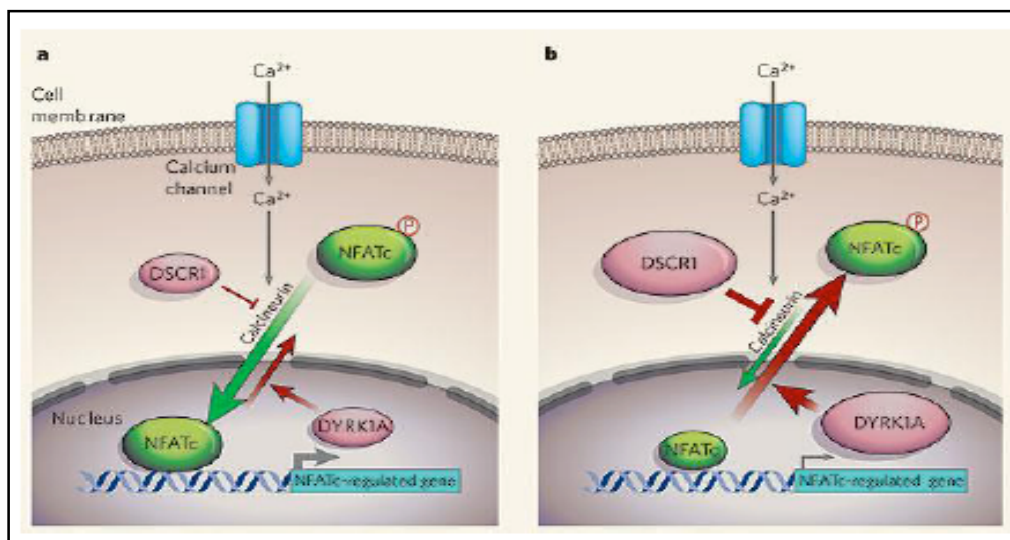


**Fig. 16 Calcineurin/NFAT signaling.** The entry of calcium ions into the cell activates the enzyme calcineurin to remove phosphate groups (P) from NFATc factors in the cytoplasm, allowing NFATc to enter the nucleus and to activate its target genes. However, once in the nucleus, NFATc can be phosphorylated, and so returns to the cytoplasm. Arron et al. and Gwack et al. (2006) implicated the *DSCR1* and *DYRK1A* proteins in regulating the levels of NFATc phosphorylation.

## 1.6 Pharmacological approaches for improving DS phenotype

Over the last several years, interesting results have been obtained testing drugs to rescue, or partially rescue, DS relevant deficits in learning and memory and abnormalities in cellular and electrophysiological features seen in the Ts65Dn mouse (Gardiner, 2014). These results suggest that some level of amelioration or prevention of cognitive deficits in people with DS may be possible.

The first demonstration of L/M (learning and memory) rescue in Ts65Dn used estrogen and was reported more than 10 years ago. The choice of estrogen was based on the observation of premature menopause and early onset cognitive decline in women with DS. Another drug that was effective was minocycline, a

derivative of tetracycline. In addition to antibiotic properties, minocycline is of interest because it is considered to have neuroprotective effects, modulating the activity of interleukin 1 beta (inflammation) and inhibiting caspases (apoptosis).

A GABA receptor (GABAAR) antagonist, pentylentetrazole (PTZ), was tested for its efficacy in L/M rescue. The proposal of PTZ for clinical trials in DS has been controversial because it is a known convulsant. Since DS subjects are at increased risk of seizures, they could be more sensitive to PTZ. Moreover, this drug is not currently US Food and Drug Administration (FDA) approved. To lessen the probability of negative side effects in people with DS, other more specific GABAAR antagonists are now being studied.

Memantine is an uncompetitive antagonist of the N-methyl-d-aspartate (NMDA) receptor and has been shown to rescue L/M in mouse models of AD. It is also currently approved by the US FDA for use in moderate to severe AD. The mechanism of action of memantine has known relationships with proteins encoded by Hsa21. There are nine Hsa21-encoded proteins, all trisomic in the Ts65Dn, which directly or indirectly interact with the NMDAR (Siddiqui et al. 2008). Among these is the regulator of *CaN*, *RCANI* that in turn is phosphorylated by the Hsa21 kinase *DYRK1A*. *RCANI* activity is further modulated by levels of reactive oxygen species that are affected by the Hsa21 proteins, the superoxide dismutase (*SOD1*), the amyloid precursor protein (*APP*), and the transcription factor *BACH1*. Activity of *CaN* is also influenced by the expression level of the Hsa21 calmodulin-binding protein, *PCP4*. *Costa et al* (2008) were the first to propose and test memantine in Ts65Dn. They showed that acute injection of memantine rescued L/M deficits. Thus, unlike GABAAR antagonists, memantine does not produce lasting positive effects.

There is extensive evidence in DS about of the potential efficacy of fluoxetine, the serotonin reuptake inhibitor. It had been shown previously in rodents that chronic treatment with fluoxetine, and other antidepressants, stimulates the production of new neurons and their incorporation into functional networks (Malberg et al. 2000). The first Ts65Dn study with fluoxetine demonstrated that adult neurogenesis is indeed impaired in untreated mice, and that 2 weeks of fluoxetine injections rescued this deficit (Clark et al. 2006). Most recently, fluoxetine has been used in prenatal treatment. Pregnant Ts65Dn mice were injected daily with 10 mg/kg fluoxetine (lower dose) from embryonic day 10 to birth (Guidi et al. 2014). When tested at P45, learning was normal. Prenatal fluoxetine treatment also rescued the abnormalities in neurogenesis seen in untreated Ts65Dn, both at birth and at 45 days.

Lithium is a common treatment for mood disorders that has been in use since the 1970s. Lithium has neuroprotective properties and has also been shown to increase adult neurogenesis in both controls and Ts65Dn mice. It has been demonstrated that when younger (~5-month-old) male Ts65Dn mice were treated for 1 month with lithium, a complete rescue of neurogenesis was seen (Contestabile et al. 2013).

Brains from individuals with DS and the Ts65Dn mice have small cerebella and reduced granule cell density. *Roper et al* (2006) first showed that an agonist of sonic hedgehog, SAG 1.1, rescued decreased cell numbers in the granule cell layer of the cerebellum. This work was particularly important because the correction, measured at P6, was obtained with a single injection of SAG 1.1 at P0.

*EGCG* (epigallocatechin-3-gallate) is a catechin found in green tea. It is a highly specific inhibitor for two Hsa21 kinases, *DYRK1A* and the *MAPKAPK5*. Reduction of activity of *DYRK1A* by *EGCG* in the Ts65Dn occurs in the context of elevated expression of other multiple Hsa21 genes. Decreasing *DYRK1A* expression in the presence of elevated expression of these Hsa21-encoded substrates and functional interactors could cause additional imbalances relevant to DS phenotypic features. It is unlikely that the benefits of *EGCG* treatment in the Ts65Dn are limited to inhibition of the activity of the *DYRK1A* kinase. *EGCG* has been shown to be a powerful antioxidant and antitumor agent. It is currently in clinical trials for obesity, several types of malignancy, Huntington's disease, Fragile X, and AD, as well as for DS.

Oxidative stress and mitochondrial dysfunction are both considered hallmarks of DS tissues and contributors to neurological phenotypes across the DS lifespan (Lott et al. 2012; Coskun et al. 2012). Cortical neurons derived from DS fetal brains show elevated levels of reactive oxygen species, and survival is enhanced by treatment with antioxidants (Busciglio et al. 1995). Several Hsa21 genes, among them *SOD1*, *BACH1*, *ETS2*, and *S100B*, are known to contribute to the regulation of oxidative stress when overexpressed (Sturgeon et al. 2012). Consistent with these observations, it was shown that levels of oxidative stress are elevated in the brains of adult Ts65Dn, and when male Ts65Dn mice were fed a diet high in vitamin E (0.4 g per kg) from the age of 4 months to ~8 months and 10 months, the levels of oxidative stress were decreased. In an attempt to prevent the developmental consequences of elevated oxidative stress, pregnant Ts65Dn female mice and their offspring were treated with a vitamin E-enriched diet and it has been observed an improvement of learning (Lockrow et al. 2009).

Some protocols are being developed to improve oxidative imbalance in DS using antioxidants such as the coenzyme Q10 (Tiano et al. 2011; Miles et al. 2007).

Considerable evidence has accumulated to suggest that prenatal and perinatal supplementation with choline can have long-term benefits for L/M (McCann et al. 2006) including the enhancement of adult neurogenesis (Glenn et al. 2007). Several clinical trials for cognitive deficits in DS have been completed recently and/or in progress. The efficacy of folate supplementation was tested in a larger trial where infants with DS, aged 3–30 months, received leucovorin (folinic acid) or placebo daily for 12 months (Blehaut et al. 2010). The choice of folate was based on the fact that seven Hsa21 genes are involved in folate metabolism, and evidence for their elevated expression and resulting perturbed concentrations of folate pathway components have been observed in DS. While

only a small effect was seen with folate, this effect was significantly increased in children who were also receiving thyroxine for hypothyroidism. Only two of the seven genes predicted to affect folate metabolism are trisomic in the Ts65Dn mice, making it an inadequate model for preclinical evaluations of folate-related supplements. The Hsa21 connection to the thyroid hormone may involve *NRIP1*, which is also not trisomic in the Ts65Dn mice (Park et al. 2009). A larger trial with folate plus thyroxine is in progress.

Although some therapeutic protocols had shown positive outcomes in Ts65Dn mice, the clinical trials did not show the expected results, and were also expensive in terms of time and resources. While prevention of cognitive deficits is an important goal, prenatal treatments come with their own more stringent and challenging requirements for safety demonstrations. The details of the Ts65Dn experiments used in preclinical evaluations are important; different drugs rescued L/M in different tasks, or they produced only partial rescue, with and without attendant rescue of neurogenesis. This suggests that combinations of drugs may be both necessary and advantageous. This approach is common in cancer therapy and viral infections, and recent methods for the rapid identification of optimally effective combinations of drugs could be easily applied to in vitro DS systems (Jaynes et al. 2013; Honda et al. 2013).

## 1.7 Drugs affecting the *PGC-1 $\alpha$* pathway

*PGC-1 $\alpha$*  is an important regulator of the mitochondrial biogenesis and can be activated via the PPAR, AMPK or Sirt1 pathway, either through increased expression (PPARs, *AMPK*) or through post-translational modification (PTMs, *AMPK*, *Sirt1*) (Wenz et al. 2008). Several substances and drugs that activate PPARs, *AMPK* and *Sirt1* are established. Recent studies have demonstrated that the activation of the *PGC-1 $\alpha$*  pathway has a potential therapeutic benefit in muscular and neurodegenerative disorders associated with mitochondrial dysfunction in cellular and murine models (Noe et al. 2013; Dillon et al. 2012; Dumont et al. 2012; Johri et al. 2012; Yatsuga and Suomalainen, 2012; Viscomi et al. 2011; Wenz et al. 2008). In some cases, this benefit led to an improvement of mitochondrial processes such as OXPHOS or fatty acid oxidation, while in other cases no significant effect was observed (Hofer et al. 2014).

Counteracting mitochondrial dysfunction in DS might provide the basis for clinical trials aimed at improving the pathological phenotypes that characterize DS or alleviate and prevent some of its related pathologies, including neurodegeneration, diabetes, obesity, and hypertrophic cardiomyopathy, thus providing a better quality of life for DS individuals and their families.

Our results (Izzo et al. 2014; Piccoli et al. 2013) indicate that the dysregulation of *NRIP1* plays a key role in the mitochondrial dysfunction observed in DS and suggest that the *NRIP1-*PGC-1 $\alpha$**  axis might represent a potential therapeutic target for restoring altered mitochondrial function in this syndrome.

Several clinical trials on the effects of antioxidant nutrients or vitamins (Lott et al. 2012; Tiano et al. 2011; Ellis et al. 2008; Miles et al. 2007) concluded that although antioxidant supplementation is safe, it neither improves cognitive performance nor prevents dementia in DS patients.

New therapies can be proposed based either on direct inhibition of *NR1P1* by specific RNAi or indirectly through the use of drugs, affecting genes involved in the same dysregulated pathways.

A possible therapeutic approach in DS could be based either on *PGC-1 $\alpha$*  activators, which have been tested in other disease mouse models (Jager et al. 2007; Rodgers et al. 2005), or on *PPAR $\gamma$*  agonists, which attenuate mitochondrial dysfunction in AD mouse models (Yamaguchi et al. 2012; Bastin et al. 2008). Such drugs are already routinely used in clinical practice for the treatment of metabolic syndromes, type 2 diabetes, and neurodegenerative diseases such as AD (Marciano et al. 2014; Watson et al. 2005).

What is puzzling is that although drugs capable of modulating the activity of *PGC-1 $\alpha$*  and/or the downstream PPAR proteins are available, no therapeutic approaches have ever been undertaken to correct the overall mitochondrial dysfunction in DS patients. In effect, *PGC-1 $\alpha$*  activity is mainly controlled by PPARs, AMP-activated kinases (AMPKs) and the NAD-dependent deacetylase *SIRT1* (Canto and Auwerx, 2009). Direct phosphorylation by *AMPK* promotes *PGC-1 $\alpha$*  dependent induction at the *PGC-1 $\alpha$*  promoter level (Jager et al. 2007); similarly, *SIRT1* stimulates *PGC-1 $\alpha$*  activity through deacetylation, thereby inducing mitochondrial biogenesis (Rodgers et al. 2005). Pharmacological activators for these proteins, such as metformin, via AMPK induction, as well as resveratrol, via SIRT1 induction, have been tested in other disease mouse models (Dong et al. 2007; Jager et al. 2007; Lagouge et al. 2006). A recent study indicates that metformin promotes neurogenesis and enhances spatial memory formation in normal adult mouse.

Other pharmacological activators include thiazolidinediones, pioglitazones, and bezafibrates. In brief, thiazolidinediones selectively stimulate *PPAR $\gamma$* . Pioglitazone attenuates mitochondrial dysfunction in animal models of central nervous system injury, improving the mitochondrial ability to produce ATP and rates of oxygen consumption (Sauerbeck et al. 2011; Nicolakakis et al. 2008). Finally, bezafibrate, a PPAR pan-agonist typically used to treat human hyperlipidemia (Yatsuga and Suomalainen, 2012), also stimulates the mitochondrial respiratory chain, mitochondrial biogenesis, and fatty acid oxidation both *in vitro* and *in vivo* (Yamaguchi et al. 2012; Johri et al. 2011; Bastin et al. 2008). Hofer et al. (2014) performed a comprehensive analysis of the effects of potential *PGC-1 $\alpha$*  activating drugs. The authors pharmaceutically targeted the PPARs (bezafibrate, rosiglitazone), AMPK (AICAR, metformin) and SIRT1 (resveratrol) pathways in HeLa cells, neuronal cells and *PGC-1 $\alpha$* -deficient MEFs demonstrating tissue-specific effects of these drugs in modulating mitochondrial processes and cellular stress programs. All the observed effects were clearly dependent on *PGC-1 $\alpha$*  modulation.

Not all analyzed drugs activate the *PGC-1 $\alpha$*  pathway or alter mitochondrial protein levels. However, they all affect supramolecular assembly of OXPHOS complexes and OXPHOS protein stability.

## **1.8 A novel approach to assess mitochondrial respiration: XF<sup>e</sup> Analyzer**

Glycolysis and oxidative phosphorylation are the two major energy-producing pathways in the cell.

XF<sup>e</sup> 96 Extracellular Flux Analyzer (Seahorse Bioscience) simultaneously interrogate these major energy producing pathways of the cell mitochondrial respiration and glycolysis in a microplate, in real-time. The XF<sup>e</sup> 96 Analyzer determines in vitro oxygen consumption rate (**OCR**), and extracellular acidification rate (**ECAR**), in order to assess cellular functions such as oxidative phosphorylation and glycolysis. The measurement of cellular bioenergetics on live cells enables time-resolved analysis and testing of multiple conditions per assay well. By incorporating automated compound addition and solid-state fluorescence sensors in a microplate format, XF technology provides the tools to:

- Simultaneously measure oxygen consumption rate (OCR) and extracellular acidification rate (ECAR) in all assay wells.
- Rapidly detect cellular responses to substrates, inhibitors, and other perturbants.
- Test more conditions with the same amount of sample, maximizing the value of each experiment.
- The XF<sup>e</sup> 96 Extracellular Flux Analyzer, XF stress test kits, reagents, consumables, and software tools work together to simplify the measurement of cellular metabolism.

The XF Cell Mito Stress Test is the standard assay for measuring mitochondrial function in cells. The XF Cell Mito Stress Test Kit makes it easy to measure the four key parameters of mitochondrial function in a microplate: basal respiration, ATP turnover, proton leak, and maximal respiration, revealing critical information not evident in basal metabolism measurements alone, by directly measuring the OCR of cells. The XF Cell Mito Stress Test uses modulators of respiration that specifically target components of ETC in the mitochondria to reveal key parameters of metabolic function. The modulators (oligomycin, FCCP, and a mix of rotenon and antimycin A) are serially injected to measure ATP production, maximal respiration, and non-mitochondrial respiration, respectively (**Fig. 17**). Each modulator targets a specific component of the ETC. Oligomycin inhibits ATP synthase (complex V) and the decrease in OCR following injection of oligomycin correlates to the mitochondrial respiration associated with cellular ATP production. Carbonyl cyanide – 4 (trifluoromethoxy) phenylhydrazone (FCCP) is an uncoupling

agent that collapses the proton gradient and disrupts the mitochondrial membrane potential. As a result, electron flow through the ETC is uninhibited and oxygen is maximally consumed by complex IV. The FCCP stimulated OCR can then be used to calculate spare respiratory capacity, defined as the difference between maximal respiration and basal respiration. Spare respiratory capacity is a measure of the cell's ability to respond to increased energy demand. The third injection is a mix of rotenon, a complex I inhibitor, and antimycin A, a complex III inhibitor. This combination shuts down mitochondrial respiration and enables the calculation of non-mitochondrial respiration driven by processes outside the mitochondria.

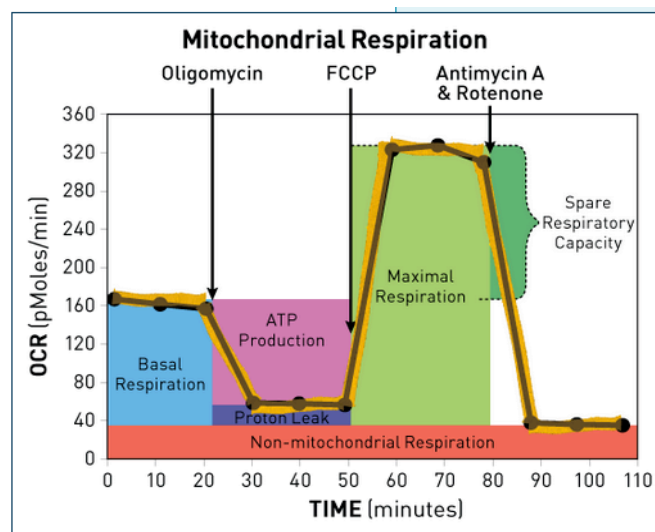


**Fig. 17 XF Cell Mito Stress Test** profile of the fundamental parameters of mitochondrial function: basal respiration, ATP turnover, proton leak, maximal respiration, and spare respiratory capacity.

The XF analyzer also provides a standard and comprehensive method to assess the three key parameters of glycolytic function: Glycolysis, Glycolytic Capacity, and Glycolytic Reserve (**Fig. 18**). Initially, cells are incubated in the glycolysis stress test medium without glucose and ECAR is assessed. The first injection is a saturating concentration of glucose (10 mM). Glucose is taken up by the cells and catabolized through the glycolytic pathway to lactate, producing ATP and protons. The extrusion of protons into the surrounding medium produces a rapid increase in ECAR. This glucose-induced response is reported as the rate of glycolysis (or Glycolytic Flux) under basal conditions. The second injection is oligomycin that inhibits mitochondrial ATP production and thus shifts the energy production to glycolysis, with the subsequent increase in ECAR revealing the maximum glycolytic capacity of the cells. The final injection is 2-DG, a glucose analog, which inhibits glycolysis through competitive binding to glucose hexokinase, the first enzyme in the glycolytic

pathway. The resulting decrease in ECAR further confirms that the ECAR produced in the experiment is due to glycolysis.

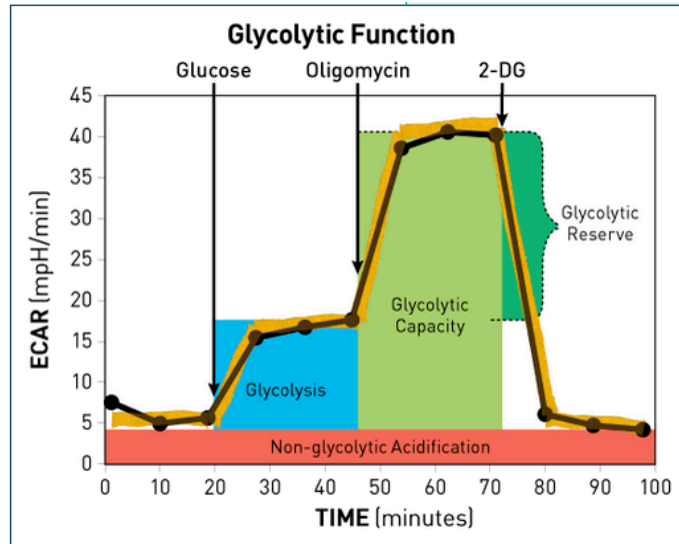


**Fig. 18 XF Glycolysis Stress Test Kit** profile of the fundamental parameters of cellular glycolysis: glycolysis, glycolytic capacity, and glycolytic reserve capacity.

## 2. AIMS OF THE STUDY

The main objective of this PhD project was to understand the molecular mechanisms implicated in some traits of the DS phenotype, especially cardiac and neurological defects, in order to develop strategies for prevention and/or therapeutic treatments.

Mitochondrial alterations, consistently observed in DS subjects and in DS mouse models, have been proposed to contribute to the severity of DS anomalies. In human cells and tissues from DS fetuses it was demonstrated that NEMGs (nuclear encoded mitochondrial genes) are globally downregulated, while ECM (extracellular matrix) genes are upregulated in comparison with euploid samples (Piccoli et al. 2013; Conti et al. 2007).

A mitochondrial dysfunction was found associated with NEMG downregulation and a more pronounced pro-oxidative state was demonstrated in DS fibroblasts from fetuses with congenital cardiopathy (Piccoli et al. 2013). These results are in line with the hypothesis that mitochondrial dysfunction might worsen the DS cardiac phenotype.

The project that our research group carried out was aimed at investigating whether NEMG downregulation or ECM upregulation might affect cardiac phenotype, to identify Hsa21 genes responsible for either NEMG downregulation or ECM upregulation, and to develop strategies to counteract the negative effects triggered by NEMG dysregulation in DS.

Through a metaanalysis of public expression data *NRIP1/RIP140* (Nuclear receptor interacting protein 1) was identified as the potential repressor of NEMGs expression, and *RUNX1* (Runt related transcription factor 1) as the potential candidate for ECM upregulation.

A strategy to counteract mitochondrial dysfunction in DS has been developed starting from the following considerations:

1) The co-repressor gene *NRIP1* negatively regulates the mitochondrial function possibly by repressing the activity of *PGC-1 $\alpha$* , a master regulator of mitochondrial biogenesis (Izzo et al. 2014; Chen et al 2012; Powelka et al. 2006, Scarpulla et al. 2012; Scarpulla et al. 2011).

2) *PGC-1 $\alpha$*  is downregulated in DS fetal fibroblasts and heart tissue (Piccoli et al. 2013; Conti et al. 2007).

The rationale of therapeutic strategies is therefore to repair mitochondrial dysfunction in DS through the restoration of the *NRIP1/PGC-1 $\alpha$*  axis.

To meet our objectives, we have transiently silenced *NRIP1* gene in DS-HFFs to evaluate its possible implication in the regulation of *PGC-1 $\alpha$*  expression and in mitochondrial dysfunction. The final aim of silencing experiments was to verify whether *NRIP1* inhibition in DS cells was able to rescue the mitochondrial function. DS-HFF samples in which *NRIP1* gene was found overexpressed have been selected.

In order to evaluate the effect of *NR1P1* silencing on mitochondrial function a phenotypic mitochondrial analysis in silenced cells versus control cells was carried out.

After demonstrating that *NR1P1* attenuation in DS cells is able to rescue mitochondrial function, the next aim of this project was to counteract mitochondrial dysfunction by pharmacologically targeting the genes controlled by *NR1P1*, namely *PGC-1 $\alpha$*  and PPAR genes. Among the possible therapeutic agents we have chosen two drugs: metformin (an activator of *PGC-1 $\alpha$* ) and pioglitazone (an agonist of *PPAR $\gamma$* ). These two drugs are already used in the clinical practice for the treatment of metabolic syndromes.

DS-HFF cultures were treated with these drugs in order to evaluate their efficiency in increasing *PGC-1 $\alpha$*  expression and ATP production and in globally ameliorating the mitochondrial function. To evaluate the drug effect on mitochondrial phenotype the same parameters described above for *NR1P1* silencing were chosen.

As the chosen drugs are already registered for human therapeutic use, should any of them demonstrate to be effective it can be immediately translated in human therapeutic protocols.

### 3. MATERIALS AND METHODS

#### Samples

The local Institutional Ethics Committee approved all experimental protocols. Primary lines of skin fibroblasts (HFFs) from fetuses at 18-22 gestational weeks were obtained from the "Telethon Bank of Fetal Biological Samples" at the University of Naples Federico II. Eight lines of fetal fibroblasts were from euploid fetuses (**N-HFF**) and ten from DS fetuses (**DS-HFF**) with and without cardiopathy (**CDS-HFF** and **NCDS-HFF** respectively) (**Tab. 1**) Fibroblasts were cultured in T25 flasks (BD Falcon) with Chang medium C (Irvine Scientific) supplemented with 1% penicillin/streptomycin (Gibco) at 37°C in 5% CO<sub>2</sub> atmosphere. All the analyses described throughout this study were carried out at cell culture passages 4-5. For silencing experiments 4 DS-HFF (BIO37, BIO55, BIO44 and BIO48) samples were used. For drug treatments 2 DS-HFFs (BIO-45 and BIO-71) were used.

**TABLE 1 Primary lines of fetal skin fibroblasts used in the study.**

<b>N-HFF</b>	<b>DS-HFF</b>	
	<b>NCDS-HFF</b>	<b>CDS-HFF</b>
BIO23	BIO37	BIO36
BIO27	BIO45	BIO44
BIO29	BIO48	BIO55
BIO30	BIO74	BIO71
BIO75		
BIO80		

**N-HFF** (euploid samples); **NCDS-HFF** (trisomic samples from fetuses without cardiopathy); **CDS-HFF** (trisomic samples from fetuses with cardiopathy)

### Transcription factors binding analysis of co-regulated genes

Pscan software (<http://www.beaconlab.it/pscan>, [Zambelli et al. 2009]) was used to look for over-represented TF motifs in the list of genes dysregulated in DS fetal hearts. We considered enriched in targets, TF with adjusted P-values < 0.05.

### Public data expression analysis

The data set GSE 19836 series (De Cegli et al. 2010) from Gene Expression Omnibus repository (GEO (<http://www.ncbi.nlm.nih.gov/geo>)) was reanalyzed to investigate the effects of Hsa21 gene overexpression over NEMG and ECM regulation. Clones of mouse embryonic stem cells in which 13 transcription factors (*Aire*, *Bach1*, *Erg*, *Ets2*, *Gabpa*, *Nrip1*, *Olig1*, *Olig2*, *Pknox1*, *Runx1*, *Sim2*, *ZFP295*, *1810007M14Rik*), one transcriptional activator (*Dscr1-Rcan1*) and 6 protein kinases (*DYRK1A*, *SNF1LK*, *Hunk*, *Pdxk*, *Pfkl*, *Ripk4*) were individually induced, were transcriptionally profiled under inducing and non-inducing conditions with Affymetrix Gene Chip Mouse 430\_2. Specifically, RNAs from three induced mouse ESCs and three controls were profiled for each inducible Hsa21 gene (De Cegli et al. 2010). In our analysis, we used GeneSpring software vers. 11.5 Multi-Omic Analysis (Agilent technologies, Inc.) for data interpretation. We considered genes differentially expressed with a Fold change (LogFC) >0.3 and < -0.3 with P<0.05. Gene ontology (GO) functional class scoring of all the lists of significantly upregulated or downregulated genes was performed using the Web-based Gene Set Analysis Toolkit V2 (<http://bioinfo.vanderbilt.edu/webgestalt/>) (Zang et al. 2005, Wang et al. 2013). Special attention was given to mitochondria- and ECM-related categories and pathways.

### Comparison of lists of differentially expressed NEMGs: meta-analysis

We compared three sets of gene expression data from different experiments, to identify genes consistently dysregulated across the three studies. The first set, SET1, included genes dysregulated by *NRIP1* modulation in mouse adipocytes (Powelka et al. 2006). The second set, SET2, included genes upregulated after *PGC-1 $\alpha$*  induction in SAOS2 cells (human osteoblast like cells) (Schreiber et al. 2004). The third set included mitochondria-related genes, downregulated in DS fetal heart tissue (Conti et al. 2007). The three sets were filtered according to the GO cell component category "mitochondrion" with Web-based Gene Set Analysis Toolkit V2. The resulting genes - 123 genes in SET1, 129 in SET2 and 70 in SET3 - were intersected using the R software (<http://www.R-project.org/>). A Venn diagram was built, which shows overlapping genes across the three sets.

### Transfection of siRNA (short interfering RNA)

*NRIP1* expression was attenuated transiently in 4 DS-HFFs lines using a specific pool of siRNAs for *NRIP1* (ON-TARGETplus SMART-pool, Dharmacon). ON-TARGET plus SMART pool Non-targeting siRNAs control

(Dharmacon) was used as control (scrambled siRNA). The siRNAs were diluted in an appropriate buffer consisting of 20 mM KCl, 6 mM HEPES pH 7.5 and 0.2 mM MgCl<sub>2</sub>, for a stock of 20 μM siRNA. INTERFERIN (Polyplus transfection) was used as transfection reagent, which avoids off-target effects. The trisomic fetal fibroblasts were transfected with two different concentrations of siRNAs, 5 nM and 20 nM. Each experiment was conducted in duplicate according to manufacturer's protocols. 72 hours after transfection, the effects of NRIP1 siRNA mediated attenuation were evaluated.

#### NRIP1 protein assay by immunofluorescence

Cultured cells, grown on 12 mm diameter round glass coverslips, were fixed in 3:1 methanol:acetic acid for 15 minutes, washed twice with PBS, and then incubated twice in 0.1 M Borate Buffer pH 8.5 for 10 minutes to neutralize the pH. After two washes with PBS, the cells were incubated with DNase 1:10 in RDD Buffer (Qiagen) at 37°C for 1 h and then treated with 2% BSA in PBS to block non-specific protein-protein interactions. The cells were then incubated with the antibody anti-NRIP1 (30 μg/ml, ab42126 Abcam, Cambridge Science Park, Cambridge, UK) overnight at + 4°C. The secondary antibody (green) was Alexa Fluor® 488 goat anti-rabbit IgG (H+L) used at a 1/200 dilution for 1 h. Cells were finally mounted in 50% glycerol in PBS. Immunofluorescence analysis was performed at a confocal laser-scanning microscope LSM 510 (Zeiss, Gottingen, Germany) equipped with an Argon ionic laser whose  $\lambda$  was set at 488 nm, and an HeNe laser whose  $\lambda$  was set at 633 nm. Emission of fluorescence was revealed by a BP 505-530 band pass filter for Alexa Fluor 488 and by a 615 long pass filter for DRAQ5. Images were acquired at a resolution of 1024 x 1024 pixels. Analysis of data was performed with ImageJ software, version 1.37. Fifty random single cells were analyzed for each imaging analysis.

#### Laser scanning confocal microscopy live cell imaging of ROS production

Cultured cells, grown for 72 hours on 25 mm diameter round glass coverslips in an Attofluor cell chamber (Molecular Probe, Leiden, NL), were incubated for 15 minutes at 37°C with 10 μM of 2,7-dichlorofluorescein diacetate (DCF-DA) which is converted to dichlorofluorescein by intracellular esterases, for detection of H<sub>2</sub>O<sub>2</sub>, or with 5 μM of MitoSOX™ Red reagent (Life Technologies, Molecular Probes), a live-cell permeant which rapidly and selectively targets the mitochondria exhibiting red fluorescence when oxidized by superoxide. Manufacturer's protocols were applied. Immunofluorescent images were captured by a confocal laser scanner microscopy Zeiss LSM 510 (Carl Zeiss, Gottingen, Germany), equipped with Argon ionic laser whose  $\lambda$  was set at 488 nm, an HeNe laser whose  $\lambda$  was set at 546 nm. Emission of fluorescence was revealed by BP 505-530 band pass filter for DCF and 560 Long Pass for MitoSOX™ Red. Images were acquired in the green or in the red channels and then saved in LSM format. They were acquired with a

resolution of 1024 x 1024 pixel with the confocal pinhole set to one Airy unit. Analysis of data was performed with ImageJ software, version 1.37. Fifty random single cells were analyzed for each imaging analysis.

#### MitoTracker immunofluorescence

The MitoTracker® Red CMXRos (Molecular Probe) is a red-fluorescent dye that diffuses into the plasma membrane depending on the potential and accumulates in the mitochondria of living cells in active respiration. Cells were grown on 12 mm diameter round glass coverslips and then incubated with 150 nM of MitoTracker® Red for 30 minutes. After incubation cells were fixed for 20 minutes in PBS containing 4% paraformaldehyde (Sigma) and then washed once with PBS 1x. Nuclei were stained with the DNA intercalant DRAQ5 (Bio status, Alexis Corporation). Cells were finally mounted in 50% glycerol in PBS. Immunofluorescence analysis was performed with a confocal laser-scanning microscope LSM 510 (Zeiss, Gottingen, Germany). The lambda of the two HeNe lasers was set at 546 nm and at 633 nm. Fluorescence emission was revealed by BP 560-615 band pass filter for MitoTracker® Red and by 615 long pass filter for DRAQ5. Double staining immunofluorescence images were acquired separately in the red and infrared channels at a resolution of 1024 x 1024 pixels, with the confocal pinhole set to one Airy unit, and then saved in LSM format. Fifty random single cells were analyzed for each imaging analysis using the ImageJ version 1.37.

#### RNA extraction and quantitative real-time PCR

Total RNA from each sample was extracted using TRIzol reagent (Gibco/BRL Life Technologies, Inc., Gaithersburg, MD) and was reverse transcribed using the iScript cDNA Synthesis kit (Bio-Rad Laboratories, Inc., Hercules, CA, USA). Real-time PCR was performed using iQ Supermix SYBR Green 2x on a Bio-Rad iCycler according to the manufacturer's protocols. PCR reactions were performed in triplicate. Primer pairs (MWG Biotech, Ebersberg, Germany) were designed using the Primer 3 software (<http://frodo.wi.mit.edu/primer3>) to obtain amplicons ranging from 100 to 150 base pairs. In order to test primer efficiency, serial dilutions of cDNAs generated from selected samples, that expressed target genes at a suitable level, were used to generate standard curves for each gene. Expression values were normalized either versus scrambled transfected cells or versus scrambled transfected euploid cells. *ABELSON* and *GAPDH* housekeeping genes were chosen as reference genes.

#### mtDNA quantification

To quantify the mtDNA content, we selected two genes: *D-LOOP* as the mitochondrial target and *ACTIN* as the nuclear target. Both targets were quantified by qRT-PCR using cDNA reverse-transcribed from RNA of three *NR1P1*-silenced trisomic samples and scrambled control. Normalization of

gene expression was obtained using *ABL* gene as housekeeping. The ratio between *D-LOOP* and *ACTIN* expression under each condition (*NR1P1*-silenced or scrambled trisomic cells) was calculated.

#### ATP measurements by chimeric photoprotein Luciferase ATP sensitive

Cells were seeded on glass coverslips (13 mm diameter) for single sample luminescence measurements and allowed to grow until 50% confluence. The cells were then transfected with a cytosolic (untargeted) firefly luciferase (cytLuc) and a mitochondrially targeted luciferase (mtLuc). Cell luminescence was measured in a luminometer constantly perfused with KRB, supplemented with 1 mM CaCl<sub>2</sub> and 20 mM luciferin. The light output of a coverslip of infected cells was in the range of 1.000-10.000 counts per second (cps) versus a background lower than 10 cps. All compounds employed in the experiments were tested for non-specific effects on the luminescence, but none was observed.

Measurements of ATP and mitochondrial mass were performed in collaboration with Prof. Pinton's Lab.

#### Western Blot

Cells were scraped into ice cold phosphate-buffered saline and lysed in a modified 10 mM Tris buffer pH 7.4 containing 150 mM NaCl, 1% Triton X-100, 10% glycerol, 10 mM EDTA and protease inhibitor cocktail. After 30 minutes of incubation on ice, the lysates were cleared via centrifugation at 12,000 g at 4°C for 10 minutes. The protein concentration was determined by the Lowry procedure. Protein extracts (18 µg) were separated on 4-12% Bis-Tris acrylamide Gel (Life Technologies, NP0323). Gel was then blotted onto nitrocellulose transfer membranes using a Bio-Rad apparatus. After transfer, the filters were blocked at room temperature for 1 h with 5% non-fat powdered milk in TTBS (150 mM NaCl, 20 mM Tris-HCl pH 7.5). After washing twice with TTBS (150 mM NaCl, 20 mM Tris-HCl pH 7.5, 0.1% Tween 20), filters were incubated overnight at 4°C with [GAPDH (Cell Signaling, 2118); LUCIFERASE (Invitrogen, 356700)]. The filters were washed extensively with TTBS and incubated for 1 h at room temperature with antirabbit peroxidase-conjugated secondary antibody [Santa Cruz, sc-2004 (goat anti-rabbit) and sc-2005 (goat anti-mouse)] plus a chemiluminescent substrate (Thermo Scientific, 34080). Results were normalized to GAPDH; indeed, equal loading of lanes was confirmed by incubation with an anti-GAPDH antibody.

#### Treatment of DS-HFFs with drugs

- Treatment with metformin

Two DS-HFFs lines (BIO-37 and BIO-71) at P3 passage were thawed and cultured in T25 flask with Chang medium C supplemented with 1% penicillin/streptomycin at 37°C in 5% CO<sub>2</sub> atmosphere. Metformin (Sigma-Aldrich, D150959) was dissolved in water to prepare a stock of 100 mM, and

then was added at final concentrations within the range between 0.5 mM and 2 mM. The cells were treated for 72h and subjected to changes every 24h, with a culture medium supplemented with the drug, while the control cells were supplemented with water. The experiments were performed in triplicate for the measurement of OCR and in duplicate for other measurements.

- Treatment with pioglitazone

Two DS-HFFs lines (BIO-71 and BIO-45) were thawed and cultured in T25 flask with Chang medium C supplemented with 1% penicillin/streptomycin at 37°C in 5% CO<sub>2</sub> atmosphere. Pioglitazone (Takeda Pharmaceuticals, Osaka, Japan) was dissolved in a DMSO solution to prepare a stock of 1 mM, and then was added to a final concentrations of 100 nM, 1 μM and 2 μM. The cells were treated for 48 and 72 hours, and subjected to changes every 24h, with a culture medium supplemented only with the drug, while the control cells were supplemented with DMSO. The experiments were performed in triplicate for the measurement of OCR and in duplicate for other measurements.

#### Measurement of OCR in cell cultures

Oxygen consumption rate (**OCR**) in adherent fibroblasts was measured with an XF<sup>e</sup> 96 Extracellular Flux Analyzer (Seahorse Bioscience, Billerica, MA, USA). Cells from 2 DS-HFFs lines (BIO-71 and BIO-37) were cultured in T25 flasks and treated with different concentrations of the drug for 48 h, with culture medium supplemented with the drug and subjected to change every 24 hour. After this time, approximately 22,000 cells/well were plated in a microplate of 96 wells. The plate was then incubated in CHANG medium C supplemented with the drug for 24h. At the end of 24h, the CHANG medium was removed from the plate and 175 μl of the OCAR medium were added in the other half of the plate. The final volume of each well was 250 μl. Finally the plate was incubated with the cells in an incubator without CO<sub>2</sub> for 1h. Experiments were performed in duplicate according to manufacturer's protocols. Each sample was plated in triplicate; for each well 12 measurements at different times, before and after the injection of inhibitors were carried out. These experiments were performed in collaboration with Prof. Matarese's Lab.

#### Measurement of mitochondrial mass

The method to assess mitochondrial mass by confocal microscopy is based on the fluorescence of the mitochondrial network after the expression of a GFP specifically targeted to the mitochondria. DS-HFF cells and controls (BIO-45 and BIO-71) were infected with adenovirus mtGFP in the culture medium, and incubated for a total of 48h after the addition of virus. Z-stack images were taken with a confocal system Nikon Eclipse Ti and analyzed by software NisElements Imaris 3.2 and 4.0. The software is able to provide, starting from the scanned image, the number of mitochondria per cell and the value of the mitochondrial mass; hence the value of the mitochondrial volume can be

obtained. Acquisitions Z-series were obtained using the software Huygens Essential 3.3.

DS-HFF and N-HFF cell cultures were first infected with adenovirus mtGFP, incubated for 48 hours after the addition of virus, and finally treated with Pioglitazone at final concentration of 1 $\mu$ M for 48h. The control cells were treated with DMSO. The images were taken with a confocal system Nikon Eclipse Ti.

#### Statistical analysis and softwares

The Student t-test was applied to evaluate the statistical significance for differences in the measured data DS-HFFs vs N-HFFs, or in treated DS-HFFs vs untreated. The threshold for statistical significance (p-value) was set at 0.05. GeneSpring software vers. 11.5 Multi-Omic Analysis (Agilent technologies, Inc.) was used to identify differentially expressed genes with a Fold change (LogFC) >0.3 and < -0.3, P<0.05.

## 4. RESULTS

### 4.1 Meta-analysis of public expression dataset

To identify which Hsa21 gene might affect either NEMG or ECM expression, we screened the Gene Expression Omnibus repository (<http://www.ncbi.nlm.nih.gov/geo>) for gene expression data related to the modulation of Hsa21 genes. We selected the GSE19836 experiment (De Cegli et al. 2010), a dataset derived from the analysis of a mouse embryonic stem cells (ESC) bank in which 32 orthologs of human chromosome 21 genes, including transcription factors and protein kinases, were individually overexpressed in an inducible manner.

#### *NRIP1* overexpression negatively regulates NEMG expression

We re-analyzed GSE19836 data focusing on the mitochondria-related categories and pathways dysregulated by the overexpression of each gene, i.e. we looked for Hsa21 genes that when overexpressed would induce NEMG downregulation. Among the 20 analyzed Hsa21 genes, only *NRIP1*, one of the 7 genes considered "effective" for the expression perturbation in the manipulated cells (De Cegli et al. 2010), was able to cause NEMG downregulation when overexpressed. Our analysis showed that *NRIP1* overexpression caused a significant enrichment of NEMGs among the 298 downregulated genes. The "Mitochondrion" was the most affected Cell Component Gene Ontology (GO) category ( $p < 10^{-3}$ ), with a cluster of 37 downregulated genes (**Tab. 2**). Motif enrichment analysis, by clustering downregulated genes based on their promoter regions, revealed a significant enrichment ( $p < 0.005$ ) in genes with the *ERRα* motif. Twenty-five downregulated genes, instead of the expected 10, showed promoter regions around the transcription start site containing the *ERRα* motif.

**TABLE 2 Mitochondria related genes downregulated after *NR1P1* overexpression**

PROBE_SET	GENE_SYMBOL	DESCRIPTION
1434866_x_at	Cpt1a	carnitine palmitoyltransferase 1a, liver
1417956_at	Cidea	cell death-inducing DNA fragmentation factor, alpha subunit-like effector A
1455106_a_at	Ckb	creatine kinase, brain
1428145_at	Acaa2	acetyl-Coenzyme A acyltransferase 2 (mitochondrial 3-oxoacyl-Coenzyme A thiolase)
1427342_at	Fastkd1	FAST kinase domains 1
1454674_at	Fez1	fasciculation and elongation protein zeta 1 (zygin I)
1428516_a_at	Alkbh7	alkB, alkylation repair homolog 7 (E. coli)
1421010_at	Mobp	myelin-associated oligodendrocytic basic protein
1424562_a_at	Slc25a4	solute carrier family 25 (mitochondrial carrier, adenine nucleotide translocator), member 4
1450048_a_at	Idh2	isocitrate dehydrogenase 2 (NADP+), mitochondrial
1418091_at	Tfcp2l1	transcription factor CP2-like 1
1422703_at	Gyk	glycerol kinase
1434499_a_at	Ldhb	lactate dehydrogenase B
1423108_at	Slc25a20	solute carrier family 25 (mitochondrial carnitine/acylcarnitine translocase), member 20
1416457_at	Ddah2	dimethylarginine dimethylaminohydrolase 2
1429021_at	Epha4	Eph receptor A4
1451504_at	Chchd3	coiled-coil-helix-coiled-coil-helix domain containing 3
1433855_at	Abat	4-aminobutyrate aminotransferase
1451744_a_at	Ptgr2	prostaglandin reductase 2
1439947_at	Cyp11a1	cytochrome P450, family 11, subfamily a, polypeptide 1
1418709_at	Cox7a1	cytochrome c oxidase, subunit VIIa 1
1431980_a_at	As3mt	arsenic (+3 oxidation state) methyltransferase
1425140_at	Lactb2	lactamase, beta 2
1419656_at	Slc25a36	solute carrier family 25, member 36
1427705_a_at	Nfkb1	nuclear factor of kappa light polypeptide gene enhancer in B cells 1, p105
1455991_at	Ccbl2	cysteine conjugate-beta lyase 2
1428140_at	Oxct1	3-oxoacid CoA transferase 1
1453738_at	C330018D20Rik	RIKEN cDNA C330018D20 gene
1451084_at	Etfdh	electron transferring flavoprotein, dehydrogenase
1456711_at	4932425I24Rik	RIKEN cDNA 4932425I24 gene
1417089_a_at	Ckmt1	creatine kinase, mitochondrial 1, ubiquitous
1418288_at	Lpin1	lipin 1
1416023_at	Fabp3	fatty acid binding protein 3, muscle and heart
1418640_at	Sirt1	sirtuin 1 (silent mating type information regulation 2, homolog) 1 (S. cerevisiae)
1434996_at	Slc25a16	solute carrier family 25, member 16

1424056_at	Usp48	ubiquitin specific peptidase 48
1437974_a_at	Hk1	hexokinase 1

The analysis of differentially expressed genes in the in the GSE19836 experiment from GEO repository showed an enrichment of genes belonging to the cellular component “Mitochondrion” (GO:0005739).

### *RUNXI* overexpression positively regulates ECM expression

We re-analyzed the GSE19836 dataset focusing on ECM-related categories and pathways dysregulated by the overexpression of each gene, i.e. we looked for Hsa21 genes that when overexpressed would induce ECM gene upregulation. Only *RUNXI* was able to cause ECM gene upregulation when overexpressed. Our analysis showed that *RUNXI* overexpression caused a significant enrichment among the 573 upregulated genes (logFC>0.3, Adj.P-val <0.01). The “extracellular matrix” (GO:0031012) was the most affected Cell Component Gene Ontology category (P-val = 3.00 e-04), with a cluster of 32 upregulated genes (**Tab. 3**). No other Hsa21 transcription factor or regulator under analysis showed a similar effect.

**TABLE 3 Extracellular Matrix genes upregulated after *RUNXI* overexpression**

PROBE_SET	GENE_SYMBOL	DESCRIPTION
1455965_at	Adams4	disintegrin-like and metallopeptidase (reprolysin type) with thrombospondin type 1 motif, 4
1416298_at	Mmp9	matrix metallopeptidase 9
1416531_at	Gsto1	glutathione S-transferase omega 1
1419613_at	Col7a1	collagen, type VII, alpha 1
1450704_at	Ihh	Indian hedgehog
1418910_at	Bmp7	bone morphogenetic protein 7
1418477_at	Matn1	matrilin 1, cartilage matrix protein
1424131_at	Col6a3	collagen, type VI, alpha 3
1437277_x_at	Tgm2	transglutaminase 2, C polypeptide
1419573_a_at	Lgals1	lectin, galactose binding, soluble 1
1426642_at	Fn1	fibronectin 1
1420569_at	Chad	Chondroadherin
1415935_at	Smoc2	SPARC related modular calcium binding 2
1420855_at	Eln	Elastin
1450673_at	Col9a2	collagen, type IX, alpha 2
1416589_at	Sparc	secreted acidic cysteine rich glycoprotein
1460187_at	Sfrp1	secreted frizzled-related protein 1
1426231_at	Vit	Vitrin
1419527_at	Comp	cartilage oligomeric matrix protein

1419091_a_at	Anxa2	annexin A2
1438312_s_at	Ltbp3	latent transforming growth factor beta binding protein
1449335_at	Timp3	tissue inhibitor of metalloproteinase 3
1417389_at	Gpc1	glypican 1
1416740_at	Col5a1	collagen, type V, alpha 1
1421279_at	Lamc2	laminin, gamma 2
1448870_at	Ltbp1	latent transforming growth factor beta binding protein
1452106_at	Npnt	Nephronectin
1460227_at	Timp1	tissue inhibitor of metalloproteinase 1
1448598_at	Mmp17	matrix metalloproteinase 17
1420891_at	Wnt7b	wingless-related MMTV integration site 7B
1422571_at	Thbs2	thrombospondin 2

The analysis of differentially expressed genes in the in the GSE19836 experiment from GEO repository showed an enrichment of genes belonging to the cellular component “extracellular matrix” (GO: 0031012).

#### NRIP1 and PGC-1 $\alpha$ modulation dysregulates the same NEMGs underexpressed in DS fetal hearts

*NRIP1* is a known repressor of the *PGC-1 $\alpha$*  protein. To investigate whether the sets of genes regulated by *NRIP1* and/or *PGC-1 $\alpha$*  overlap the NEMGs downregulated in DS fetal hearts (Conti et al. 2007), we performed a meta-analysis comparing three sets of gene expression data.

SET1 included 123 genes which were both upregulated after *NRIP1* silencing and downregulated after *NRIP1* re-expression in mouse adipocytes (Powelka et al. 2006). SET2 included 129 genes, which were upregulated after *PGC-1 $\alpha$*  induction in SAOS2 cells (human osteoblast-like cells) (Schreiber et al. 2004). SET3 included the 70 genes downregulated in DS fetal heart tissues (Conti et al. 2007) belonging to the ‘mitochondrion’ GO category. The comparison was aimed at identifying genes consistently dysregulated across these studies. The Venn Diagram in **Figure 19** shows that the three sets of genes overlap each other for at least 25 genes. Fifteen genes are consistently dysregulated across all three experiments. Most of these genes are included in the electron transport chain, mainly in complex I, and in oxidative phosphorylation pathways. It is also interesting to note that 42 genes overlap between the sets of genes inversely regulated by *NRIP1* and *PGC-1 $\alpha$*  (SET1 and SET2), in agreement with the antagonistic functions of the two coregulators (Fritah et al. 2010).

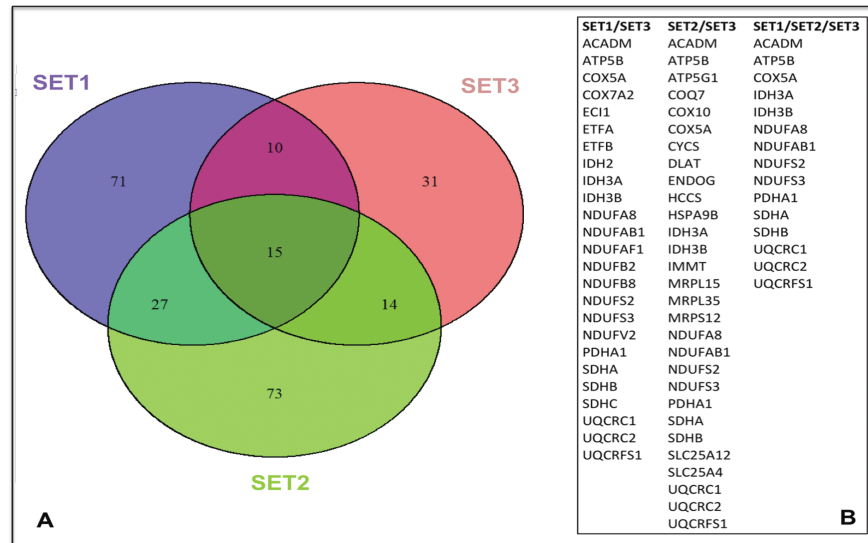


**Fig. 19 Venn Diagram comparing NEMGs downregulated in DS fetal hearts with those dysregulated by *NR1P1* and/or *PGC-1a*.** **A)** Twenty-five out of the 70 mitochondrial genes that are downregulated in DS fetal hearts (SET3) (Conti et al. 2007) overlap the list of *NR1P1* regulated genes (SET1) (Powelka et al. 2006) and 29 overlap the list of *PGC-1a* regulated genes (SET2) (Schreiber et al. 2004). **B)** List of mitochondria-related genes overlapping in the three sets of data.

Promoter analysis of genes downregulated in DS fetal hearts shows enrichment for transcription factors repressed by *NR1P1*

The promoter regions (-450bp to +50bp from transcription start site) of mitochondrial genes downregulated in DS fetal heart tissues (Conti et al. 2007) were analyzed in order to recognize DNA binding motifs for both *NR1P1* and *ERRα* matrices using PSCAN software (Zambelli et al. 2009). The list of downregulated genes was ranked according to the prediction of binding affinity of their promoter regions to *NR1P1* and *ERRα* binding sites with a cut-off of affinity score =0.80 and p-value <0.003. Interestingly, 40% of the 80 mitochondrial genes downregulated in fetal hearts, have consensus DNA binding sites for the nuclear respiratory factor *NR1P1* in their 5' flanking regions (**Tab. 4**); 20% of them show a high affinity for the estrogen-related receptor *ERRα* (**Tab. 5**).

**TABLE 4 Mitochondrial genes downregulated in DS heart tissues with *NRF1* binding site in their promoter regions.**

GENE NAME	DESCRIPTION
ECGF1	Endothelial Cell Growth Factor 1
SCO2	SCO Cytochrome Oxidase Deficient Homolog 2
PIN4	Protein (Peptidylprolyl Cis/Trans Isomerase) NIMA-Interacting, 4
IDH3A	Isocitrate Dehydrogenase 3 (NAD+) Alpha
UQCRC1	Ubiquinol-Cytochrome C Reductase Core Protein 1
NDUFB8	NADH Dehydrogenase (Ubiquinone) 1 Beta Subcomplex, 8, 19kDa
RPL10	Ribosomal Protein L10
ENDOG	Endonuclease G
SDHA	Succinate Dehydrogenase Complex, Subunit A, Flavoprotein (Fp)
UQCRC2	Ubiquinol-Cytochrome C Reductase Core Protein II
ETFB	Electron-Transfer-Flavo protein, Beta Polypeptide
GLUD1	Glutamate Dehydrogenase 1
NDUFAB1	NADH Dehydrogenase (Ubiquinone) 1, Alpha/Beta Subcomplex, 1, 8kDa
CYCS	Cytochrome C, Somatic <sup>1</sup>
SDHB	Succinate Dehydrogenase Complex, Subunit B, Iron Sulfur
HSPA9	Heat Shock 70kDa Protein 9
MRPL15	Mitochondrial Ribosomal Protein L15 <sup>1</sup>
SLC25A12	Solute Carrier Family 25 (Aspartate/Glutamate Carrier), Member 12
VDAC1	Voltage-Dependent Anion Channel 1
HCCS	Holocytochrome C Synthase
IDH3B	Isocitrate Dehydrogenase 3 (NAD+) Beta
IDH2	Isocitrate Dehydrogenase 2 (NADP+), Mitochondrial
COX4NB	ER Membrane Protein Complex Subunit 8
COQ7	Coenzyme Q7 Homolog, Ubiquinone
ETFFA	Electron-Transfer-Flavoprotein, Alpha Polypeptide
GOT1	Glutamic-Oxaloacetic Transaminase 1, Soluble
NDUFA13	NADH Dehydrogenase (Ubiquinone) 1 Alpha Subcomplex, 13
NDUFS2	NADH Dehydrogenase (Ubiquinone) Fe-S Protein 2, 49kDa (NADH Coenzyme Q Reductase)
PDHA1	Pyruvate Dehydrogenase (Lipoamide) Alpha 1
DLAT	Dihydrolipoamide S-Acetyltransferase
GCSH	Glycine Cleavage System Protein H (Aminomethyl Carrier)
MOSC2	Mitochondrial Amidoxime Reducing Component 2
AK2	Adenylate kinase 2

*NRF1* target genes are sorted with a cut-off affinity score =0.80

**TABLE 5 Mitochondrial genes downregulated in DS heart tissues with *ERRα* binding site in their promoter regions.**

GENE NAME	DESCRIPTION
HSPA9	Heat Shock 70kDa Protein 9
MOSC2	Mitochondrial Amidoxime Reducing Component 2
SDHA	Succinate Dehydrogenase Complex, Subunit A, Flavoprotein (Fp)
TXN2	Thioredoxin 2
MRPL35	Mitochondrial Ribosomal Protein L15 <sup>L</sup>
BDH1	3-Hydroxybutyrate Dehydrogenase, Type 1
NDUFB8	NADH Dehydrogenase (Ubiquinone) 1 Beta Subcomplex, 8, 19kDa
COX7A2	Cytochrome C Oxidase Subunit VIIa Polypeptide 2
SDHB	Succinate Dehydrogenase Complex, Subunit B, Iron Sulfur
DLAT	Dihydrolipoamide S-Acetyltransferase
NDUFAB1	NADH Dehydrogenase (Ubiquinone) 1, Alpha/Beta Subcomplex, 1, 8kDa
COQ7	Coenzyme Q7 Homolog, Ubiquinone
MRPS12	Mitochondrial Ribosomal Protein S12
TIMM23	Translocase Of Inner Mitochondrial Membrane 23 Homolog
ETFFA	Electron-Transfer-Flavoprotein, Alpha Polypeptide
ATP5B	ATP Synthase, H <sup>+</sup> Transporting, Mitochondrial F1 Complex, Beta Polypeptide
IDH3B	Isocitrate Dehydrogenase 3 (NAD <sup>+</sup> ) Beta
ECI1	Enoyl-CoA Delta Isomerase 1
MRPL15	Mitochondrial Ribosomal Protein L15 <sup>L</sup>
ETFB	Electron-Transfer-Flavo protein, Beta Polypeptide
COX4NB	ER Membrane Protein Complex Subunit 8
CYCS	Cytochrome C, Somatic <sup>L</sup>
UQCRCF1	Ubiquinol-Cytochrome C Reductase, Rieske Iron-Sulfur Polypeptide 1
SLC25A4	Solute Carrier Family 25 (Mitochondrial Carrier; Adenine Nucleotide Translocator), Member 4
GOT1	Glutamic-Oxaloacetic Transaminase 1, Soluble
PIN4	Protein (Peptidylprolyl Cis/Trans Isomerase) NIMA-Interacting, 4
SCO2	SCO Cytochrome Oxidase Deficient Homolog 2
NFS1	NFS1 Cysteine Desulfurase
CKMT2	Creatine Kinase, Mitochondrial 2
IMMT	Inner Membrane Protein, Mitochondrial
DLST	Dihydrolipoamide S-Succinyltransferase (E2 Component Of 2-Oxo-Glutarate Complex)
MIPEP	Mitochondrial Intermediate Peptidase
COX10	Cytochrome C Oxidase Assembly Homolog 10 (Yeast

*ERRα* target genes are sorted with a cut-off affinity score =0.80

Promoter analysis of genes upregulated in DS fetal hearts shows enrichment for the transcription factor *RUNX1*

We performed a transcription factor-binding site (TFBS) analysis on the list of ECM genes upregulated in DS fetal hearts with the PSCAN software, in order to scan promoters of these genes for consensus sequences according to the JASPAR database. This analysis identified *RUNX1* as a transcription factor with high binding specificity to ECM genes upregulated in DS hearts (**Tab.6**). About 60% of ECM genes overexpressed in DS hearts show consensus sequences for *RUNX1*.

Molecular and functional studies are currently in progress in order to evaluate the effects of *RUNX1* modulation on ECM gene expression and on cellular phenotype in euploid and trisomic fetal skin fibroblasts.

**TABLE 6 ECM genes upregulated in DS hearts with consensus sequence for *RUNX1***

GENE NAME	DESCRIPTION
ECM2	extracellular matrix protein 2, female organ and adipocyte specific
COL6A2	collagen, type VI, alpha 2
GPC3	glypican 3
APP	amyloid beta (A4) precursor protein
ADAMTS5	ADAM metalloproteinase with thrombospondin type 1 motif, 5
ITGB4	integrin, beta 4
COL18A1	collagen, type XVIII, alpha 1
MMP11	matrix metalloproteinase 11 (stromelysin 3)
FLRT2	fibronectin leucine rich transmembrane protein 2
APP	amyloid beta (A4) precursor protein
COL3A1	collagen, type III, alpha 1
DCN	decorin
ADAMTS7	ADAM metalloproteinase with thrombospondin type 1 motif, 7
COLEC10	collectin sub-family member 10 (C-type lectin)
WNT4	wingless-type MMTV integration site family, member 4
HAPLN1	hyaluronan and proteoglycan link protein 1
COL5A1	collagen, type V, alpha 1
DCN	Decorin
C1QTNF3	C1q and tumor necrosis factor related protein 3
LAMA4	laminin, alpha 4
FBLN1	fibulin 1
COL9A3	collagen, type IX, alpha 3
APP	amyloid beta (A4) precursor protein
VCAN	versican
COL13A1	collagen, type XIII, alpha 1
COL14A1	collagen, type XIV, alpha 1
DTL	denticleless E3 ubiquitin protein ligase homolog (Drosophila)
ASPN	Aspirin

## 4.2 OCR is decreased in DS-HFFs

As preliminary experiments before testing the role of *NR1P1* in causing the mitochondrial dysfunction in DS cells, we examined some features of the mitochondrial activity of the cell lines to be used thereafter. The first parameter we measured was the OCR. We compared two lines of trisomic fetal fibroblasts (DS-HFF) and two euploid lines (N-HFF) by XF<sup>e</sup> 96 Extracellular Flux Analyzer (Seahorse Bioscience, Billerica, MA, USA), a novel approach to evaluate mitochondrial respiration.

After an OCR baseline measurement, oligomycin (OL), carbonyl cyanide 4-(trifluoromethoxy) phenylhydrazone (FCCP) and antinomycin/rotenon (ANT/ROT) solutions were sequentially added to each well to reach working concentrations and changes in the OCR were analyzed.

The results of the XF<sup>e</sup> Analyzer measurements indicated a decrease of OCR by approximately 70% in DS-HFFs when compared to N-HFFs (Fig. 20).

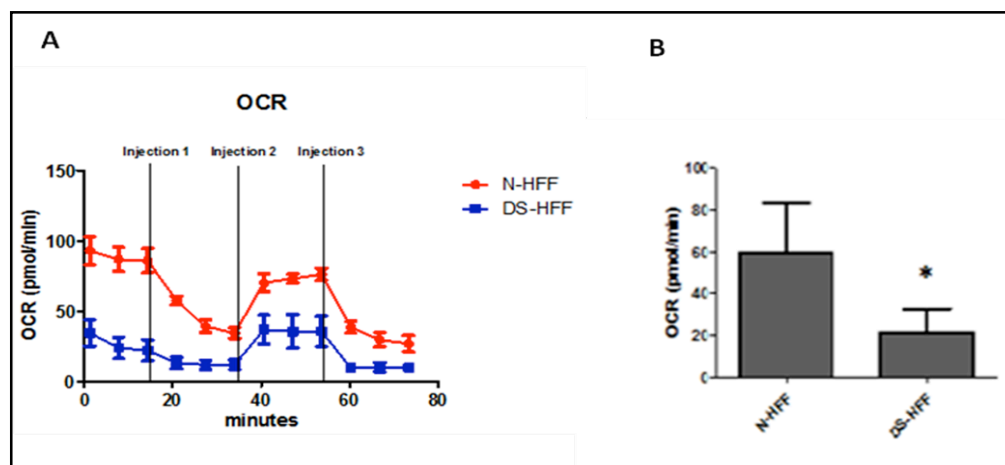


**Fig. 20** XF Cell Mito Stress Test profile of the key parameters of mitochondrial respiration. (A) Sequential compound injections measure: basal OCR (injection 1-oligomycin), ATP linked (injection 2 -carbonyl cyanide 4-trifluoromethoxy phenylhydrazone, FCCP) and maximal OCR (injection 3 -antonomycin/rotenone, ANT/ROT). (B) The XF<sup>e</sup> Analyzer showed a decrease of OCR by approximately 70% in DS-HFFs when compared to N-HFFs. Values represent the average determination $\pm$ SEM for DS-HFFs and N-HFFs carried out in triplicate. \*  $p < 0.05$ . P-value was expressed for trisomic cells vs euploid cells.

## 4.3 DS-HFFs show a very fragmented mitochondrial network

In order to test whether a decreased mitochondrial biogenesis in DS-HFFs was associated to a variation of mitochondrial mass, parameters such as the number, volume and mitochondrial mass of individual cells were compared between DS-HFFs and N-HFFs. The trisomic and euploid cells were transfected with a mitochondrially targeted GFP (mtGFP) and incubated for 48 hours. The analysis of mtGFP distribution by confocal microscopy showed that

there was a significant difference in the mitochondrial number and volume when comparing trisomic cells and controls: in particular, DS-HFF cells had a greater number of isolated mitochondria (**Fig. 21A**), and a smaller average mitochondrial volume (**Fig. 21B**). However, mitochondrial mass determination did not show significant differences between trisomic cells and euploid controls (**Fig. 21C**).

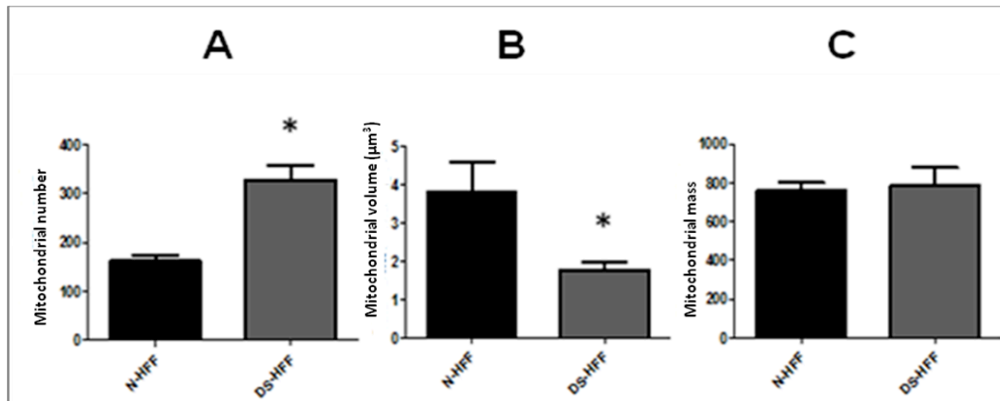


**Fig. 21 Mitochondrial morphology in DS-HFF and N-HFF.** (A) The number of mitochondria was significantly higher in trisomic cells compared to controls. (B) The mitochondrial volume was significantly lower in trisomic cells compared to controls. (C) By comparing the values of the mitochondrial mass there were no significant differences between cells trisomic and euploid controls. \* P <0.05. P-value was expressed for trisomic cells vs. euploid cells.

Confocal microscopy images showed a mitochondrial network much less fragmented in control cells when (**Fig. 22A**) compared to DS-HFF cells (**Fig. 22B**).

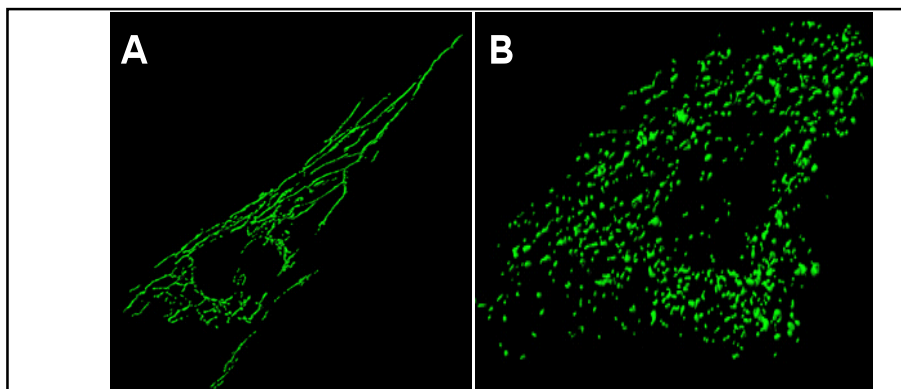


**Fig. 22 Mitochondrial network in DS-HFF and control cells.** (A) Confocal microscopy images obtained with Nikon Eclipse Ti showed the mitochondrial network in euploid cells. (B) Mitochondrial network in trisomic cell. The mitochondrial network appeared more fragmented in trisomic cells respect to controls.

#### 4.4 The Hsa21 gene *NRIP1* is a major regulator of *PGC-1 $\alpha$*

To test the hypothesis that *NRIP1* overexpression perturbs mitochondrial function and that this effect is associated with *PGC-1 $\alpha$*  downregulation, we performed silencing experiments of *NRIP1* gene in DS-HFFs. We attenuated *NRIP1* expression by either 5 or 20 nM siRNA in DS-HFFs. Seventy-two hours after transfection we performed qRT-PCR demonstrating a significant inverse correlation between *NRIP1* silencing and *PGC-1 $\alpha$*  upregulation in a siRNA dosage-dependent way (Fig. 23).

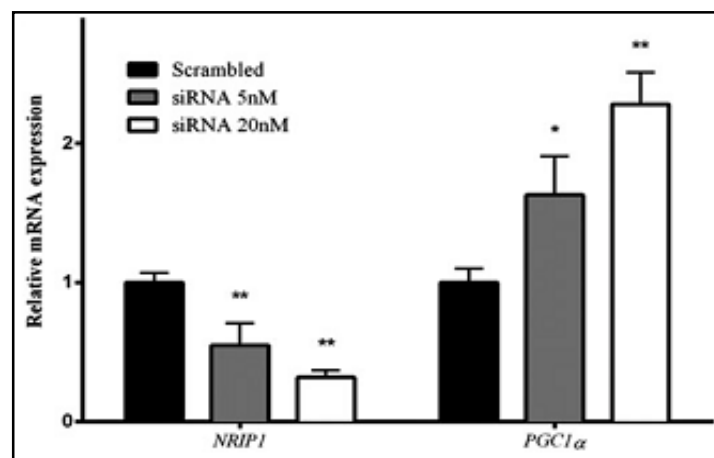


**Fig. 23 *NRIP1* attenuation modulates *PGC-1 $\alpha$*  expression in DS-HFFs.** *NRIP1* and *PGC-1 $\alpha$*  expression levels in trisomic cells transfected with a scrambled siRNA and with a *NRIP1*-specific SMART pool of siRNAs. A decrease in the *NRIP1* expression level corresponds to an increase of *PGC-1 $\alpha$*  expression level in a siRNA-dependent way. Values represent the average determination  $\pm$  SEM for 4 *NRIP1*-silenced DS-HFFs carried out in triplicate. \* $p$ <0.05, \*\* $p$ <0.01. P-values express statistical significance for *NRIP1*-silenced versus scrambled comparisons.

#### 4.5 *NRIP1* siRNA transfection decreases *NRIP1* in the nucleus of DS-HFFs

To have a deeper understanding of mechanisms by which *NRIP1* exerts his repressive activity, we investigated the localization of *NRIP1* protein by immunofluorescence methods demonstrating that the *NRIP1* protein localized to the cell nucleus, both in euploid and in trisomic fibroblasts (Fig. 24). Fluorescent signal was more intense in nuclei of DS-HFFs (Fig. 24B) than in N-HFFs (Fig. 24A), indicating a higher concentration of the *NRIP1* protein in trisomic cells. In these cells, some fluorescent signal was also present in the cytoplasm (Fig. 24B) likely due to the overexpression of the *NRIP1* protein.

The attenuation of *NRIP1* expression caused a decrease of the fluorescent signal in silenced versus scrambled DS-HFFs in a siRNA dosage-dependent way (**Fig. 24**). Quantitative evaluation of fluorescence intensities in euploid, trisomic and siRNA transfected cells (**Fig. 24F**) indicated that siRNA transfection reduced *NRIP1* protein levels of trisomic cells down to the range of diploid cells or even lower (**Fig. 24D and E**). In particular, signal from 5 nM *NRIP1* siRNA transfected cells was comparable with euploid HFFs.

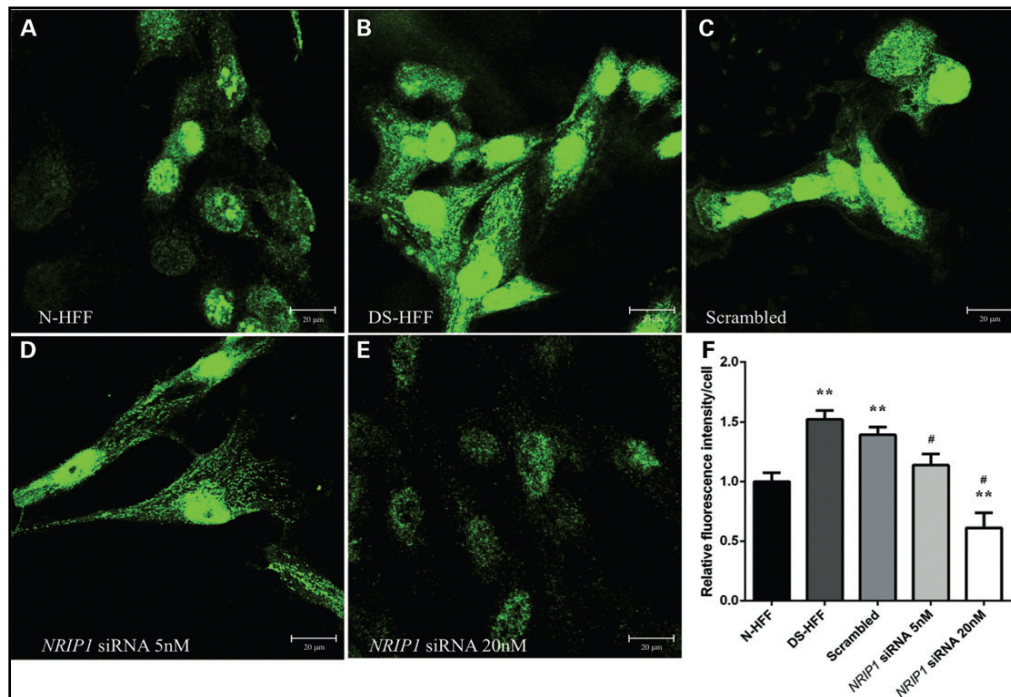


**Fig. 24 NRIP1 immunofluorescence in *NRIP1*-silenced DS-HFFs.** Representative images of NRIP1 immunofluorescence analysis in **A)** euploid cells, **B)** trisomic cells and trisomic cells transfected **C)** with a scrambled siRNA, **D)** with 5 nM *NRIP1* siRNA and **E)** 20 nM *NRIP1* siRNA. **F)** Semi-quantitative analysis of the immunodetected signals by the ImageJ software (means  $\pm$  SEM of three assayed samples). Fifty randomly selected, different cells for each sample/experimental condition were analyzed. A decrease of the fluorescent signal is observed in silenced versus scrambled DS-HFFs. Signal from 5 nM *NRIP1* siRNA transfected cells is comparable with euploid HFFs. Statistical significance: \*\*= $p < 0.01$  for trisomic versus euploid comparisons; #= $p < 0.05$  for *NRIP1*-silenced versus scrambled comparisons.

#### 4.6 *NRIP1* silencing improves mitochondrial function in DS-HFFs

To investigate whether *NRIP1* affects mitochondrial function in DS possibly through the downregulation of *PGC-1 $\alpha$*  and other NEMGs, we evaluated functional parameters in DS-HFFs after *NRIP1* silencing compared to not silenced cells. We evaluated redox state of DS-HFF silenced cells by

measuring NEMGs expression, ROS production, mitochondrial activity, mitochondrial biogenesis and ATP production.

#### NRIP1 silencing affects NEMG expression in DS-HFFs

To determine the effects of *NRIP1* attenuation by siRNA on other mitochondria-related genes, we compared the expression of seven genes in silenced versus scrambled cells using qRT-PCR. Three genes, i.e. *COX5A*, *NDUFA1* and *NDUFS3*, were chosen from the list of 15 genes that resulted consistently dysregulated across the three sets compared in the meta-analysis (Fig. 19). The fourth gene, *NRF1*, which is downregulated in DS hearts (Conti et al. 2007) and fibroblasts (Piccoli et al. 2013), was chosen because of its role both as a *PGC-1 $\alpha$*  partner and as its target. Finally, three other genes, i.e. *ANT1/SLC25A4*, *ANT2/SLC25A5* and *ANT3/SLC25A6*, which are downregulated in DS fetal fibroblasts (our unpublished data), were also chosen as *PGC-1 $\alpha$*  targets (Schreiber et al. 2004). *ANT1/SLC25A4* is downregulated in SET3 and after *NRIP1* overexpression in the De Cegli's dataset (Tab. 2) (De Cegli et al. 2010). The expression ratio of these genes in *NRIP1*-silenced DS-HFFs versus scrambled transfected DS-HFFs demonstrated that five out of seven analyzed genes were significantly upregulated after *NRIP1* attenuation by siRNA (Fig. 25).

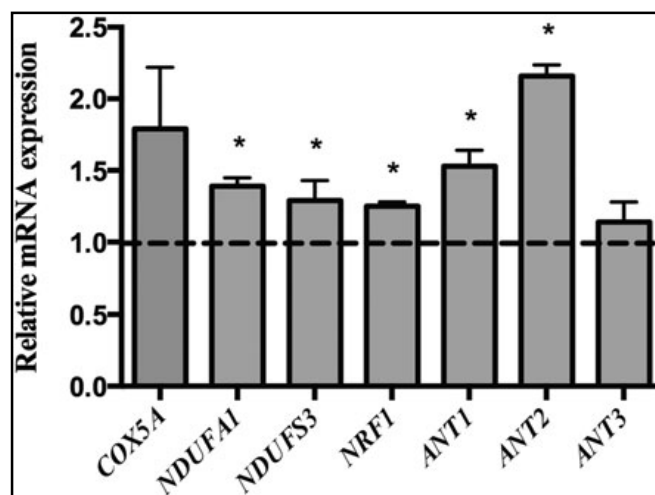


**Fig. 25 Mitochondria-related gene expression in *NRIP1*-silenced DS-HFFs.** Relative mRNA expression of seven mitochondria-related genes was measured in *NRIP1*-silenced DS-HFFs versus scrambled transfected DS-HFFs. Five out of the seven genes show a significant increase in their expression level. Values represent the average determination  $\pm$  SEM for three DS-HFFs samples carried out in triplicate. A pool of scrambled transfected euploid cells was used as calibrator.  $\ast = p < 0.05$ . P-value expresses statistical significance for *NRIP1*-silenced versus scrambled comparisons.

### NRIP1 silencing decreases mitochondrial ROS

Since the mitochondrial respiratory chain is known to be the major source of ROS within the cell (Kussmaul and Hirst, 2006; Li and Trush, 1998), the intracellular redox state was assessed by confocal microscopy using DCF. The intensity of DCF was measured in silenced DS-HFFs compared either to non transfected DS-HFF or to N-HFF samples.

Seventy-two hours after transfection with *NRIP1* siRNA, trisomic cells showed a fluorescent signal of DCF up to 50% decreased in silenced DS-HFFs in a siRNA-dosage dependent way (Fig. 26).

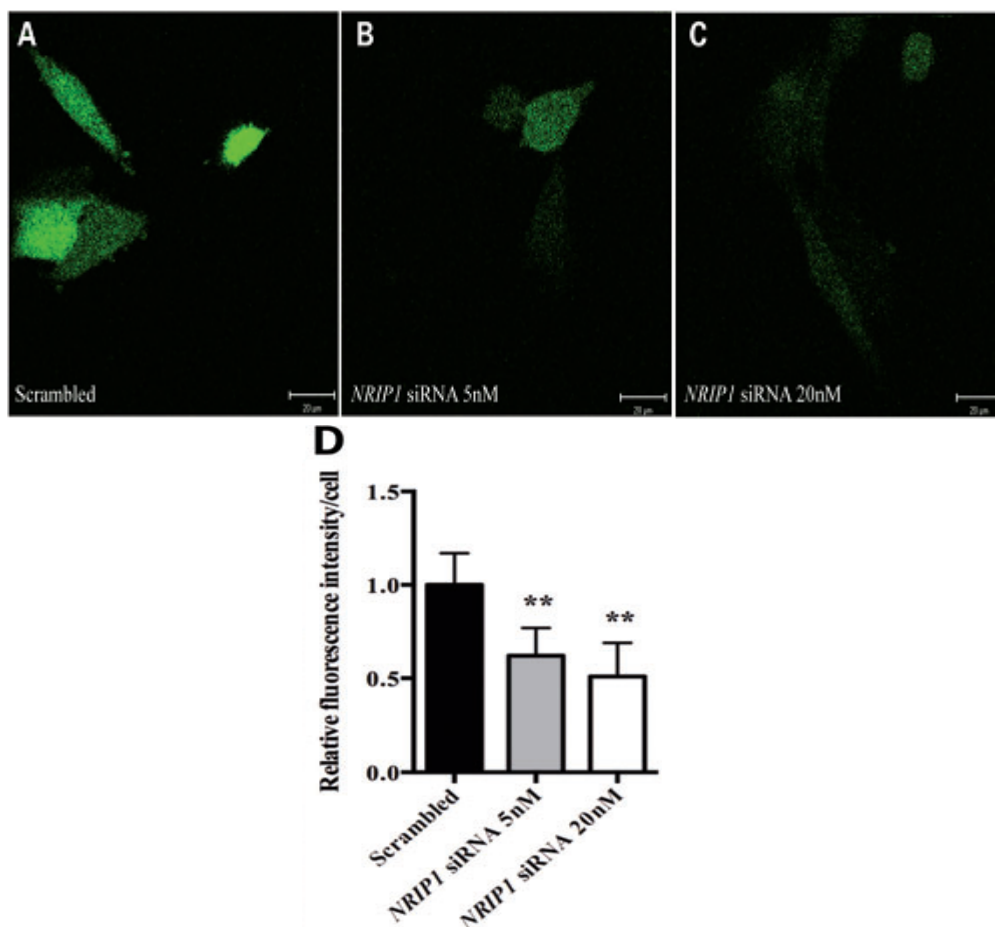


**Fig. 26** Live cell imaging of confocal microscopy analysis of the DCF fluorescence in transfected DS-HFFs: **A)** scrambled, **B)** 5 nM *NRIP1* siRNA and **C)** 20 nM *NRIP1* siRNA. **D)** Semi-quantitative analysis of the DCF-related fluorescence by the ImageJ software (means  $\pm$  SEM of three assayed samples). Fifty randomly selected, different cells for each sample/experimental condition were analyzed. A significant decrease of DCF-related fluorescence is observed after *NRIP1* attenuation in a siRNA-dependent way. Pixel intensity was measured in about 50 cells after *NRIP1* silencing. \*\*= $p < 10^{-4}$ . P-value expresses statistical significance for *NRIP1*-silenced versus scrambled comparisons.

ROS production was also evaluated by confocal microscopy using a MitoSOX™ Red reagent, a fluorogenic dye specifically targeted to mitochondria in live cells. Oxidation of MitoSOX™ Red reagent by superoxide produces red fluorescence. This reagent is a live-cell permeant that is rapidly and selectively targeted to mitochondria. Our aim was to investigate whether this parameter is correlated to *NR1P1* expression. MitoSOX™ fluorescent intensity was decreased in DS-HFFs silenced cells, thus suggesting that the decrease in ROS was in part associated to mitochondrial activity (**Fig. 27**).

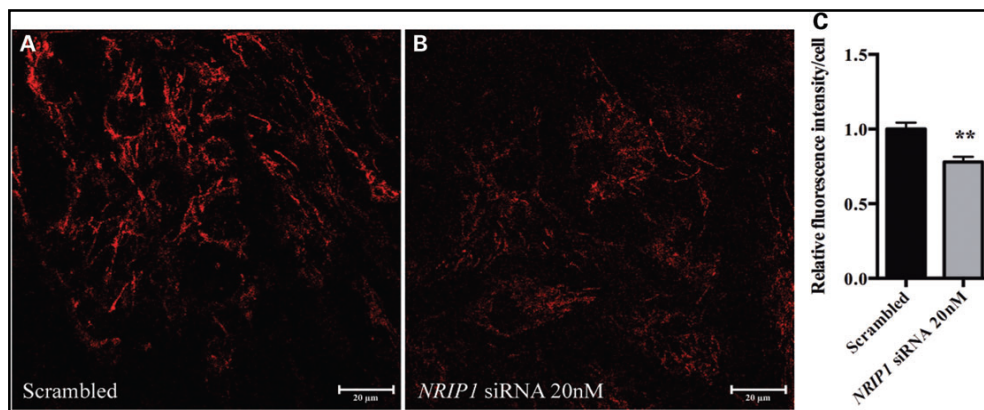


**Fig. 27 Intra-mitochondrial superoxide decrease in *NR1P1*-silenced DS-HFFs measured using MitoSOX Red.** Confocal microscopy live cell imaging of the MitoSOX Red fluorescence in transfected DS-HFFs: **A)** scrambled cells and **B)** 20 nM *NR1P1* siRNA transfected cells. Note that the distribution of MitoSOX Red signal resembles the mitochondrial network. **C)** Semiquantitative analysis of the MitoSOX-related fluorescence by the ImageJ software (means  $\pm$  SEM of three assayed samples). Fifty randomly selected, different cells for each sample/experimental condition were analyzed. A reduction of the fluorescent signal over the mitochondrial network is detected. \*\*= $p < 0.01$ . P-value expresses statistical significance for *NR1P1*-silenced versus scrambled comparisons.

#### *NR1P1* silencing increases mitochondrial activity

In order to establish whether ROS decrease in *NR1P1*-silenced DS-HFFs depends on a rescue of respiratory chain complex activities, mitochondrial activity was evaluated using MitoTracker Red dye, a reagent that stains mitochondria in live cells according to their membrane potential. Mitotracker fluorescent intensity was increased in DS-HFFs silenced cells in a siRNA concentration dependent way, thus indicating an increase in respiratory activity (**Fig. 28**).

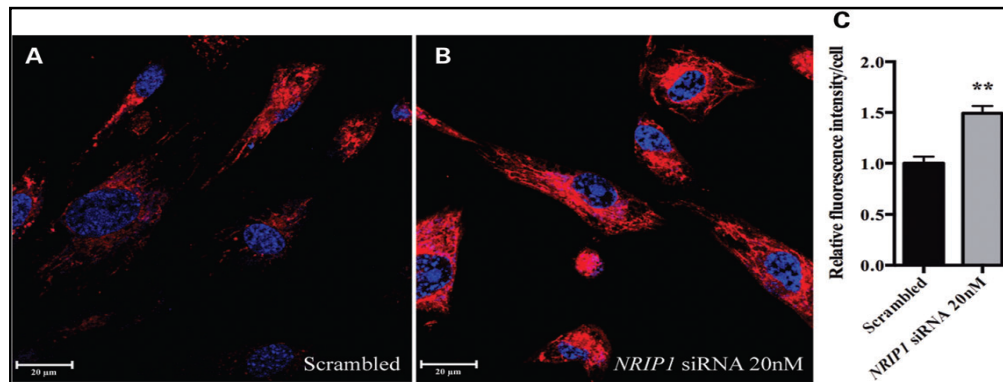


**Fig. 28 Mitochondrial activity in DS *NRIP1*-silenced DS-HFFs.** Confocal microscopy live cell imaging of the Mitotracker fluorescence in transfected DS-HFFs: **A)** scrambled cells and **B)** with 20 nM *NRIP1* siRNA transfected cells **C)** Semi-quantitative analysis of the Mitotracker-related fluorescence by the ImageJ software (means  $\pm$  SEM of five assayed samples). Fifty randomly selected, different cells for each sample/experimental condition were analyzed. An increase of Mitotracker-related fluorescence is observed in *NRIP1*-silenced DS-HFFs. **\*\***= $p < 0.005$ . P-value expresses statistical significance for *NRIP1*-silenced versus scrambled comparisons.

#### *NRIP1* silencing increases mtDNA content

As an indirect measure of the mitochondrial biogenesis, we quantified by qRT-PCR the gene expression of gene *D-LOOP* and *ACTIN*, mtDNA and nuclear DNA markers respectively, in *NRIP1*-silenced trisomic samples versus scrambled controls. The average ratio *D-LOOP/ACTIN* indicated an increase of 2.5-fold in silenced trisomic cells, after *NRIP1* attenuation by siRNA (**Fig. 29**), thereby suggesting that mtDNA content increases after *NRIP1* attenuation by siRNA and consequent *PGC-1 $\alpha$*  overexpression.

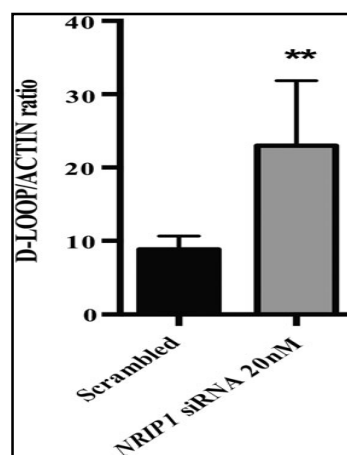


**Fig. 29 mtDNA content in *NRIP1*-silenced DS-HFFs.** Ratio between the mtDNA marker *D-LOOP* and the nuclear DNA marker *ACTIN* was increased after *NRIP1* attenuation by siRNA. The ratio was calculated upon normalization to a reference gene (*ABELSON*) by qRT-PCR. Values represent the average determination  $\pm$  SEM for three *NRIP1*-silenced trisomic samples carried out in triplicate. **\***= $p < 0.05$ . P-value expresses statistical significance for *NRIP1*-silenced versus scrambled comparisons.

### *NR1P1* silencing strongly increases cellular ATP content

The universal energy carrier ATP defines the energy state in living cells and depends mainly on mitochondrial function (Bonora et al. 2012). In *NR1P1*-silenced DS-HFFs, we investigated ATP concentration using a chimera of the ATP-sensitive photoprotein luciferase specifically targeted to mitochondria (mtLuc) to obtain a dynamic monitoring of [ATP]<sub>m</sub>. Luciferase has been widely employed to measure ATP content both in isolated mitochondria and in intact cells; its reaction with luciferin produces a flash of yellow green light with a peak emission at 560 nm, the intensity of which is proportional to the amount of substrates in the reaction mixture. Silenced DS-HFFs showed more than 50% increase of ATP content (Fig. 30), calculated by the luminescence values of the plateau generated after the addition of luciferin. Since basal ATP content is highly dependent on the abundance of transfected luciferase, we determined the exact amount of the luciferase transduced under our experimental conditions through an immunoblot assay. We found that the levels of luciferase protein transduced in *NR1P1*-silenced DS-HFFs were comparable with those detected in control cells transfected with the non-targeting scrambled siRNA (Fig. 31). In parallel, *NR1P1*-silenced cells were slightly decreased in mitochondrial ATP production 72 hours after transfection. This was calculated by subtracting the basal cellular luminescence plateau, generated after the addition of luciferin, from the luminescence values of the second plateau, generated after the addition of the Ca<sup>2+</sup> mobilizing agent histamine (Fig. 30).

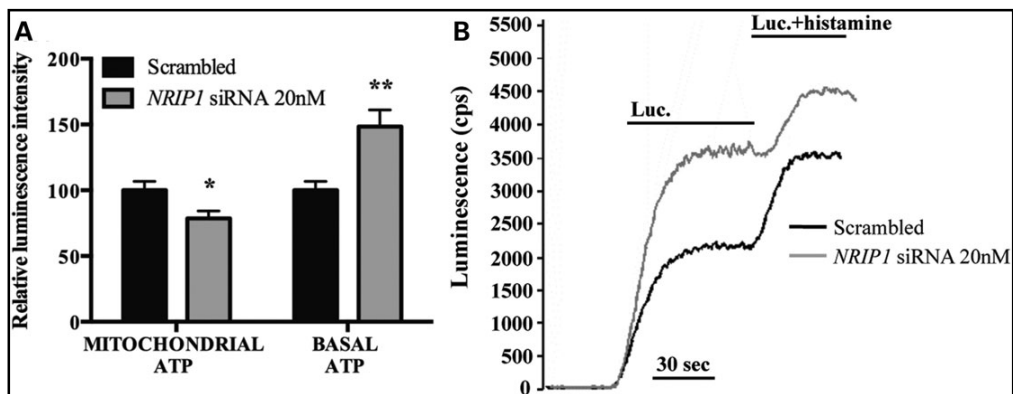


**Fig. 30 Mitochondrial ATP measurement.** **A)** The barplot of the mitochondrial ATP content and of the basal ATP content in scrambled and *NR1P1* siRNA transfected DS-HFFs. **B)** The traces show mitochondrial [ATP]<sub>m</sub> changes elicited by mitochondrial [Ca<sup>2+</sup>] increase in cells perfused with 100 mM histamine as agonist. mtLuc luminescence data are expressed as a percentage of the initial value  $\pm$  SEM. The traces are representative of four independent experiments. \*= $p < 0.05$ , \*\*= $p < 10^{-4}$ . P-values express statistical significance for *NR1P1*-silenced versus scrambled comparisons.

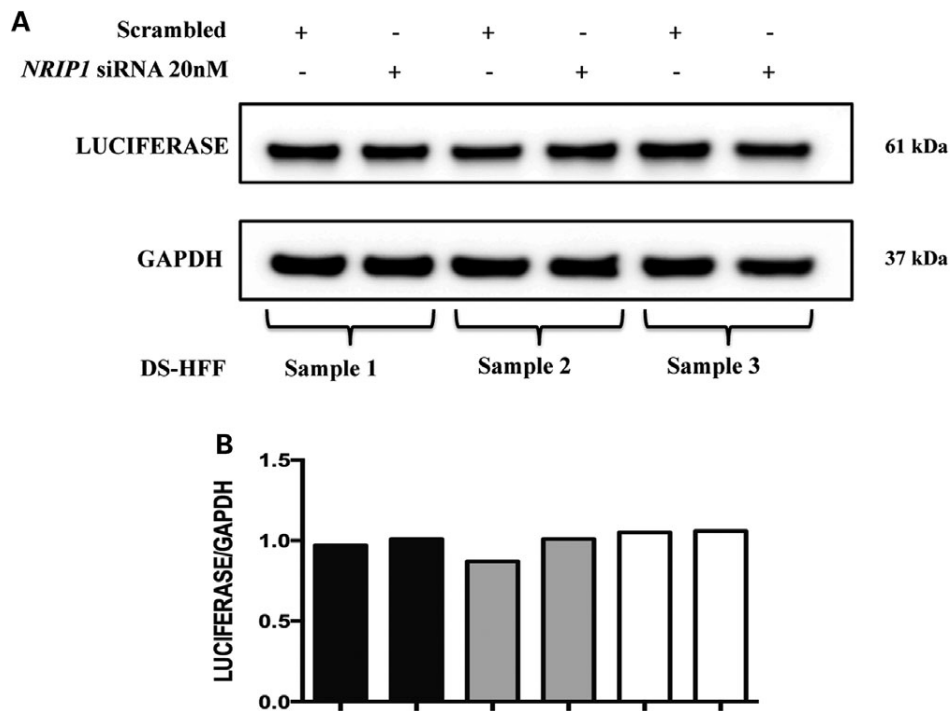


**Fig. 31 Luciferase expression following *NR1P1* attenuation by siRNA.** A) Representative immunoblot of luciferase protein in three *NR1P1*-silenced or scrambled DS-HFFs transfected with a luciferase-encoding plasmid specifically targeted to mitochondria (mtLuc) and cultured in complete medium for 72 h. B) Quantification of luciferase accumulation by the LUCIFERASE/GAPDH ratio.

## 4.7 Drug testing in DS-HFFs cultures

The mitochondrial rescue obtained by *NR1P1* silencing, possibly mediated by restoring *PGC-1 $\alpha$*  levels, suggested the possibility to pharmacologically induce *PGC-1 $\alpha$*  activity in DS-HFFs. Two drugs have been tested: Metformin and Pioglitazone. Metformin, usually used to treat type 2 diabetes, activates the AMPK pathway in liver and muscles, affecting mitochondrial biogenesis and function. Pioglitazone interacts with *PPAR $\gamma$* , a nuclear receptor regulating the transcription of genes involved in glucidic and lipidic metabolism.

### 4.7.1 Metformin counteracts mitochondrial dysfunction in DS-HFFs

#### Metformin treatment increases the expression of mitochondria related genes

To understand the impact of Metformin on the activation of the signaling pathway of *PGC-1 $\alpha$* , two DS-HFF cell lines were treated with different concentrations of the drug (0.5 mM, 1 mM and 2 mM) for 72 hours. The analysis of *PGC-1 $\alpha$*  gene by qRT-PCR demonstrated that the expression levels increased in treated DS-HFF cells at Metformin concentrations of 0.5 mM and

1 mM (**Fig. 32A**). The treatment with 2 mM Metformin did not cause significant changes compared to untreated trisomic control (**Fig. 32A**). The expression of *NRF1*, the main TF of mitochondrial enzymes was significantly increased at all Metformin concentrations (**Fig. 32B**). To evaluate the effects of Metformin treatment on mitochondrial biogenesis, the expression of *D-LOOP* and *ACTIN* was measured by qRT-PCR (**Fig. 32C**). The expression values of mtDNA (calculated from the ratio of genes *D-LOOP/ACTIN*) increased in treated DS-HFF at Metformin concentrations of 0.5 mM and 1 mM, while the treatment with 2 mM Metformin did not cause significant changes compared to untreated trisomic control (**Fig. 32C**). The expression of *TFAM*, a mitochondrial transcription factor, was increased after treatment at concentrations of 0,5 mM and 1 mM Metformin (**Fig. 32D**). The treatment with 2 mM Metformin did not cause significant changes compared to untreated trisomic control.

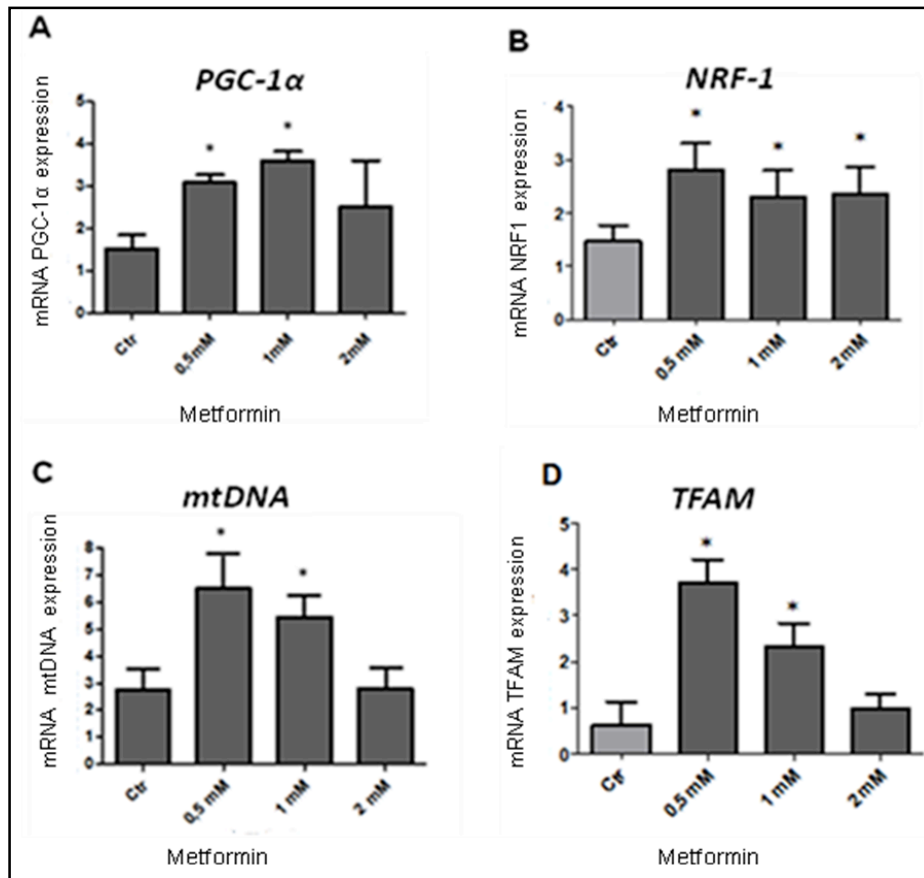


**Fig. 32** qRT-PCR analysis in Metformin treated DS-HFF cells for 72h. (A) The expression levels of *PGC-1α* increased in treated DS-HFF cells for 72h at different Metformin concentrations when compared to untreated controls. (B) The expression values of *NRF1* increased at all Metformin concentration. (C) mtDNA, calculated as the ratio of genes *D-LOOP/ACTIN*, increased in treated DS-HFF cells at Metformin concentrations of 0.5 mM and 1 mM, while the treatment with 2 mM Metformin did not cause significant changes compared to untreated trisomic controls. The values represent the mean  $\pm$  determined SEM; analysis were performed in triplicate. (D) The expression levels of *TFAM* increased in treated DS-HFF cells at Metformin concentrations of 0.5 mM and 1 mM, while the treatment with 2 mM Metformin did not cause significant changes compared to untreated trisomic controls. Values represent the average determination  $\pm$  SEM for two DS-HFFs samples carried out in triplicate. \*= $p < 0.05$ . P-value expressed statistical significance for treated trisomic cells versus untreated trisomic cells.

#### Metformin treatment increases OCR in DS-HFFs

To verify whether the increase of *PGC-1α* and mtDNA in treated trisomic cells were associated with an improvement of mitochondrial function, the rate of OCR was assayed by XF<sup>e</sup> 96 Extracellular Flux Analyzer. DS-HFF cells treated for 72 hours with different Metformin concentrations showed an increase of OCR inversely proportional to the concentration of the drug used. Best results were obtained at 0.5 mM Metformin concentration with a more

than 50% increase in comparison to non treated controls. In contrast, OCR was decreased in DS-HFF cells treated with 2 mM Metformin (**Fig. 33**).

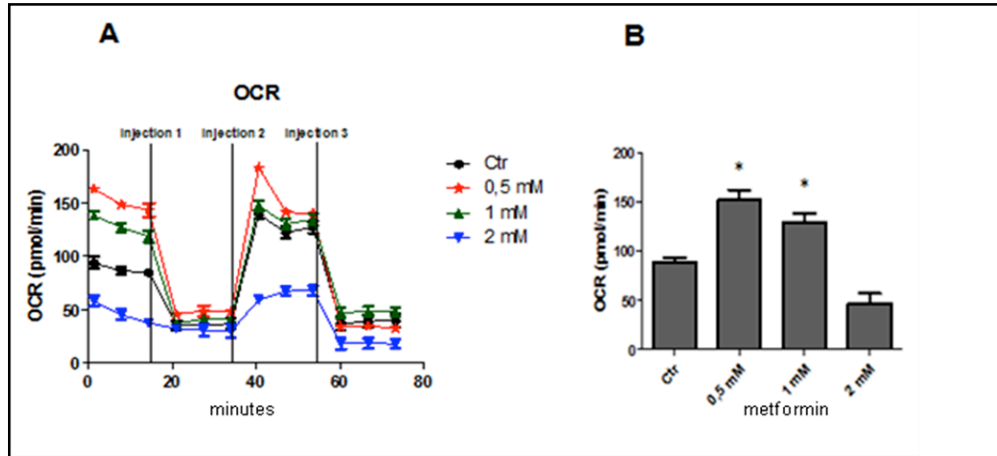


**Fig. 33 Measurement of OCR in DS-HFF cells treated with different Metformin concentrations for 72h.** (A) XF<sup>c</sup> Analyzer detected an increase of OCR of about two times in DS-HFF cells treated with 0.5mM Metformin concentration when compared to untreated trisomic control. In contrast, a reduction of mitochondrial parameters was observed in DS-HFF treated at higher Metformin concentration (2 mM) when compared to untreated controls. (B) Quantification of OCR values in Metformin treated trisomic cells compared to untreated controls. The optimal concentration at which there was the best result was of 0.5 mM. Values represent the average determination  $\pm$ SEM for two DS-HFF samples carried out in triplicate. \* =  $p < 0.05$ . P-value expressed statistical significance for treated trisomic cells versus untreated trisomic cells.

#### Metformin treatment increases mitochondrial activity

Mitochondrial function after Metformin treatment was assessed by MitoTracker Red, as previously described. Three trisomic cell lines were treated for 72 hours with Metformin at a 0.5 mM concentration. Confocal microscopy showed a 70% increase in red fluorescence in treated DS-HFFs (**Fig. 34B**) when compared with non treated DS-HFFs (**Fig. 34A**). The semi-quantitative analysis of Mitotracker fluorescence by ImageJ software is shown (**Fig. 34C**).

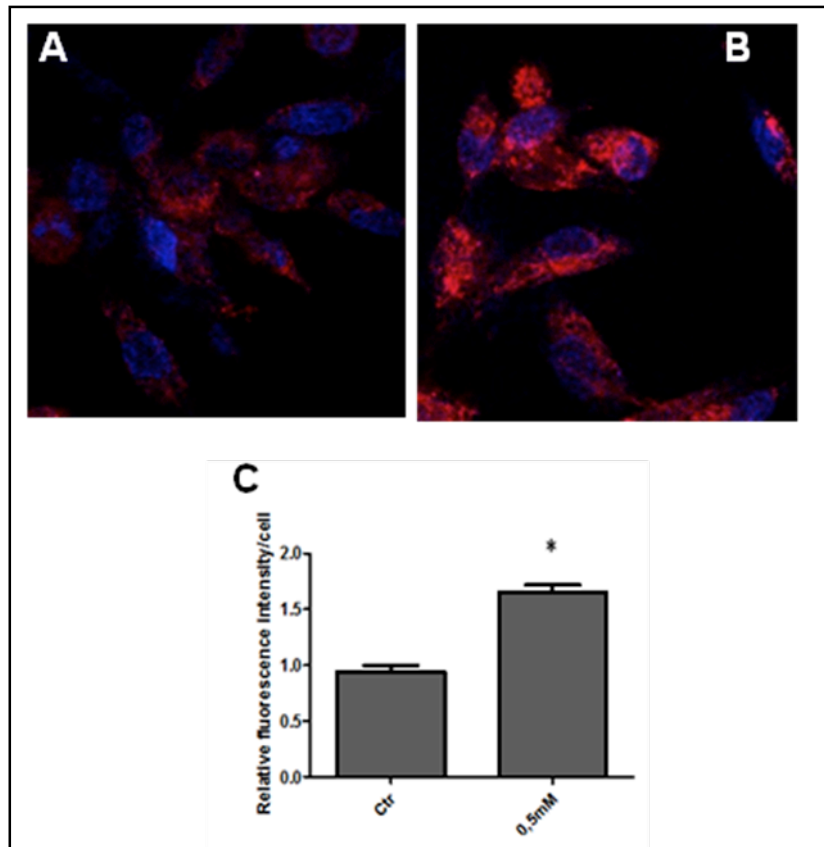


**Fig. 34 Mitochondrial activity was increased in DS-HFF cells treated with Metformin.** Confocal microscopy live cell imaging of the Mitotracker fluorescence in treated DS-HFFs: (A) untreated controls and (B) cells treated at the concentration of 0.5 mM Metformin for 72h. The cells were randomly selected, fifty cells for each sample/experiment were analyzed. An increase in Mitotracker-related fluorescence was observed in DS-HFF cells treated with Metformin compared to untreated controls. (C) Semiquantitative analysis of the Mitotracker-related fluorescence using ImageJ software, which showed an increase in fluorescence up to 70% more in treated DS-HFF cells, compared to untreated trisomic controls. \*= $p < 0.05$ . The P-value expressed statistical significance for treated trisomic cells vs. untreated trisomic cells.

Moreover, the analysis showed comparable fluorescence in untreated N-HFFs (Fig. 35A) and in DS-HFF treated with Metformin (Fig. 35B)

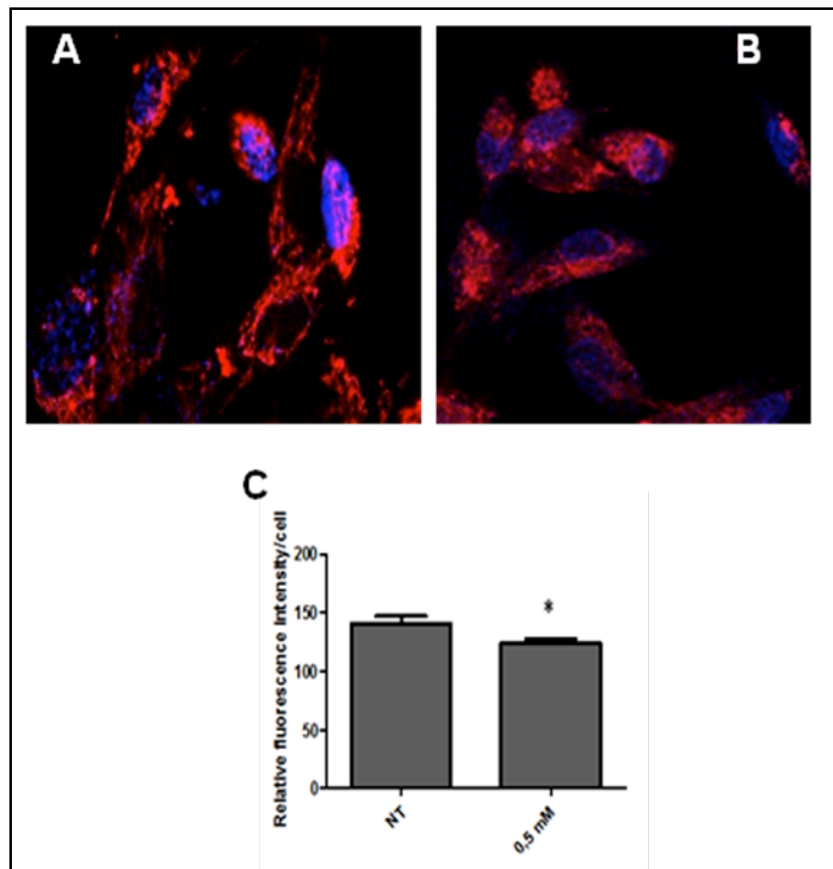


**Fig. 35 Comparison of mitochondrial activity in DS-HFF treated with Metformin and euploid untreated controls.** Confocal microscopy live cell imaging of the Mitotracker fluorescence in treated DS-HFFs: (A) untreated euploid controls and (B) trisomic cells treated with 0.5 mM Metformin for 72h. The cells were randomly selected, fifty cells for each sample/experiment were analyzed. (C) Semiquantitative analysis of the Mitotracker-related fluorescence using ImageJ software. The comparison between treated DS-HFF and untreated euploid control (NT) showed a very similar fluorescence.  $*=p<0.05$ . The P-value expressed statistical significance for treated trisomic cells vs. untreated euploid cells.

#### 4.7.2 Pioglitazone counteracts mitochondrial dysfunction in DS-HFFs

##### Pioglitazone treatment increases cellular ATP content

ATP production in DS-HFFs was assessed as described above in 2 DS-HFF cultures treated with Pioglitazone at different concentrations (100 nM, 1  $\mu$ M and 2 $\mu$ M), for either 48 or 72 hours. ATP production was increased in treated cells in a dosage dependent way (Fig. 36). The increase was very significant at 72 hours: the treatment with 1  $\mu$ M Pioglitazone raised the ATP content up to the values observed in euploid cells.

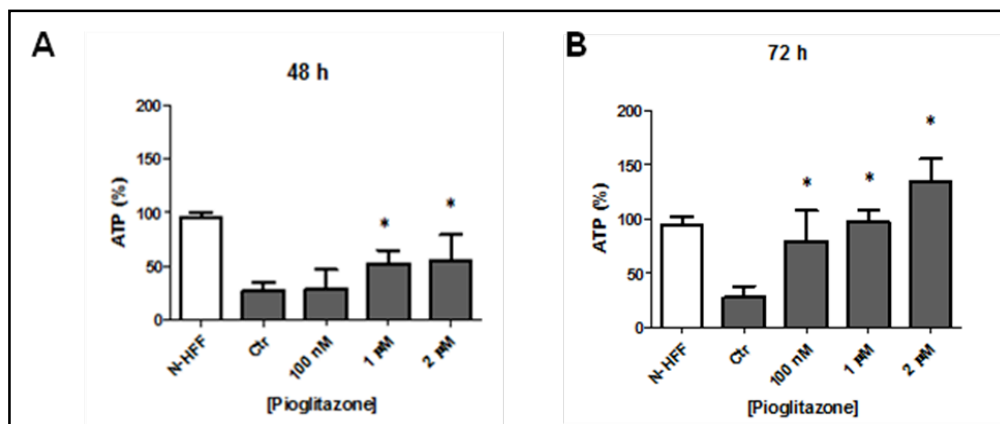


**Fig. 36 ATP concentration dosage in Pioglitazone DS-HFF cells.** (A). DS-HFF cells treated with Pioglitazone at different concentrations for 48 hours showed an increase of up to 50% of mitochondrial ATP-dosage compared to untreated control. (B) DS-HFF cells treated with Pioglitazone at different concentrations for 72 showed an increase of ATP three times greater than trisomic untreated controls . \*=p<0.05. The P-value expressed statistical significance for trisomic treated cells vs. untreated cells.

#### Pioglitazone treatment affects mitochondrial network in DS-HFFs

Pioglitazone is a drug that acts as an agonist of *PPAR $\gamma$* , therefore able to affect the biogenesis and mitochondrial function. To evaluate the effects of Pioglitazone on mitochondrial morphology, DS-HFF cells were infected with the addition of an adenovirus mtGFP in the culture medium, incubated for the next 72 hours, and subjected to treatment with 1  $\mu$ M Pioglitazone for 72h. As shown in **Figure 37** the mitochondrial network is much less fragmented if compared to untreated trisomic control.

More experiments are needed to plot data and to analyze statistical significance.

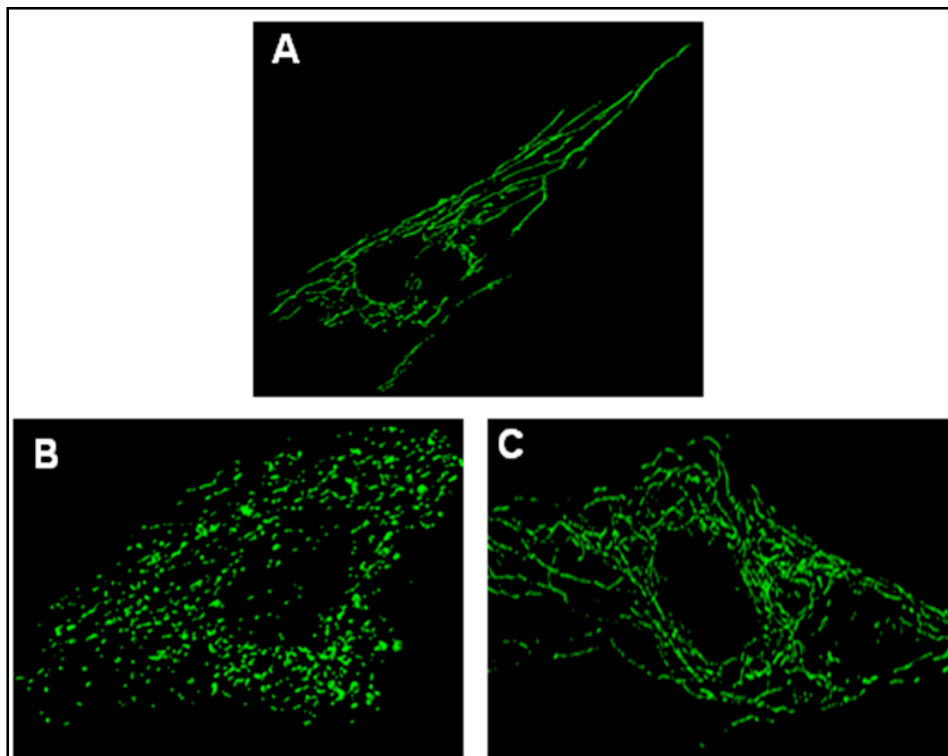


**Fig. 37 Mitochondrial network in Pioglitazone DS-HFF treated at concentration of 1  $\mu$ M.** (A) Confocal microscopy images showed mitochondrial network in a euploid cell. (B) Mitochondrial network in a trisomic untreated cell. (C) Mitochondrial network in a trisomic cell treated with 1  $\mu$ M Pioglitazone for 72h. Confocal microscopy images obtained with Nikon Eclipse Ti showed that the mitochondrial network in DS-HFF cells is much less fragmented as a result of treatment with the drug.

#### Pioglitazone treatment increases the expression of mitochondria related genes

To understand the impact of Pioglitazone on the activation of *PGC-1 $\alpha$*  signaling pathway, two DS-HFF cell lines were treated with different concentrations of the drug (100 nM, 1  $\mu$ M and 2  $\mu$ M) for 72 hours. The analysis of *PGC-1 $\alpha$*  gene expression by qRT-PCR demonstrated that the expression levels increased in treated DS-HFF cells at all Pioglitazone concentrations (**Fig. 38**).

Also the expression of *PPAR $\gamma$* , the direct target of Pioglitazone, was significantly increased at all the concentrations (**Fig. 38**).

To evaluate the effects of Pioglitazone treatment on mitochondrial biogenesis, the expression of *D-LOOP* and *ACTIN* was measured by qRT-PCR (**Fig. 38**). The expression values of mtDNA (calculated from the ratio of genes *D-LOOP/ACTIN*) increased in treated DS-HFFs at Pioglitazone concentrations of 1  $\mu$ M and 2  $\mu$ M, while treatment with 100 nM Pioglitazone did not cause significant changes if compared to untreated trisomic controls.

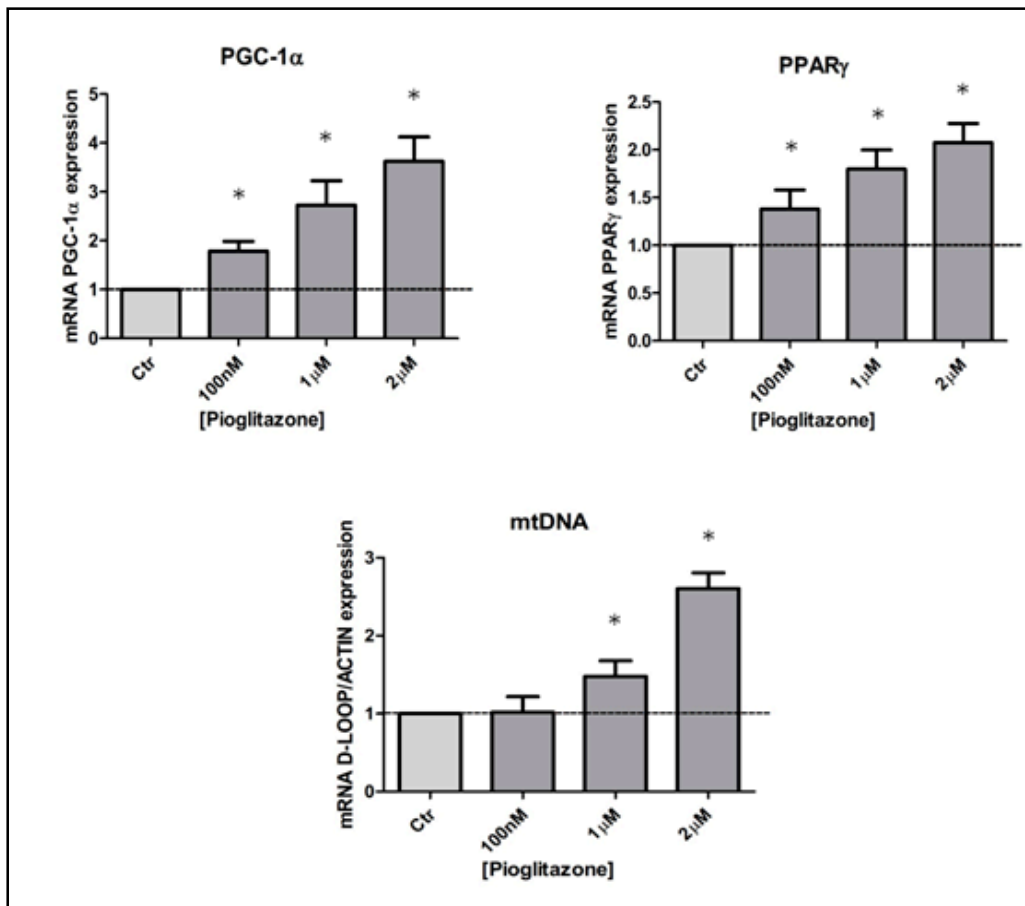


**Fig. 38** qRT-PCR analysis in Pioglitazone treated DS-HFF cells for 72h. The expression levels of *PGC-1 $\alpha$*  increased in treated DS-HFF cells for 72h at different Pioglitazone concentrations when compared to untreated controls. Also *PPAR $\gamma$*  expression increased at all Pioglitazone concentrations tested. The expression of *mtDNA*, calculated as the ratio of genes D-LOOP/Actin, increased in treated DS-HFF cells at Pioglitazone concentrations of 1  $\mu$ M and 2  $\mu$ M, while the treatment with 100nM Pioglitazone did not cause significant changes compared to untreated trisomic controls. Values represent the average determination  $\pm$  SEM for two DS-HFFs samples carried out in triplicate. \*= $p < 0.05$ . P-value expressed statistical significance for treated trisomic cells versus untreated trisomic cells.

#### Pioglitazone treatment increases OCR in DS-HFFs

To verify whether the increase of *PGC-1 $\alpha$* , *PPAR $\gamma$*  and *mtDNA* in treated trisomic cells were associated with an improvement of mitochondrial function, the rate of OCR was assessed by XF<sup>c</sup> 96 Extracellular Flux Analyzer. DS-HFF cells treated for 72 hours with different Pioglitazone concentrations showed an increase of OCR. Best results were obtained at 2  $\mu$ M Pioglitazone concentration with an increase of about 60% in comparison with non treated controls (**Fig. 39**).

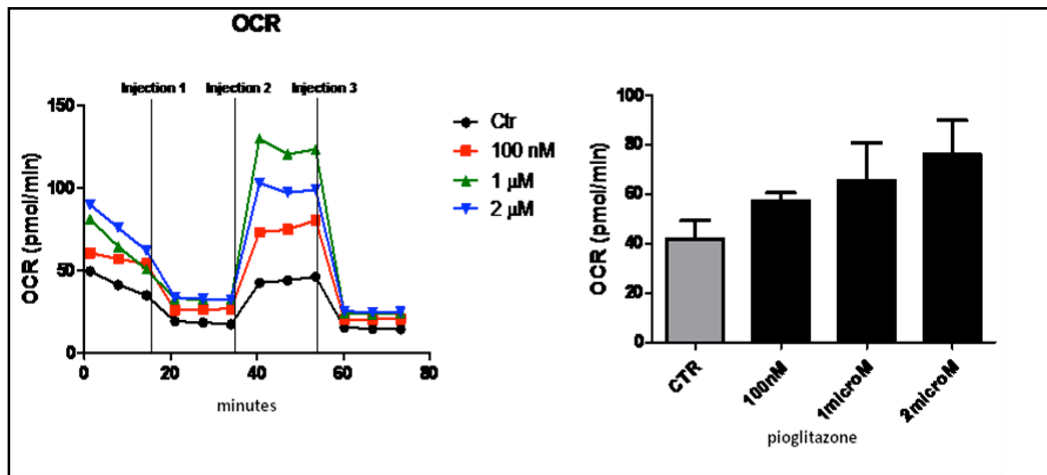


**Fig. 39 Measurement of OCR in DS-HFF cells treated with different Pioglitazone concentrations for 72h.** (A) XF<sup>c</sup> Analyzer detected an increase of OCR in DS-HFF cells treated at all Pioglitazone concentrations when compared to untreated trisomic control. (B) Quantification of OCR values in Pioglitazone treated trisomic cells compared to untreated controls. The optimal concentration at which there was approximately 60% of OCR increase was 2 μM Pioglitazone. Values represent the average determination ±SEM for two DS-HFF samples carried out in triplicate. \*= $p < 0.05$ . P-value expressed statistical significance for treated trisomic cells versus untreated trisomic cells.

## 5. DISCUSSION

Since 2005, the research group in which I have been working has been committed at unraveling the molecular consequences of TS21 on the development of specific DS phenotypic traits. The first strategy was to compare the overall gene expression profile of hearts from human fetuses with and without TS21. The analysis showed that most Hsa21 genes were approximately 1.5 fold upregulated and 441 non-Hsa21 genes were dysregulated in all trisomic samples (Conti et al. 2007).

Functional analysis of differentially expressed genes revealed both a prevalence of NEMGs, among downregulated genes, and a prevalence of ECM genes among the upregulated ones (Conti et al. 2007). As a consequence of that, the corresponding protein levels and enzymatic activities may be dysregulated in DS subjects. It has been proposed that NEMG hypoexpression might be the cause of the molecular, functional and morphological alterations found in mitochondria from DS cells and tissues.

Indeed, abnormal mitochondrial cristae morphology, reduced oxygen consumption, increased ROS production and increased levels of intra-mitochondrial calcium (Piccoli et al. 2013) have been demonstrated in skin fibroblasts from fetuses with TS21. They also showed an abnormal mitochondrial distribution, with smaller and more numerous mitochondria than euploid fetal fibroblasts. The global mitochondrial mass was not significantly different.

The pro-oxidative state observed in DS-HFFs (Piccoli et al. 2013) led us to test the hypothesis that NEMGs regulation might be under the control of one regulatory gene affected by trisomy of Hsa21.

Many Hsa21 genes have been proposed as possible candidates for mitochondrial abnormalities, such as *APP* (Askanas et al. 1996), the transcription factor *GABPA* (O'Leary et al. 2004), the copper-zinc superoxide dismutase *SOD1* (Shin et al. 2004), *DYRK1A*, *DSCRI/RCAN1* (Bushdid et al. 2003) and *NR1P1*. The analysis of expression profiling of cells in which each of these genes was induced (De Cegli et al. 2010), clearly demonstrated that only *NR1P1* gene is able to cause NEMG downregulation, when overexpressed, and that no other Hsa21 gene tested exerts such an effect.

*NR1P1* is a corepressor for nuclear receptors and transcription factors controlling energy homeostasis in white adipose tissue (Powelka et al. 2006), muscle (Seth et al. 2007), and heart (Fritah et al. 2010). It links nuclear receptors to chromatin remodeling enzymes, including the HDAC enzymes, involved in chromatin condensation and transcriptional repression, and this function is modulated by post translational modifications which include phosphorylation and methylation (White et al. 2008). *NR1P1* is also target of acetylation, which inhibits the recruitment of the C-terminal binding protein (CtBP) (Vo et al. 2001). The upregulation of *NR1P1* in adipocytes inhibited a panel of *PGC-1 $\alpha$*  target genes through its partners, such as PPARs, ERRs and

NRFs (Hallberg et al. 2008) (**Fig. 40**). mRNA expression analysis revealed that *ERRα*, *PPARα*, *PPARβ*, NRF1, as well as some of their target genes, were repressed by *NR1P1* and induced by *PGC-1α* in a dose dependent manner in neonatal rat cardiomyocytes (Chen et al. 2012).

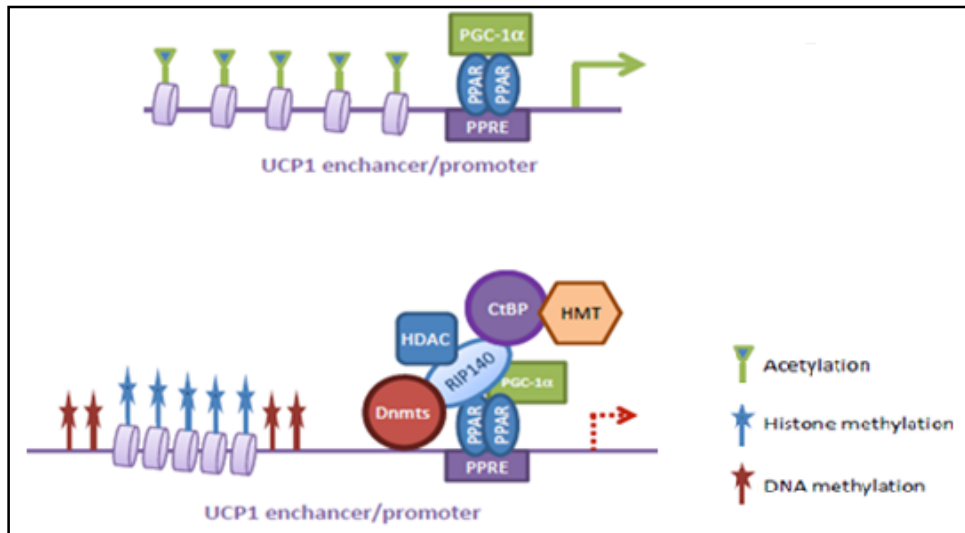


**Fig. 40 Corepressor function of *NR1P1* in regulating target gene transcription.** *NR1P1* acts as a transcriptional corepressor for PPARs, blocking *UCP1* promoter activation through the recruitment of DNA methyltransferase (Dnmt), C terminal binding protein (CtBP), histone methyltransferase (HMT) and histone deacetylase (HDAC) (Seth et al. 2007).

This highly conserved gene shows a 1.5- to 4-fold upregulation both in the heart and fibroblasts from DS subjects (Piccoli et al. 2013; Conti et al. 2007). The upregulation of *NR1P1* protein was also demonstrated in DS hippocampus (Gardiner, 2006) together with the upregulation of *SUMO3*, another gene mapping to Hsa21, which might modulate *NR1P1* repressive activity. Indeed, the lysines located in *NR1P1* repression domain 3 and 4 represent a *SUMO3* attachment consensus region and they are evolutionary conserved across vertebrates (Rytinki and Palvimo, 2009). The simultaneous upregulation of both Hsa21 genes might exert a synergistic effect.

The analysis of genes, which possibly may affect mitochondrial function, highlighted that *PGC-1α* transcription and activity are negatively regulated by *NR1P1* (Scarpulla et al. 2011) (**Fig. 41**).

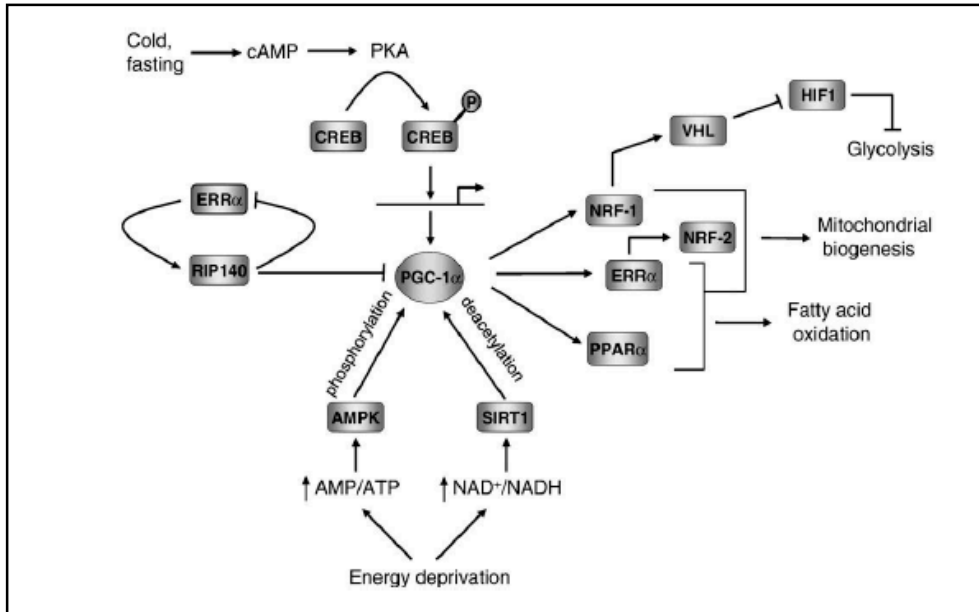


**Fig. 41 Regulatory network governing mitochondrial functions orchestrated by *PGC-1 $\alpha$* .** Interactions among some key participants in the transcriptional network regulating mitochondrial biogenesis are depicted schematically. The diagram summarizes the regulation of *PGC-1 $\alpha$*  by transcriptional and post-transcriptional pathways and its interactions with some of its target transcription factors involved in metabolic regulation. Potential suppression of glycolysis through *NRF-1* control of *VHL* expression and negative control by the *NRIP1/RIP140* co-repressor are also shown (Scarpulla et al. 2011).

*Powelka et al*, (2007) demonstrated that *NRIP1* significantly affects oxidative metabolism and mitochondrial biogenesis, and Seth et al, (2007) demonstrated that *NRIP1* overexpression represses nuclear mitochondrial genes involved in all respiratory chain complexes. Moreover *NRIP1* affects also the genes encoding enzymes within the glycolytic, TCA cycle, fatty acid oxidative pathways which were upregulated in response to *NRIP1* depletion.

Even a mild *NRIP1* overexpression is able to repress NEMGs involved in all respiratory chain complexes (Seth et al. 2007).

*NRIP1* is known to suppress both oxidative metabolism and mitochondrial biogenesis through *ERR $\alpha$*  (Powelka et al. 2006). It engages in a direct interaction with *PGC-1 $\alpha$*  in suppressing the *ERR $\alpha$*  and *NRF1* dependent expression of *CIDEA*, a gene involved in both programmed cell death and metabolism (Hallberg et al. 2008). Thus, *PGC-1 $\alpha$*  utilizes a network of positive and negative transcriptional regulators to establish and modulate metabolic functions (Fig. 41).

The lists of genes regulated by *NRIP1* and *PGC-1 $\alpha$*  largely overlap each other and to the list of NEMGs hypoexpressed in DS fetal hearts (Fig. 19, Table S1, appendix 1).

To biologically validate the results deriving from the bioinformatic strategy, we verified the potential role of *NRIP1* in mitochondrial dysfunction in a cell

model of DS in which *NRIP1* is upregulated. When *NRIP1* was transiently attenuated in human trisomic fibroblasts, an inverse correlation between *NRIP1* and *PGC-1 $\alpha$*  expression was demonstrated. Accordingly, this attenuation induced the upregulation of genes controlled by both *NRIP1* and *PGC-1 $\alpha$* . Moreover, *NRIP1* siRNA-mediated attenuation in DS-HFFs, and the consequent *PGC-1 $\alpha$*  and *NRF1* upregulation, elicited a significant increase in mtDNA.

A functional analysis of mitochondrial activity was performed in *NRIP1* silenced DS-HFFs vs control scrambled cells. ROS production decreased, and mitochondrial activity increased, in silenced cells demonstrating that the induction of NEMG expression counteracts mitochondrial impairment and partially rescues mitochondrial function. Notably, *NRIP1* silencing also increased cellular ATP content. These results, together with the finding that *NRIP1* attenuation by siRNA leads to an increase in the adenine nucleotide translocators *ANT1/SLC25A4* and *ANT2/SLC25A5*, suggest that a more efficient exchange of ATP is induced.

It is known that *NRIP1* also directly inhibits a panel of *PGC-1 $\alpha$*  related genes through its transcriptional partners (Hallberg et al. 2008). In particular, the transcription factors *NRF1* and *ERR $\alpha$* , as well as their targets, are repressed by *NRIP1* and induced by *PGC-1 $\alpha$*  in a dose dependent manner, in neonatal rat cardiomyocytes (Chen et al. 2012). *PGC-1 $\alpha$*  null mice (Mitra et al. 2012; Leone et al. 2005), as well as knock-in *NRIP1* mice (Seth et al. 2007), show reduced expression of mitochondrial genes in multiple tissues.

The role of *NRIP1* in DS might extend to several phenotypic aspects. The *NRIP1*-dependent repression of genes involved in mitochondrial function is closely linked with post-natal impaired cardiac function. Indeed, the most obvious phenotype of mice expressing exogenous *NRIP1* is the impaired postnatal heart function (Fritah et al. 2010). The transgenic mice are characterized by rapid onset of cardiac hypertrophy and ventricular fibrosis resulting in increased mortality. These data suggest that *NRIP1* might play a role in DS in postnatal heart defects such as cardiac hypertrophy, but also embryo heart development might be affected, as congenital heart defects have been associated to a more severe pro-oxidative state in DS fetuses (Piccoli et al. 2013).

*NRIP1* and *PGC-1 $\alpha$*  are also involved in glucose uptake and therefore in the physiopathology of diabetes through the regulation of the insulin sensitive glucose transporter *GLUT4* expression and its subcellular localization (Fritah et al. 2012). These findings might correlate with the fact that cardiac hypertrophy and diabetes are two important post-natal complications of DS.

It is known that mitochondria play a central role in many neurodegenerative diseases such as Alzheimer, Parkinson, Amyotrophic Lateral Sclerosis and Huntington diseases. Impaired energy metabolism, defect of mitochondrial enzymes activities, abnormalities of mitochondrial respiration, mtDNA mutations and oxidative stress are common characteristics of these neurodegenerative conditions (Petrozzi et al. 2007). The similarity of

neurodegenerative processes between DS and AD and the high prevalence of AD in DS patients suggest that AD and DS share common brain alterations possibly due to similar molecular pathways involved in the pathogenesis, such as mitochondrial dysfunction and oxidative stress (Dumont and Beal, 2011).

It is interesting to note that the bioinformatic functional analysis indicated that many genes regulated by both *NR1P1* and *PGC-1 $\alpha$* , and dysregulated in DS, characterize the mitochondrial dysfunction pathways described in neurodegenerative diseases such as AD and Parkinson's disease [KEGG Pathways <http://www.genome.jp/kegg/> (Kanehisa et al. 2000)].

This suggests that the pathway regulated by the *NR1P1/PGC-1 $\alpha$*  axis may be the target of a potential pharmacological strategy to counteract mitochondrial dysfunction and consequently mitigate the DS phenotype.

Therapeutic protocols have already been used in the past to counteract the oxidative stress observed in DS. Several clinical studies have tested the effects of antioxidant nutrients and vitamins (Lott et al. 2012; Tiano et al. 2011; Ellis et al. 2008; Miles et al. 2007). They concluded that the intake of these agents did not improve cognitive performance, nor prevented dementia in DS. Better results were obtained on learning and memory in the mouse model Ts65Dn using pentylenetetrazole, Memantine, Fluoxetine, Lithium, Epigallocatechin-3-gallate (EGCG) and antioxidants such as vitamin E, (Gardiner, 2014) but the clinical trials have not yielded the expected results.

To counteract mitochondrial dysfunction in DS we searched for drugs that interfere on the pathways regulated by *NR1P1/PGC-1 $\alpha$* . Even though drugs capable of modulating the activity of *PGC-1 $\alpha$*  are already used for the treatment of metabolic diseases and neurodegenerative diseases, such as AD, they have never been used in clinical trials in DS patients. Two drugs were evaluated in the present study: Metformin, an activator of *PGC-1 $\alpha$*  and Pioglitazone, an agonist of PPAR $\gamma$ .

Metformin is a drug commonly used as a hypoglycemic agent in type 2 diabetes because it inactivates gluconeogenesis (Caton et al. 2010). Metformin activates *AMPK* in the liver and muscles causing the phosphorylation and thus activation of *PGC-1 $\alpha$* , and upregulates *SIRT1* that in turn activates *PGC-1 $\alpha$*  by deacetylation (**Fig. 42**).

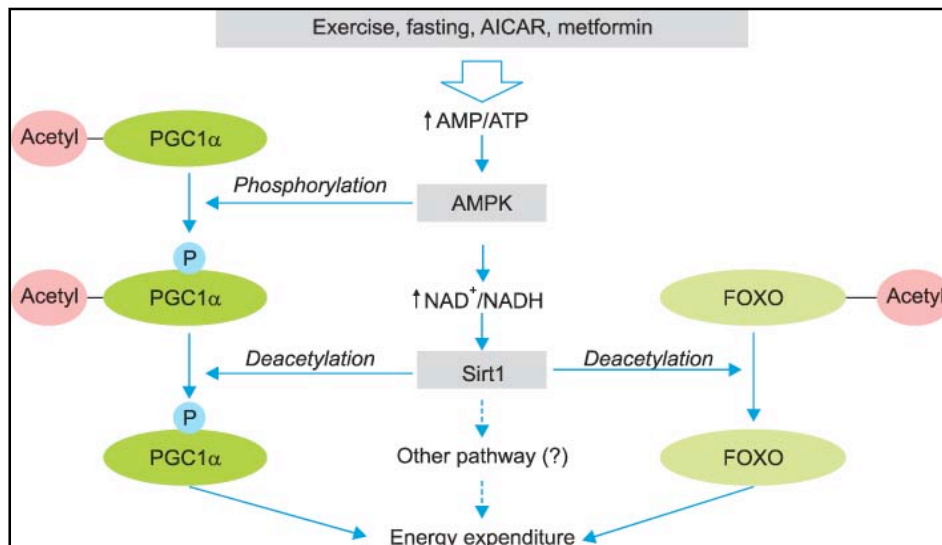


**Fig. 42 Representation of the mechanism of action of Metformin.** The drug activates *AMPK*, which in turn phosphorylates *PGC-1 $\alpha$* . Metformin also activates *SIRT1* that in turn deacetylates *PGC-1 $\alpha$*  activating it.

By activating the *PGC-1 $\alpha$*  pathway, Metformin can affect mitochondrial biogenesis and function, slowly permeating into mitochondria. All the tests of mitochondrial function we performed showed increased expression levels of *PGC-1 $\alpha$*  and a global improvement of mitochondrial activity at Metformin concentrations of 0.5-1 mM. Correspondingly, analysis by XF<sup>e</sup> 96 Extracellular Flux Analyzer showed an increase of OCR of about two times.

Since it is known that Metformin also has an inhibitory effect on the activity of mitochondrial complex I, one of the aims of the research was to identify concentrations that had effect on the activation of *PGC-1 $\alpha$*  but not on the inhibition of respiratory activity.

At 2mM Metformin concentration (the highest that has been analyzed) there was a significant OCR decrease with a consequent reduction of mitochondrial activity. At this drug dose also *PGC-1 $\alpha$*  transcription was decreased.

The therapeutic dosage of the hypoglycemic agent Metformin is 50 $\mu$ M which corresponds to a blood concentration from 0.05 to 1 mM. This dosage should be optimal to obtain maximum effect on mitochondrial function without inhibition of respiratory activity.

The second drug we tested, Pioglitazone, is a high affinity ligand for the nuclear receptor *PPAR $\gamma$* , a downstream gene of the *PGC-1 $\alpha$*  pathway. The binding with the drug activates the *PPAR $\gamma$*  receptor, which forms a heterodimer with the retinoid-X receptor leading to transcription of adipogenic genes (**Fig. 43**).

The treatment of type 2 diabetes with Pioglitazone significantly reduces insulin resistance (Fullert et al. 2002), and has beneficial effects on plasma lipid profile leading to a lower risk of acute myocardial infarction, stroke or heart failure (Goldberg et al. 2005; Aronoff et al. 2000). However, the clinical use of

Pioglitazone is also limited by the occurrence of certain adverse events, including weight gain, fluid retention, and possibly bladder cancer (Cariou et al. 2012; Hirose et al. 2002).

The therapeutic dosage of the drug as a hypoglycemic agent ranges from 15 to 30 mg/day, which should correspond to a blood concentration of 3-5  $\mu\text{M}$ .

The aim of this study was therefore to evaluate if the mitochondrial function might be improved at dosages that have limited side effects.

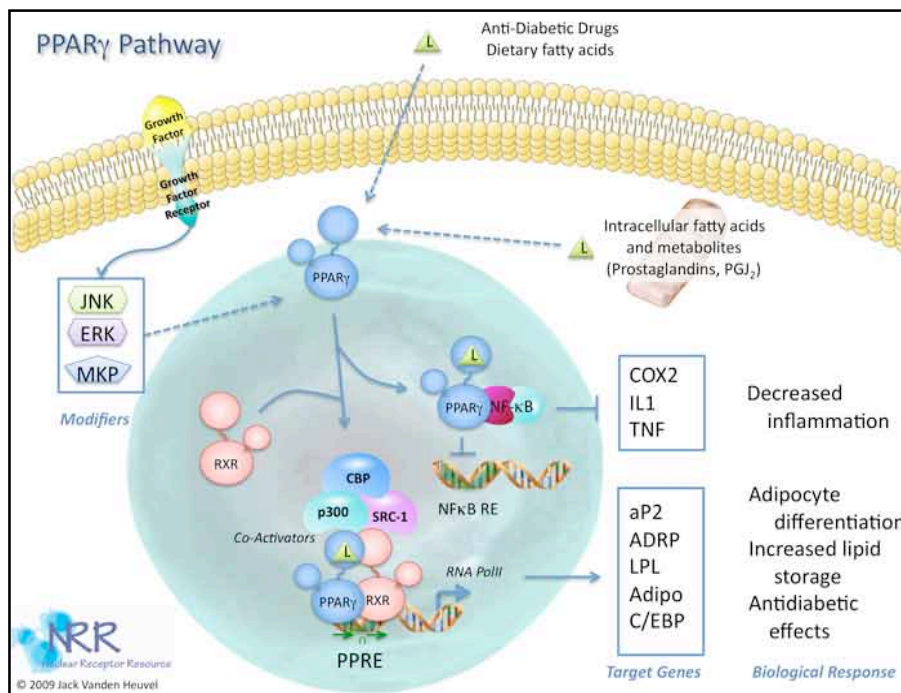


**Fig. 43 Representation of mechanism of action of Pioglitazone.** The drug binds to the *PPAR- $\gamma$*  receptor that forms a dimer with RXR receptor leading to transcription of downstream genes.

We evaluated the therapeutic effect of Pioglitazone treatment on mitochondrial phenotype in vitro for 48-72 hours, at concentrations from 100 nM to 2  $\mu\text{M}$ . All concentrations showed an impact on the phenotype as assessed by mitochondrial ATP production and organization of the mitochondrial network. The trisomic cell lines treated with Pioglitazone for 72 hours showed a less fragmented mitochondrial network, with a reduced number of isolated mitochondria and a greater average mitochondrial volume if compared to non-treated controls.

In the last part of the study, we looked for a regulator of ECM genes that maps to Hsa21 and that is upregulated in DS samples, by virtue of a gene dosage effect. To this aim, we re-analyzed the same GEO series discussed above (De Cegli et al. 2010). Our analysis demonstrated that only one gene is able to

cause the overexpression of 32 ECM genes, when overexpressed, and that no other Hsa21 tested gene exerts such an effect. This gene is *RUNXI* that is included in the smallest critical region recently identified for CHDs in DS (Liu et al. 2013).

The protein encoded by this gene represents the alpha subunit of *CBF*, a transcription factor involved in the development of normal hematopoiesis. The association of *RUNXI* with ECM genes regulation is supported by experiments that demonstrated that ectopic expression of *RUNXI* in 3T3 fibroblasts induced deep alterations in the distribution of *N-cadherin*, an increased expression of *Integrin  $\beta$ 5*, and increased survival at confluence (Wotton et al. 2008).

Furthermore, transcription factor-binding site (TFBS) analysis of ECM genes upregulated in DS fetal hearts identified *RUNXI* as the transcription factor with the highest specificity of binding. About 60% of ECM genes overexpressed in DS hearts showed consensus sequences for *RUNXI* (**Tab. 6**).

Our interest in ECM proteins is justified by the role they play in cardiac morphogenesis. Since 1984 it is known that cells derived from endocardial cushions and outflow tract of DS fetuses are more adherent in vitro when compared with controls (Wright et al. 1984).

ECM proteins are widely represented among the upregulated genes in DS fetal hearts (Conti et al. 2007). Since DS is a major cause of congenital heart defects, their dysregulation may represent a key pathological mechanism. Specific changes in the expression and accumulation of ECM components have been observed during human cardiomyocyte differentiation from human embryonic stem cells (Chan et al. 2010). Heart valvulogenesis is initiated in the atrioventricular junction and outflow tract by signaling events originating in the myocardium that induce endocardial cells to undergo an epithelial to mesenchymal transformation (**EMT**) and to migrate into *cardiac jelly*. This is an acellular and extracellular matrix-rich space that separates the myocardial and endocardial cell layers in the primitive heart during the early steps of heart development (Wirrig et al. 2007). As a result of EMT, endocardial cushions are formed that are composed of highly proliferative, undifferentiated, mesenchymal valve progenitor cells embedded in an unorganized ECM. The cushions will then elongate and undergo ECM remodeling in order to form functionally mature valves with decreased proliferation of endocardial cushions cells and increased organization and complexity of the ECM. The process by which endocardial cushions develop into mature valve leaflets is marked by the expression of specific ECM proteins and remodeling enzymes. Proteoglycans (aggrecan and versican/*VCAN*) and hyaluronan play critical role in heart development. Normal development of the heart requires synthesis, deposition and degradation of the ECM components versican and hyaluronan.

Fetal heart transcriptome profiling that we performed demonstrated that *VCAN* and Cartilage link protein 1 (*Crtl1*; also known as Hyaluronan and Proteoglycan Binding Protein 1- *Hapln1*), an ECM protein that stabilizes the interaction between hyaluronan and *VCAN*, are upregulated in DS fetal hearts in comparison to control fetal hearts. Intriguingly, we found that *VCAN*,

*CRTL1* and *ADAMTSs*, crucial genes implicated in the embryonic development and in particular in the heart morphogenesis, are among the genes with consensus sequence for *RUNXI*.

*VCAN* is a chondroitin sulfate proteoglycan abundantly expressed within the extracellular matrix compartment of the developing and mature cardiovascular system. It binds to a number of other ECM components, as well as to cellular receptors, to influence cell adhesion, proliferation, migration and survival. It is necessary for cardiac cushion formation, atrioventricular valve development, ventricular septation, and outflow tract development (Chan et al. 2010). Alterations in its expression have been associated with vascular diseases (Wight and Merrilees, 2004). Analysis of *Vcan* transgenic mice has established the requirement for versican in cardiac development and its role in skeletogenesis. The *ADAMTS* family includes several versican-degrading proteases that are active during remodeling of the embryonic provisional matrix, especially during sculpting of versican-rich tissues. Versican is cleaved at specific peptide bonds by *ADAMTS* proteases, and the cleavage products are detectable by neo-epitope antibodies. Myocardial compaction, closure of the secondary palate (in which neural crest derived cells participate), endocardial cushion remodeling, myogenesis and interdigital web regression are developmental contexts in which *ADAMTS*-mediated versican proteolysis has been identified as a crucial requirement (Nandadasa et al. 2014).

*VCAN* dysregulation can induce changes in the distribution of periostin, another important molecule of the heart cushion extracellular matrix, and then may affect the developing valves by altering the structural integrity of the ECM through altered interaction with other molecules such as fibronectin, collagen and other proteoglycans (Norris et al. 2007). These molecules were found dysregulated in our data as well. Additionally, since it interacts directly with integrins, attachment-dependent signaling may be altered thus affecting cell migration and EMT in the cushion primordia of the septa and valves (Yan and Shao, 2006).

*Crtll* is a glycoprotein found in the extracellular matrix. It is expressed in endocardial and endocardially-derived cells in the developing heart, including cells in the atrioventricular (AV) and outflow tract (OFT) cushions (Binette et al. 1994). *Crtll* is involved in the formation and stabilization of proteoglycan and hyaluronan aggregates (Matsumoto et al. 2006) and is important for preventing aggregate degradation by proteases, such as members of the *ADAMTS* and *MMP* families (Miwa et al. 2006). Alteration in the expression of *Crtll* results in impairment of growth and development of several tissues, including the cartilage, heart, and central nervous system (Wirrig et al. 2007). Craniofacial abnormalities and shortened long bones are important phenotypic traits of DS subjects. *Crtll* null mice are characterized by craniofacial abnormalities and shortened long bones, possibly due to a reduction of aggrecan within the cartilage, resulting in an inability of chondrocytes to undergo differentiation and hypertrophy (Watanabe et al. 1999). Cardiac malformations seen in *Crtll* knockout mice include muscular ventricular septal

defects, atrioventricular septal defects, and thin myocardium (Wirrig et al. 2007).

The role of *RUNXI* in regulating ECM proteins and the role of ECM overexpression in the pathogenesis of DS-CHD will be elucidated by future experiments in which we plan to modulate *RUNXI* expression in iPSCs from DS fibroblasts induced to cardiac differentiation.

## 6. CONCLUSIONS

This study was aimed to identify Hsa21 genes responsible for either NEMG or ECM dysregulation; to develop strategies to counteract mitochondrial dysfunction in DS; to investigate how NEMG downregulation or ECM upregulation might affect cardiac phenotype.

The results we obtained indicate that the Hsa21 gene *NRIP1* plays a key role in the NEMG downregulation observed in DS, and suggest that the *NRIP1-PGC-1 $\alpha$*  axis represents a potential therapeutic target for restoring altered mitochondrial function in this syndrome. This provides the basis for clinical trials aimed at alleviating and preventing some DS pathologies, including neurodegeneration, diabetes, obesity, and hypertrophic cardiopathy, thus providing a better quality of life for DS individuals and their families. Few therapeutic approaches have been undertaken in this direction mainly based on the use of antioxidants and nutraceuticals with poor results.

We have here demonstrated that *in vitro* treatments with Metformin, a *PGC-1 $\alpha$*  activator, or Pioglitazone a *PPAR $\gamma$*  agonist, were both able to induce an improvement of mitochondrial function and morphology in DS cells. At lower concentrations than those commonly used for the diseases for which they are registered, these drugs caused an increase of OCR and ATP production and a decrease in the oxidative status of the cells.

Mitochondrial dysfunction play a central role in many neurodegenerative diseases such as AD, Parkinson's disease (PD), Huntington's diseases (HD), and Amyotrophic Lateral Sclerosis (ALS) (Petrozzi et al. 2007), which share with DS the NEMG dysregulation. This open new frontiers for the use of these drugs in other diseases, including neurodegenerative diseases.

Last, we have investigated which Hsa21 gene may be responsible for the upregulation of ECM proteins observed in DS and how this upregulation might affect the heart development. The mechanisms governing regulation of ECM protein expression during heart development are complex and involve many signaling pathways (Combs et al. 2009). We have identified in the Hsa21 gene *RUNX1* a possible candidate for ECM regulation and also we have focused our attention on 2 important non-Hsa21 genes, *VCAN* and *CTRL1*, upregulated in DS hearts (Conti et al. 2007), which play a key role in regulating ECM distribution during the cardiogenesis.

Of course mitochondrial dysfunction and ECM alterations are just two potential mechanisms responsible for the DS phenotypic traits. Recently, it has been proposed that the variable phenotypic expression in DS might be caused by epigenetic modifications. Altered patterns of DNA methylation have been observed in DS tissues (Jones et al. 2013). Several genes that map on Hsa21, such as DNA methyltransferase III, or transcriptional regulators *HMGNI* and *NRIP1*, could be important for epigenetic modifications, as histones bind and regulate the configuration of chromatin (Dekker et al. 2014). New experiments are needed also in this direction.

## 7. FUTURE PERSPECTIVES

The results of this study lay the bases for future investigations. We are planning to test other drugs, namely Resveratrol, which activates *PGC-1 $\alpha$*  acting on *SIRT1*, bezafibrate, a PPAR pan-agonist, and AICAR, on mitochondrial dysfunction. We will also test the effect drug associations.

We are producing stem cells (iPSCs) directly induced from human fetal fibroblasts with TS21. Recent studies of the transcriptome of DS-iPSC cells have shown that genes related to mitochondria are dysregulated in both undifferentiated stem cells and in differentiated neuronal cells (Weick et al. 2013). These demonstrations make iPSC a good cell model for the study of mitochondrial phenotype during differentiation and for drug testings directly on cell lines at various stages of differentiation without the use of any animal models. We plan also to induce iPSCs to differentiate into cardiomyocytes, in order to perform a molecular and functional study to evaluate the effects of *RUNX1* modulation on ECM gene expression.

Gene therapy in DS is opening new scenarios. RNAi is a useful tool to silence specific genes in biological systems. Its efficacy was demonstrated in the treatment of several diseases in vivo, but its therapeutic use in treating neurological diseases has been hampered by the lack of an efficient way to deliver siRNA across the blood brain barrier (BBB). Initial attempts using intracranial injections of lentiviral vectors turned out to be inadequate (Zabel, 2013; Fillat and Altafaj, 2012). Alternative delivery with the Adeno associated (AAV) virus system gave encouraging results (Fillat and Altafaj, 2012; McCown, 2011; Worgall et al. 2008;). AAV vectors were used indeed to correct *DYRK1A*-induced motor defects in DS (Ortiz-Abalia et al. 2008).

Despite the capacity of AAV vectors to cross the BBB, the use of non viral systems, based on cationic lipids, polymers, dendrimers or different types of nanoparticles, seems more attractive as these vectors are demonstrating to be non immunogenic, easy to prepare and non expensive (Alvarez-Erviti et al. 2011).

## ACKNOWLEDGEMENTS

At the end of this work, I would like to thank all people that, in different ways, encouraged my studies and allowed the creation of this thesis.

My heartfelt thanks go to *Prof. Lucio Nitsch*, my tutor in this research work, for being always available with his precious suggestions and comments. He also gave me the opportunity to know the interesting field of prenatal cytogenetics that I love with the same intensity of the research field.

Thanks to *Dr. Anna Conti* for her the continuous availability and support in all steps of this thesis. I would also like to thank her for all what I have learned and for her patience, motivation and enthusiasm.

An affectionate thank go to *Dr. Floriana Fabbrini*. She introduced me to the research field and gave me the passion for cytogenetics. I will always be grateful to her.

Thanks to *Dr. Antonella Izzo* for contributing to my training and professional growth and, above all, for showing me affection since the first moment. She is for me not only my research supervisor but also a dear friend.

I would like to thanks *Dr. Rosanna Manco* and *Dr. Ferdinando Bonfiglio* for their special support and friendship.

Thanks to all my laboratory group, especially *Valentina, Francesca, Nunziatina, Chiara e Filomena* for their help and moral support.

I would like to thanks *Prof. Nazzareno Capitano*, *Dr. Claudia Piccoli* and *Prof. Paolo Pinton* for their help in mitochondrial functional studies; *Dr. Marina Prisco* for electron microscope analyses of mitochondrial ultrastructure; *Prof. Matarese's* group for OCR measurements by the XF<sup>o</sup> Analyzer and *Dr. Maria Nitti* for performing ATP and mitochondrial mass measurements after drug treatments.

Last but not least, I would like to thanks my family. My parents represent the source of love, courage and energy that I needed to overcome obstacles.

Thanks to my husband Alessandro, always present in these long years of study and life together, for his immense patience, moral support and encouragement. I could not imagine a better person at my side.

I conclude thanking my children, Mara and Lorenzo, which are the sense of all my thoughts, gestures, and sacrifice...the sense of my life.

## REFERENCES

- Abu-Issa R, Kirby ML. Heart field: from mesoderm to heart tube. *Annu Rev Cell Dev Biol* 2007;23:45-68.
- Alvarez-Erviti L, Seow Y, Yin H, Betts C, Lakhali S, Wood MJ. Delivery of siRNA to the mouse brain by systemic injection of targeted exosomes. *Nat Biotechnol* 2011;29:341-345.
- Amano K, Sago H, Uchikawa C, Suzuki T, Kotliarova SE, Nukina N, Epstein CJ, Yamakawa K. Dosage-dependent overexpression of genes in the trisomic region of Ts1Cje mouse model for Down syndrome. *Hum Mol Genet* 2004;13:1333-1340.
- Arbuzova S, Hutchin T, Cuckle H. Mitochondrial dysfunction and Down's syndrome. *Bioessays* 2002;24:681-684.
- Armstrong EJ, Bischoff J. Heart Valve Development. *Endothelial Cell Signaling and Differentiation. Circulation Research* 2004;95:459-470.
- Aronoff S, Rosenblatt S, Braithwaite S, Egan JW, et al. Pioglitazone hydrochloride monotherapy improves glycemic control in the treatment of patients with type 2 diabetes: a 6-month randomized placebo-controlled dose-response study, The Pioglitazone 001 Study Group. *Diabetes Care*. 2000;23:1605–1611.
- Arron JR, Winslow MM, Polleri A, Chang CP, Wu H, Gao X, Neilson JR, Chen L, Heit JJ, Kim SK, Yamasaki N, Miyakawa T, Francke U, Graef IA, Crabtree GR. NFAT dysregulation by increased dosage of DSCR1 and DYRK1A on chromosome 21. *Nature* 2006;441:595-600.
- Askanas V, McFerrin J, Baque S, Alvarez RB, Sarkozi E, Engel WK. Transfer of beta amyloid precursor protein gene using adenovirus vector causes mitochondrial abnormalities in cultured normal human muscle. *Proc Natl Acad Sci USA* 1996;93:1314-1319.
- Bambrick LL, Fiskum G. Mitochondrial dysfunction in mouse trisomy 16 brain. *Brain Res* 2008;1188:9-16.
- Barlow GM, Xiao-Ning Chen, Zheng Y Shi, Gary E Lyons, David M Kurnit, Livija Celle, Nancy B Spinner, Elaine Zackai, Mark J Pettenati, Alexander J Van Riper, Michael J Vekemans, Corey H Mjaatvedt and Julie R Korenberg. Down syndrome congenital heart disease: A narrowed region and a candidate gene. *Genetics in Medicine* 2001;3: 91–101.
- Bastin J, Aubey F, Rotig A, Munnich A, Djouadi F. Activation of peroxisome proliferator-activated receptor pathway stimulates the mitochondrial respiratory chain and can correct deficiencies in patients' cells lacking its components. *J Clin Endocrinol Metab* 2008;93:1433-1441.
- Binette F, Cravens J, Kahoussi B, Haudenschield DR, Goetinck PF. Link protein is ubiquitously expressed in non-cartilaginous tissues where it enhances and stabilizes the interaction of proteoglycans with hyaluronic acid. *J Biol Chem* 1994;269:19116-22.
- Blehaut H, Mircher C, Ravel A, et al. Effect of leucovorin (folinic acid) on the developmental quotient of children with Down's syndrome (trisomy 21) and influence of thyroid status. *PLoS One* 2010;5:e8394.
- Bonora M, Patergnani, Rimessi S, De Marchi A, Suski E, Bononi JM, Giorgi A, Marchi C, Missiroli S, Poletti S, F. et al. ATP synthesis and storage. *Purinergic Signal* 2012;8:343–357.

- Busciglio J, and Yankner, B.A. Apoptosis and increased generation of reactive oxygen species in Down's syndrome neurons in vitro. *Nature* 1995;378:776–779.
- Busciglio J, Pelsman A, Wong C, Pigino G, Yuan M, Mori H, and Yankner BA. Altered metabolism of the amyloid beta precursor protein is associated with mitochondrial dysfunction in Down's syndrome. *Neuron* 2002;33:677–688.
- Bushdid PB, Osinska H, Waclaw RR, Molkentin JD, Yutzey KE. NFATc3 and NFATc4 are required for cardiac development and mitochondrial function.; *Circ Res* 2003;92:1305-1313.
- Camello-Almaraz MC, Gomez-Pinilla PJ, Pozo MJ and Camello PJ. Mitochondrial reactive oxygen species and Ca<sup>2+</sup> signaling. *Am J Physiol Cell Physiol* 2006;291:C1082–C1088.
- Cantó C, Auwerx J. PGC-1alpha, SIRT1 and AMPK, an energy sensing network that controls energy expenditure. *Curr Opin Lipidol* 2009;20,98-105.
- Cariou B, Charbonnel B, Staels B. Thiazolidinediones and PPARgamma agonists: time for a reassessment. *Trends Endocrinol Metab: TEM* 2012;23:205–215.
- Caton PW, Nayuni NK, Kieswich J, Khan NQ, Yaqoob MM, Corder R. Metformin suppresses hepatic gluconeogenesis through induction of SIRT1 and GCN5. *J Endocrinol* 2010;205:97-106.
- Caviedes P, Caviedes R and Rapoport SI. Altered calcium currents in cultured sensory neurons of normal and trisomy 16 mouse fetuses, an animal model for human trisomy 21 (Down syndrome). *Biol Res* 2006;39:471-81.
- Chan CK, Rolle MW, Potter-Perigo S, Braun KR, Van Biber BP, Laflamme MA, Murry CE, Wight TN. Differentiation of cardiomyocytes from human embryonic stem cells is accompanied by changes in the extracellular matrix production of versican and hyaluronan. *J Cell Biochem.* 2010;111:585-96.
- Chen Q, Vazquez EJ, Moghaddas S, Hoppel CL, and Lesnefsky EJ. Production of reactive oxygen species by mitochondria: central role of complex III. *J Biol Chem* 2003; 278: 36027–36031.
- Chen Y, Wang Y, Chen J, Chen X, Cao W, Chen S, Xu S, Huang H. and Liu P. Roles of transcriptional corepressor RIP140 and coactivator PGC-1alpha in energy state of chronically infarcted rat hearts and mitochondrial function of cardiomyocytes. *Mol. Cell Endocrinol* 2012;362:11–18.
- Clark S, Schwalbe J, Stasko MR, Yarowsky PJ, Costa AC. Fluoxetine rescues deficient neurogenesis in hippocampus of the Ts65Dn mouse model for Down syndrome. *Exp Neurol* 2006;200:256–261.
- Combs MD, Yutzey KE. Heart Valve Development. *Regulatory Networks in Development and Disease. Circulation Research* 2009;105:408-421
- Contestabile A, Greco B, Ghezzi D, Tucci V, et al. Lithium rescues synaptic plasticity and memory in Down syndrome mice. *J Clin Invest* 2013;123:348–361.
- Conti A, Fabbrini F, D'Agostino P, Negri R, Greco D, Genesio R, D'Armiento M, Olla C, Paladini D, Zannini M, Nitsch L. Altered expression of mitochondrial and extracellular matrix genes in the heart of human fetuses with chromosome 21 trisomy. *BMC Genomics* 2007;8:268.
- Cork LC. Neuropathology of Down Syndrome and Alzheimer Disease. *Am J Med Genet Suppl* 1990; 7:282-286.
- Coskun PE, Busciglio J. Oxidative Stress and Mitochondrial Dysfunction in Down's Syndrome: Relevance to Aging and Dementia. *Curr Gerontol Geriatr Res* 2012;2012:383170.

- Costa AC, Scott-McKean JJ, Stasko MR. Acute injections of the NMDA receptor antagonist memantine rescue performance deficits of the Ts65Dn mouse model of Down syndrome on a fear conditioning test. *Neuropsychopharmacology* 2008;33:1624–1632.
- Crabtree GR, Olson EN. NFAT signaling: choreographing the social lives of cells. *Cell* 2002;109:s67-79.
- Dauphinot L, Lyle R, Rivals I, Dang MT, Moldrich RX, Golfier G, Ettwiller L, Toyama K, Rossier J, Personnaz L, Antonarakis SE, Epstein CJ, Sinet PM, Potier MC. The cerebellar transcriptome during postnatal development of the Ts1Cje mouse, a segmental trisomy model for Down syndrome. *Hum Mol Genet* 2005;14:373-84.
- De Cegli R, Romito A, Iacobacci S, Mao L, Lauria M, Fedele AO, Klose J, Borel C, Descombes P, Antonarakis SE, et al. A mouse embryonic stem cell bank for inducible overexpression of human chromosome 21 genes. *Genome Biol* 2010;11, R64.
- Delabar JM, Theophile D, Rahmani Z, Chettouh Z, Blouin JL, Prieur M, Noel B, Sinet PM: Molecular mapping of twenty-four features of Down syndrome on chromosome 21. *Eur J Hum Genet* 1993;1:114-124.
- Dekker AD, De Deyn PP, Rots MG. Epigenetics: the neglected key to minimize learning and memory deficits in Down syndrome. *Neurosci Biobehav Rev* 2014;45:72–84.
- Dillon LM, Hida A, Garcia S, Prolla, et al. Long-term bezafibrate treatment improves skin and spleen phenotypes of the mtDNA mutator mouse. *PLoS ONE* 2012;7:e44335.
- Dong W, Gao D, Zhang X. Mitochondria biogenesis induced by resveratrol against brain ischemic stroke. *Med Hypotheses* 2007;69:700-701.
- Douglas C. Wallace. A Mitochondrial Paradigm of Metabolic and Degenerative Diseases, Aging, and Cancer: A Dawn for Evolutionary Medicine *Annu Rev Genet* 2005;39:359.
- Dumont M, Beal MF. Neuroprotective strategies involving ROS in Alzheimer disease. *Free Radic Biol Med* 2011;51:1014-1026.
- Dunlevy L, Bennett M, Slender A, Lana-Elola E, Tybulewicz VL, Fisher EM, Mohun T. Down's syndrome-like cardiac developmental defects in embryos of the transchromosomal Tc1 mouse. *Cardiovasc Res* 2010;88:287-95.
- Ellis JM, Tan HK, Gilbert RE, Muller DP, Henley W, et al. Supplementation with antioxidants and folic acid for children with Down's syndrome: Randomised controlled trial. *British Medical Journal* 2008;336:594-597.
- Epstein CJ. Epilogue: toward the twenty-first century with Down syndrome--a personal view of how far we have come and of how far we can reasonably expect to go. *Prog Clin Biol Res* 1995;393:241-6.
- Epstein CJ, Korenberg JR, Anneren G, Antonarakis SE, Ayme S, Courchesne E, Epstein LB, Fowler A, Groner Y, Huret JL et al. Protocols to establish genotype-phenotype correlations in Down syndrome. *Am J Hum Genet* 1991; 49:207-235.
- Ferencz C, Neill CA, Boughman JA, Rubin JD, Brenner JI, Perry LW. Congenital cardiovascular malformations associated with chromosome abnormalities: an epidemiologic study. *J Pediatr* 1989;114:79-86.
- Fillat C and Altafaj X. 2012. *Progress in Brain Research*. Vol. 197.

- FitzPatrick DR, Ramsay J, McGill NI, Shade M, Carothers AD, Hastie ND. Transcriptome analysis of human autosomal trisomy. *Hum Mol Genet* 2002;11:3249-56.
- Fritah A, Steel JH, Parker N, Nikolopoulou E, Christian M, Carling D, and Parker MG. Absence of RIP140 reveals a pathway regulating glut4-dependent glucose uptake in oxidative skeletal muscle through UCP1-mediated activation of AMPK. *PLoS One* 2012;7, e32520.
- Fritah A, Christian M, and Parker MG. The metabolic coregulator RIP140: an update. *Am. J. Physiol. Endocrinol. Metab.* 2010;299:E335–E340.
- Fullert S, Schneider F, Haak E, Rau H, et al. Effects of pioglitazone in nondiabetic patients with arterial hypertension: a double-blind, placebo-controlled study. *J Clin Endocrinol Metab* 2002;87:5503–5506.
- Gardiner KJ. Pharmacological approaches to improving cognitive function in Down syndrome: current status and considerations. *Drug Des Devel Ther* 2014;9:103-125.
- Gardiner K. Transcriptional dysregulation in Down syndrome: predictions for altered protein complex stoichiometries and post-translational modifications, and consequences for learning/behavior genes ELK, CREB, and the estrogen and glucocorticoid receptors. *Behav Genet* 2006;36:439-53.
- Gardiner K. Predicting pathway perturbations in Down syndrome. *J Neural Transm Suppl* 2003;(67):21-37.
- Glenn MJ, Gibson EM, Kirby ED, Mellott TJ, Blusztajn JK, Williams CL. Prenatal choline availability modulates hippocampal neurogenesis and neurogenic responses to enriching experiences in adult female rats. *Eur J Neurosci* 2007;25:2473–2482.
- Goldberg RB, Kendall DM, Deeg MA, et al. A comparison of lipid and glycemic effects of pioglitazone and rosiglitazone in patients with type 2 diabetes and dyslipidemia. *Diabetes Care* 2005;28:1547–1554.
- Guidi S, Stagni F, Bianchi P, Ciani E, Giacomini A, De Franceschi M, Moldrich R, Kurniawan N, Mardon K, Giuliani A, Calzà L, Bartesaghi R. Prenatal pharmacotherapy rescues brain development in a Down's syndrome mouse model. *Brain* 2014;137(Pt 2):380-401.
- Gunter TE, Yule DI, Gunter KK, Eliseev RA, Salter JD. Calcium and mitochondria 2004; 567:96-102.
- Gwack Y, Sharma S, Nardone J, Tanasa B, Iuga A, Srikanth S, Okamura H, Bolton D, Feske S, Hogan PG, Rao A. A genome-wide *Drosophila* RNAi screen identifies DYRK-family kinases as regulators of NFAT. *Nature* 2006;441:646-50.
- Hallberg M, Morganstein DL, Kiskinis E, Shah K, Kralli A, Dilworth SM, White R, Parker MG, and Christian M. A functional interaction between RIP140 and PGC-1alpha regulates the expression of the lipid droplet protein CIDEA. *Mol. Cell Biol* 2008;28:6785–6795.
- Helguera P, Seiglie J, Rodriguez J, Hanna M, Helguera G. and Busciglio J. Adaptive downregulation of mitochondrial function in down syndrome. *Cell. Metab* 2012;17:132–140.
- Hirose H, Kawai T, Yamamoto Y, et al. Effects of pioglitazone on metabolic parameters, body fat distribution, and serum adiponectin levels in Japanese male patients with type 2 diabetes. *Metab: Clin Exp* 2002;51:314–317.
- Hofer A, Noe N, Tischner C, Kladt N, Lellek V, Schauf A, Wenz T. Defining the action spectrum of potential PGC-1 $\alpha$  activators on a mitochondrial and cellular level in vivo. *Hum Mol Genet.* 2014;23:2400-15.

- Honda Y, Ding X, Mussano F, Wiberg A, Ho CM, Nishimura I. Guiding the osteogenic fate of mouse and human mesenchymal stem cells through feedback system control. *Sci Rep* 2013;3:3420.
- Huo L and Scarpulla RC. Mitochondrial DNA instability and peri-implantation lethality associated with targeted disruption of nuclear respiratory factor 1 in mice. *Mol Cell Biol* 2001;21:644-654.
- Izzo A, Manco R, Bonfiglio F, Cali G, de Cristofaro T, Patergnani S, Cicatiello R, Scrima R, Pinton P, Conti A, Nitsch L. NRIP1/RIP140 siRNA-mediated attenuation counteracts mitochondrial dysfunction in Down syndrome. *Hum Mol Genet* 2014;23:4406-19.
- Jager S, Handschin C, St-Pierre J, and Spiegelman BM. AMP-activated protein kinase (AMPK) action in skeletal muscle via direct phosphorylation of PGC-1alpha. *Proc Natl Acad Sci USA*, 2007;104:12017–12022.
- Jaynes J, Ding X, Xu H, Wong WK, Ho CM. Application of fractional factorial designs to study drug combinations. *Stat Med* 2013;32:307–318.
- Johri A, Calingasan NY, Hennessey TM, Sharma A, Yang L, Wille E, Chandra A, Beal MF. Pharmacologic activation of mitochondrial biogenesis exerts widespread beneficial effects in a transgenic mouse model of Huntington's disease. *Hum Mol Genet* 2012;21:1124-1137.
- Jones MJ, Farré P, McEwen LM, et al. Distinct DNA methylation patterns of cognitive impairment and trisomy 21 in Down syndrome. *BMC Med Genomics* 2013;6:58.
- Kahlem P, Sultan M, Herwig R, Steinfath M, Balzereit D, Eppens B, Saran NG, Pletcher MT, South ST, Stetten G, Lehrach H, Reeves RH, Yaspo ML. Transcript level alterations reflect gene dosage effects across multiple tissues in a mouse model of down syndrome. *Genome Res* 2004;14:1258-1267.
- Kanehisa M, and Goto S. KEGG: kyoto encyclopedia of genes and genomes. *Nucleic Acids Res* 2000;28:27–30.
- Kim SH, Vlkolinskya R, Cairnsb N, and Lubeca G. Decreased levels of complex III core protein 1 and complex V b chain in brains from patients with Alzheimer's disease and Down syndrome. *CMLS* 2000;1810–1816.
- Korenberg JR, Chen XN, Schipper R, Sun Z, Gonsky R, Gerwehr S, Carpenter N, Daumer C, Dignan P, Disteché C et al. Down syndrome phenotypes: the consequences of chromosomal imbalance. *Proc Natl Acad Sci USA* 1994;91:4997-5001.
- Korenberg JR, Kawashima H, Pulst SM, Ikeuchi T, Ogasawara N, Yamamoto K, Schonberg SA, West R, Allen L, Magenis E, et al. Molecular definition of a region of chromosome 21 that causes features of the Down syndrome phenotype. *Am J Hum Genet* 1990;47:236-46.
- Kumar P, Wu H, McBride JL, Jung KE, Kim MH, Davidson BL, Lee SK, Shankar P, Manjunath N. Transvascular delivery of small interfering RNA to the central nervous system. *Nature* 2007;448:39-43.
- Kussmaul L and Hirst J. The mechanism of superoxide production by NADH:ubiquinone oxidoreductase (complex I) from bovine heart mitochondria. *Proc Natl Acad Sci USA* 2006;103:7607–7612.
- Lagouge M, Argmann C, Gerhart-Hines Z, Meziane H, Lerin C, Daussin F, Messadeq N, Milne J, Lambert P, Elliott P, Geny B, Laakso M, Puigserver P and Auwerx J. Resveratrol Improves Mitochondrial Function and Protects against Metabolic Disease by Activating SIRT1 and PGC-1a. *Cell* 2006;127:1109-1122.

- de Lange FJ, Moorman A, Anderson RH, Männer J, Soufan AT, Corrie de Gier-de Vries, Schneider MD, Webb S, van den Hoff M, Christoffels VM. Lineage and Morphogenetic Analysis of the Cardiac Valve. *Circulation Research* 2004;95:645-654.
- Lehman JJ, Barger PM, Kovacs A, Saffitz JE, Medeiros DM, Kelly DP. Peroxisome proliferator-activated receptor gamma coactivator-1 promotes cardiac mitochondrial biogenesis. *J Clin Invest* 2000;106:847-56.
- Leone TC, Lehman JJ, Finck BN, Schaeffer PJ, Wende AR, Boudina S, Courtois M, Wozniak DF, Sambanda N, Bernal-Mizrachi C, et al. PGC-1alpha deficiency causes multi-system energy metabolic derangements: muscle dysfunction, abnormal weight control and hepatic steatosis. *PLoS Biol* 2005;3:e101.
- Li CM, Guo M, Salas M, Schupf N, Silverman W, Zigman WB, Husain S, Warburton D, Thaker H, Tycko B. Cell type-specific overexpression of chromosome 21 genes in fibroblasts and fetal hearts with trisomy 21. *BMC Med Genet* 2006;7:24.
- Li Y and Trush MA. Diphenyleneiodonium, an NAD(P)H oxidase inhibitor, also potently inhibits mitochondrial reactive oxygen species production. *Biochem Biophys Res Commun* 1998;253:295–299.
- Li Z, Yu T, Morishima M, Pao A, LaDuca J, Conroy J, Nowak N, Matsui S-I, Shiraishi I and Yu YE. Duplication of the entire 22.8 Mb human chromosome 21 syntenic region on mouse chromosome 16 causes cardiovascular and gastrointestinal abnormalities. *Hum Mol Genet* 2007;16:1359-1366
- Liu C, Morishima M, Jiang X, Yu T, Meng K, Ray D, Pao A, Ye P, Parmacek MS, Yu YE. Engineered chromosome-based genetic mapping establishes a 3.7 Mb critical genomic region for Down syndrome-associated heart defects in mice. *Hum Genet* 2014;133:743-53.
- Liu C, Belichenko PV, Zhang L, Fu D, Kleschevnikov AM, Baldini A, Antonarakis SE, Mobley WC, Yu YE. Mouse models for Down syndrome-associated developmental cognitive disabilities. *Dev Neurosci*. 2011;33:404-13.
- Lockrow J, Prakasam A, Huang P, Bimonte-Nelson H, Sambamurti K, Granholm AC. Cholinergic degeneration and memory loss delayed by vitamin E in a Down syndrome mouse model. *Exp Neurol* 2009;216:278–289.
- Lott IT. Neurological phenotypes for Down syndrome across the life span. *Prog Brain Res* 2012;197:101–121.
- Lyle R, Gehrig C, Neergaard-Henrichsen C, Deutsch S, Antonarakis SE. Gene expression from the aneuploid chromosome in a trisomy mouse model of down syndrome. *Genome Res* 2004;14:1268-1274.
- Malberg JE, Eisch AJ, Nestler EJ, Duman RS. Chronic antidepressant treatment increases neurogenesis in adult rat hippocampus. *J Neurosci* 2000;20:9104–9110.
- Mao R, Wang X, Spitznagel EL Jr, Frelin LP, Ting JC, Ding H, Kim JW, Ruczinski I, Downey TJ, Pevsner J. Primary and secondary transcriptional effects in the developing human Down syndrome brain and heart. *Genome Biol* 2005;6:R107.
- Marciano DP, Chang MR, Corzo CA, Goswami D, Lam VQ, Pascal BD, and Griffin PR. The therapeutic potential of nuclear receptor modulators for treatment of metabolic disorders: PPARgamma, RORs, and Rev-erbs. *Cell Metab* 2014;19:193 208.

- Matsumoto K, Kamiya N, Suwan K, Atsumi F, Shimizu K, Shinomura T, Yamada Y, Kimata K, Watanabe H. Identification and characterization of versican/PDGF-M aggregates in cartilage. *J Biol Chem* 2006;281:18257-63.
- McCann JC, Hudes M, Ames BN. An overview of evidence for a causal relationship between dietary availability of choline during development and cognitive function in offspring. *Neurosci Biobehav Rev* 2006;30:696–712.
- McCormick MK, Schinzel A, Petersen MB, Stetten G, Driscoll DJ, Cantu ES, Tranebjaerg L, Mikkelsen M, Watkins PC, Antonarakis SE. Molecular genetic approach to the characterization of the "Down syndrome region" of chromosome 21. *Genomics* 1989;5:325-331.
- McCown TJ. Adeno-Associated Virus (AAV) vectors in the CNS. *Current Gene Therapy* 2011;11:181-188.
- Miles MV, Patterson BJ, Chalfonte-Evans ML, Horn PS, et al. Coenzyme Q10 (ubiquinol-10) supplementation improves oxidative imbalance in children with trisomy 21. *Pediatr Neurol* 2007;37:398-403.
- Mitra R, Noguee DP, Zechner JF, Yea K, Gierasch CM, Kovacs A, Medeiros DM, Kelly DP, and Duncan JG. The transcriptional coactivators, PGC-1alpha and beta, cooperate to maintain cardiac mitochondrial function during the early stages of insulin resistance. *J. Mol. Cell. Cardiol* 2012;52:701–710.
- Miwa HE, Gerken TA, Hering TM. Effects of covalently attached chondroitin sulfate on aggrecan cleavage by ADAMTS-4 and MMP-13. *Matrix Biol* 2006;25:534-45.
- Moore CS. Postnatal lethality and cardiac anomalies in Ts65Dn Down syndrome mouse model. *Mammalian Genome* 2006;17:1005-1012.
- Nandadasa S, Foulcer S, Apte SS. The multiple, complex roles of versican and its proteolytic turnover by ADAMTS proteases during embryogenesis. *Matrix Biol*. 2014;35:34-41.
- Nicolakakis N, Aboukassim T, Ongali B, Lecrux C, Fernandes P, Rosa-Neto P, Tong XK, Hamel E. Complete rescue of cerebrovascular function in aged Alzheimer's disease transgenic mice by antioxidants and pioglitazone, a peroxisome proliferator-activated receptor gamma agonist. *J Neurosci* 2008;28:9287-9296.
- Noe N, Dillon L, Lellek V, Diaz F, Hida A, Moraes CT, Wenz T. Bezafibrate improves mitochondrial function in the CNS of a mouse model of mitochondrial encephalopathy. *Mitochondrion* 2013;13:417-426.
- Norris RA, Damon B, Mironov V, Kasyanov V, Ramamurthi A, Moreno-Rodriguez R, Trusk T, Potts JD, Goodwin RL, Davis J, Hoffman S, Wen X, Sugi Y, Kern CB, Mjaatvedt CH, Turner DK, Oka T, Conway SJ, Molkentin JD, Forgacs G, Markwald RR. Periostin regulates collagen fibrillogenesis and the biomechanical properties of connective tissues. *J Cell Biochem* 2007;101:695-711.
- O'Doherty A, Ruf S, Mulligan C, Hildreth, V, Errington, ML, Cooke S, Sesay A, Modino S, Vanes L, Hernandez D, Linehan JM, Sharpe PT, Brandner S, Bliss TV, Henderson DJ, Nizetic D, Tybulewicz VL, Fisher EM. An aneuploid mouse strain carrying human chromosome 21 with Down syndrome phenotypes. *Science* 2005;309:2033–2037.
- O'Leary DA, Pritchard MA, Xu D, Kola I, Hertzog PJ, and Ristevski S. Tissue specific overexpression of the HSA21 gene GABPalpha: implications for DS. *Biochim. Biophys. Acta* 2004;1739:81–87.

- Olson LE, Roper RJ, Sengstaken CL, Peterson EA, Aquino V, Galdzicki Z, Siarey R, Pletnikov M, Moran TH, Reeves RH. Trisomy for the Down syndrome "critical region" is necessary but not sufficient for brain phenotypes of trisomic mice. *Hum Mol Genet* 2007;16:774-782.
- Olson LE, Richtsmeier JT, Leszl J, Reeves RH. A chromosome 21 critical region does not cause specific Down syndrome phenotypes. *Science* 2004;306:687-690.
- Ortiz-Abalia J, Sahun I, Altafaj X, Andreu N, Estivill X, Dierssen M, Fillat C. 2008. Targeting Dyrk1A with AAVshRNA attenuates motor alterations in TgDyrk1A, a mouse model of Down syndrome. *Am J Hum Genet* 83:479-488.
- Park J, Song WJ, Chung KC. Function and regulation of Dyrk1A: towards understanding Down syndrome. *Cell Mol Life Sci* 2009;66:3235–3240.
- Park SC, Mathews RA, Zuberbuhler JR, Rowe RD, Neches WH, Lenox CC. Down syndrome with congenital heart malformation. *Am J Dis Child* 1977; 131:29-33.
- Peiris H, Dubach D, Jessup CF, Unterweger P, Raghupathi R, Muyderman H, Zanin MP, Mackenzie K, Pritchard MA, Keating DJ. RCAN1 Regulates Mitochondrial Function and Increases Susceptibility to Oxidative Stress in Mammalian Cells. *Oxid Med Cell Longev* 2014; 2014:520316.
- Person AD, Klewer SE, Runyan RB. Cell Biology of Cardiac Cushion Development. *Int Rev Cytol* 2005;243:287–335.
- Petrozzi , Ricci G, Giglioli NJ, Siciliano G, and Mancuso M. Mitochondria and neurodegeneration. *Biosci. Rep* 2007;27:87–104.
- Piccoli C, Izzo A, Scrima R, Bonfiglio F, Manco R, Negri R, Quarato G, Cela O, Ripoli M, Prisco M, Gentile F, Cali G, Pinton P, Conti A, Nitsch L, Capitanio N. Chronic Pro-oxidative State and Mitochondrial Dysfunctions are more Pronounced in Fibroblasts from Down Syndrome Foeti with Congenital Heart Defects. *Hum Mol Genet* 2013;22:1218-32.
- Powelka AM, Seth A, Virbasius JV, Kiskinis E, Nicoloso SM, Guilherme A, Tang X, Straubhaar J, Cherniack AD, Parker MG et al. Suppression of oxidative metabolism and mitochondrial biogenesis by the transcriptional corepressor RIP140 in mouse adipocytes. *J. Clin. Invest* 2006;116:125–136.
- Puigserver P, Ribot J, Serra F, Gianotti M, Bonet ML, Nadal-Ginard B, Palou A. Involvement of the retinoblastoma protein in brown and white adipocyte cell differentiation: functional and physical association with the adipogenic transcription factor C/EBPalpha. *Eur J Cell Biol* 1998;77:117-123.
- Rahmani Z, Blouin JL, Creau-Goldberg N, Watkins PC, Mattei JF, Poissonnier M, Prieur M, Chettouh Z, Nicole A, Aurias A et al. Critical role of the D21S55 region on chromosome 21 in the pathogenesis of Down syndrome. *Proc Natl Acad Sci U S A* 1989;86:5958-5962.
- Reeves RH, Irving NG, Moran TH, Wohn A, Kitt C, Sisodia SS, Schmidt C, Bronson RT and Davisson MT. A mouse model for Down syndrome exhibits learning and behaviour deficits. *Nat Genet* 1995;11:177–184.
- Roat E, Prada N, Ferraresi R, Giovenzana C, Nasi M, Troiano L, Pinti M, Nemes E, Lugli E, Biagioni O, Mariotti M, Ciacci L, Consolo U, Balli F, Cossarizza A. Mitochondrial alterations and tendency to apoptosis in peripheral blood cells from children with Down syndrome. *FEBS letters* 2007;581:521-525.
- Rodgers JT, Lerin C, Haas W, Gygi SP, Spiegelman SP, and Puigserver P. Nutrient control of glucose homeostasis through a complex of PGC-1alpha and SIRT1. *Nature* 2005;434:113–118.

- Roper RJ, Baxter LL, Saran NG, Klinedinst DK, Beachy PA, Reeves RH. Defective cerebellar response to mitogenic Hedgehog signaling in Down [corrected] syndrome mice. *Proc Natl Acad Sci U S A* 2006;103:1452–1456.
- Rytinki MM, and Palvimo JJ. SUMOylation attenuates the function of PGC-1alpha. *J. Biol. Chem.*, 2009;284:26184–26193.
- Russell LK, Mansfield CM, Lehman JJ, Kovacs A, Courtois M, Saffitz JE, Medeiros DM, Valencik ML, McDonald JA, Kelly DP. Cardiac-Specific Induction of the Transcriptional Coactivator Peroxisome Proliferator-Activated Receptor  $\gamma$  Coactivator-1 $\alpha$  Promotes Mitochondrial Biogenesis and Reversible Cardiomyopathy in a Developmental Stage-Dependent Manner. *Circ Res* 2004;94:525-533.
- Sago H, Carlson EJ, Smith DJ, Kilbridge J, Rubin EM, Mobley WC, Epstein CJ, Huang TT. Ts1Cje, a partial trisomy 16 mouse model for Down syndrome, exhibits learning and behavioral abnormalities. *Proc Natl Acad Sci U S A* 1998;95:6256–6261.
- Sauerbeck A, Gao J, Readnower R, Liu M, Pauly JR, Bing G, Sullivan P. Pioglitazone attenuates mitochondrial dysfunction, cognitive impairment, cortical tissue loss, and inflammation following traumatic brain injury. *Exp Neurol* 2011;227:128-135.
- Scarpulla, R.C., Vega, R.B. and Kelly, D.P. Transcriptional integration of mitochondrial biogenesis. *Trends Endocrinol. Metab.*, 2012; 23, 459–466.
- Scarpulla, R.C. Metabolic control of mitochondrial biogenesis through the PGC-1 family regulatory network. *Biochim. Biophys. Acta* 2011;1813:1269–1278.
- Schuchmann S and Heinemann U. Increased mitochondrial superoxide generation in neurons from trisomy 16 mice: a model of Down's syndrome. *Free Radic Biol Med.* 2000; 28:235-250.
- Schreiber, S.N., Emter, R., Hock, M.B., Knutti, D., Cardenas, J., Podvinec, M., Oakeley, E.J. and Kralli, A. The estrogen-related receptor alpha (ERRalpha) functions in PPARgamma coactivator 1alpha (PGC-1alpha)-induced mitochondrial biogenesis. *Proc. Natl Acad. Sci. USA*, 2004;101, 6472–6477.
- Seth, A., Steel, J.H., Nichol, D., Pocock, V., Kumaran, M.K., Fritah, A., Mobberley, M., Ryder, T.A., Rowlerson, A., Scott, J. et al. The transcriptional corepressor RIP140 regulates oxidative metabolism in skeletal muscle. *Cell Metab* 2007;6:236–245.
- Shin JH, London J, Le Pecheur M, Hoger H, Pollak D, Lubec G. Aberrant neuronal and mitochondrial proteins in hippocampus of transgenic mice overexpressing human Cu/Zn superoxide dismutase 1. *Free Radic Biol Med* 2004;37:643-53.
- Shinohara T, Tomizuka K, Miyabara S, Takehara S, Kazuki Y, Inoue J, Katoh M, Nakane H, Iino A, Ohguma A, Ikegami S, Inokuchi K, Ishida I, Reeves RH, Oshimura M. Mice containing a human chromosome 21 model behavioral impairment and cardiac anomalies of Down's syndrome. *Hum Mol Genet* 2001;10:1163–1175.
- Shokolenko I, Susan LeDoux, Glenn Wilson and Mikhail Alexeyev. Mitochondrial DNA Damage, Repair, Degradation and Experimental Approaches to Studying These Phenomena 2011;307:649-2.
- Shukkur EA, Shimohata A, Akagi T, Yu W, Yamaguchi M, Murayama M, Chui D, Takeuchi T, Amano K, Subramhanya KH, Hashikawa T, Sago H, Epstein CJ, Takashima A and Yamakawa K. Mitochondrial dysfunction and tau

- hyperphosphorylation in Ts1Cje, a mouse model for Down syndrome. *Hum Mol Genet* 2006;15:2752-2762.
- Siarey RJ, Kline-Burgess A, Cho M, Balbo A, Best TK, Harashima C, Klann E, Galdzicki Z. Altered signaling pathways underlying abnormal hippocampal synaptic plasticity in the Ts65Dn mouse model of Down syndrome. *J Neurochem*. 2006;98:1266-77.
  - Siddiqui A, Lacroix T, Stasko MR, Scott-McKean JJ, Costa AC, Gardiner KJ. Molecular responses of the Ts65Dn and Ts1Cje mouse models of Down syndrome to MK-801. *Genes Brain Behav* 2008;7:810–820.
  - Snarr BS, Kern CB, Wessels A. Origin and fate of cardiac mesenchyme. *Dev Dyn* 2008;237:2804-2819.
  - Snarr BS, Wirrig EE, Phelps AL, Trusk TC and Wessels A. A spatiotemporal evaluation of the contribution of the dorsal mesenchymal protrusion to cardiac development. *Developmental Dynamics* 2007;5:1287–1294.
  - Sommer CA and Henrique-Silva F. Trisomy 21 and Down syndrome *Braz. J. Biol.* 2008;68: 447-452, 449.
  - Sturgeon X, Le T, Ahmed MM, Gardiner KJ. Pathways to cognitive deficits in Down syndrome. *Prog Brain Res.* 2012;197:73–100.
  - Johri A, Calingasan NY, Hennessey TM, Sharma A, Yang L, Wille E, Chandra A, Beal MF. Pharmacologic activation of mitochondrial biogenesis exerts widespread beneficial effects in a transgenic mouse model of Huntington's disease. *Hum Mol Genet* 2012;21:1124-1137.
  - Tiano L, Carnevali P, Padella L, et al. Effect of Coenzyme Q10 in mitigating oxidative DNA damage in Down syndrome patients, a double blind randomized controlled trial. *Neurobiol Aging* 2011;32:2103-2105.
  - Valenti D, Manente GA., Moro L, Marra E and Vacca RA. Deficit of complex I activity in human skin fibroblasts with chromosome 21 trisomy and overproduction of reactive oxygen species by mitochondria: involvement of the cAMP/PKA signaling pathway. *Biochem J* 2011;435:679-688.
  - Valenti, D., Tullo, A., Caratozzolo, M.F., Merafina, R.S., Scartezzini, P., Marra, E. and Vacca, R.A. Impairment of F1F0-ATPase, adenine nucleotide translocator and adenylate kinase causes mitochondrial Energy deficit in human skin fibroblasts with chromosome 21 trisomy. *Biochem. J* 2010;431: 299–310.
  - Viscomi C, Bottani E, Civiletto G, Cerutti R, Moggio M, Fagiolari G, Schon EA, Lamperti C, Zeviani M. In vivo correction of COX deficiency by activation of the AMPK/PGC-1 $\alpha$  axis. *Cell Metab.* 2011;14:80-90.
  - Vo N, Fjeld C, and Goodman RH. Acetylation of nuclear hormone receptor-interacting protein RIP140 regulates binding of the transcriptional corepressor CtBP. *Mol Cell Biol* 2001;21:6181-6188.
  - Wang J, Duncan D, Shi Z, Zhang B. WEB-based GENE SeT AnaLysis Toolkit (WebGestalt). *Nucleic Acids Res*, 2013;41:W77-83.
  - Watanabe H, Yamada Y. Mice lacking link protein develop dwarfism and craniofacial abnormalities. *Nat Genet* 1999;21:225-9.
  - Watson GS, Cholerto BA, Reger MA, Baker LD, Plymate SR, Asthana S, Fishel MA, Kulstad JJ, Green PS, Cook DG et al. Preserved cognition in patients with early Alzheimer disease and amnesic mild cognitive impairment during treatment with rosiglitazone: a preliminary study. *Am. J. Geriatr. Psychiatr* 2005;13:950–958.
  - Weich S, Bebbington P, Rai D, Stranges S, McBride O, Spiers N, Meltzer H, Brugha T. The population impact of common mental disorders and long-term

- physical conditions on disability and hospital admission. *Psychol Med* 2013;43:921-31.
- Wenz T, Diaz F, Spiegelman BM, Moraes CT. Activation of the PPAR/PGC-1alpha pathway prevents a bioenergetic deficit and effectively improves a mitochondrial myopathy phenotype. *Cell Metab* 2008;8:249-256.
  - Wessels A, Markman MW, Vermeulen JL, Anderson RH, Moorman AF, Lamers WH. The development of the atrioventricular junction in the human heart. *Circulation Research* 1996;78:110-117.
  - White R, Parker MG, Christian M. A functional interaction between RIP140 and PGC-1alpha regulates the expression of the lipid droplet protein CIDEA. *Mol Cell Biol* 2008;28:6785-6795.
  - Wight TN, Merrilees MJ. Proteoglycans in atherosclerosis and restenosis: key roles for versican. *Circ Res* 2004;94:1158-67.
  - Wirrig EE, Snarr BS, Chintalapudi MR, O'neal JL, Phelps AL, Barth JL, Fresco VM, Kern CB, Mjaatvedt CH, Toole BP, Hoffman S, Trusk TC, Argraves WS, Wessels A. Cartilage link protein 1 (Crtl1), an extracellular matrix component playing an important role in heart development. *Dev Biol* 2007;310:291-303.
  - Worgall S, Sondhi D, Hackett NR, Kosofsky B, Kekatpure MV, Neyzi N, Dyke JP, Ballon D, Heier L, Greenwald BM, Christos P, Mazumdar M, Souweidane MM, Kaplitt MG, Crystal RG. Treatment of late infantile neuronal ceroid lipofuscinosis by CNS administration of a serotype 2 adeno-associated virus expressing CLN2 cDNA. *Hum Gene Ther* . 2008;19:463-474.
  - Wotton S, Terry A, Kilbey A, Jenkins A, Herzyk P, Cameron E, Neil JC. Gene array analysis reveals a common Runx transcriptional programme controlling cell adhesion and survival. *Oncogene* 2008;27:5856-5866.
  - Wright TC, Orkin RW, Destrepes M, Kurnit DM. Increased adhesiveness of Down syndrome fetal fibroblasts in vitro. *Proc Natl Acad Sci U S A*. 1984;81:2426-30.
  - Yamaguchi, S., Li, H., Purevsuren, J., Yamada, K., Furui, M., Takahashi, T., Mushimoto, Y., Kobayashi, H., Hasegawa, Y., Taketani, T. et al. Bezafibrate can be a new treatment option for mitochondrial fatty acid oxidation disorders: evaluation by in vitro probe acylcarnitine assay. *Mol Genet Metab* 2012;107:87–91.
  - Yamato F, Takaya J, Yasuhara A, Teraguchi M, Ikemoto Y, Kaneko K. Elevated intracellular calcium in neutrophils in patients with Down syndrome. *Pediatr Int* 2009;51:474-7.
  - Yan W, Shao R. Transduction of a mesenchyme-specific gene periostin into 293T cells induces cell invasive activity through epithelial-mesenchymal transformation. *J Biol Chem* 2006;281:19700-19708.
  - Yatsuga S, Suomalainen A. Effect of bezafibrate treatment on late-onset mitochondrial myopathy in mice. *Hum Mol Genet* 2012;21:526-535.
  - Zabel MD. Lipopeptide Delivery of siRNA to the Central Nervous System; Nanotechnology for Nucleic Acid Delivery. *Methods Mol Biol* 2013;948:251-262.
  - Zaffran S, Kelly RG. New developments in the second heart field. *Differentiation* 2012;84:17-24.
  - Zambelli F, Pesole G, Pavesi G. Pscan: finding over-represented transcription factor binding site motifs in sequences from co-regulated or co-expressed genes. *Nucleic Acids Res*. 2009;37:W247-252

- Zhang B, Kirov S, Snoddy J. WebGestalt: an integrated system for exploring gene sets in various biological contexts. *Nucleic Acids Res* 2005;33:W741-748.

## APPENDIX 1

**TABLE S1 List of genes encoding mitochondrial proteins downregulated in DS fetal hearts.**

<b>Affymetrix Probe ID</b>	<b>DSH/NH ratio</b>	<b>Gene Name</b>	<b>Genbank ID</b>
214274_s_at	0.647	ACAA1	AI860341
215210_s_at	0.548	ACADM	S72422
205412_at	0.756	ACAT1	NM_000019
208967_s_at	0.757	AK2	U39945
201322_at	0.739	ATP5B	NM_001686
208972_s_at	0.739	ATP5G1	AL080089
211715_s_at	0.554	BDH1	BC005844
205295_at	0.699	CKMT2	NM_001825
209746_s_at	0.721	COQ7	AF032900
203858_s_at	0.74	COX10	NM_001303
218057_x_at	0.738	COX4NB	BC001472
201597_at	0.764	COX7A2	NM_001865
201633_s_at	0.727	CYB5B	AW235051
208905_at	0.702	CYCS	BC005299
209759_s_at	0.729	DCI	BC002746
211150_s_at	0.568	DLAT	J03866
204824_at	0.638	ENDOG	NM_004435
201931_at	0.698	ETFA	NM_000126
202942_at	0.692	ETFB	NM_001985
213133_s_at	0.713	GCSH	AW237404
221415_s_at	0.545	GJA10	NM_030772
200947_s_at	0.758	GLUD1	NM_005271
208813_at	0.671	GOT1	BC000498
203745_at	0.678	HCCS	AI801013
200691_s_at	0.645	HSPA9B	NM_004134
210046_s_at	0.743	IDH2	U52144
202070_s_at	0.709	IDH3A	NM_005530
210418_s_at	0.751	IDH3B	AF023265
200955_at	0.704	IMMT	NM_006839
36830_at	0.711	MIPEP	U80034
219527_at	0.701	MOSC2	NM_017898
218027_at	0.716	MRPL15	NM_014175
203781_at	0.741	MRPL33	NM_004891
218890_x_at	0.745	MRPL35	NM_016622
204331_s_at	0.735	MRPS12	AA587905
220864_s_at	0.638	NDUFA13	NM_015965

202077_at	0.748	NDUFAB1	NM_005003
218201_at	0.669	NDUFB2	NM_004546
201226_at	0.663	NDUFB8	NM_005004
201966_at	0.62	NDUFS2	NM_004550
201740_at	0.72	NDUFS3	NM_004551
201757_at	0.763	NDUFS5	NM_004552
202941_at	0.76	NDUFV2	NM_021074
218455_at	0.712	NFS1	NM_021100
202780_at	0.705	OXCT1	NM_000436
200980_s_at	0.598	PDHA1	BF739979
214225_at	0.677	PIN4	BE674061
203649_s_at	0.657	PLA2G2A	NM_000300
205241_at	0.724	SCO2	NM_005138
201093_x_at	0.591	SDHA	NM_004168
202675_at	0.744	SDHB	NM_003000
202004_x_at	0.722	SDHC	NM_003001
203340_s_at	0.688	SLC25A12	AI887457
217961_at	0.705	SLC25A38	NM_017875
202825_at	0.607	SLC25A4	NM_001151
216841_s_at	0.734	SOD2	X15132
218119_at	0.634	TIMM23	NM_006327
203092_at	0.612	TIMM44	AF026030
220415_at	0.635	TNNI3K	NM_015978
209077_at	0.74	TXN2	AL022313
201903_at	0.75	UQCRC1	NM_003365
200883_at	0.716	UQCRC2	NM_003366
208909_at	0.744	UQCRFS1	BC000649
217140_s_at	0.637	VDAC1	AJ002428
217249_x_at	0.68	WUGSC:H_RG162B04.1	AC004544

**TABLE S2 List of genes encoding ECM proteins overexpressed in DSH.**

Affymetrix Probe ID	DSH/NH ratio	Gene name	GenBank ID
222162_s_at	1.93	<b>ADAMTS1</b>	AK023795
219935_at	1.5	<b>ADAMTS5</b>	NM_007038
220706_at	2.24	ADAMTS7	NM_014272
214953_s_at	1.668	<b>APP</b>	X06989
219087_at	1.829	ASPN	NM_017680
220988_s_at	1.466	C1QTNF3	NM_030945
219025_at	1.342	CD248	NM_020404
211809_x_at	1.721	COL13A1	M59217
203477_at	1.413	COL15A1	NM_001855
209081_s_at	1.57	COL18A1	AF018081
202310_s_at	1.546	COL1A1	K01228
202403_s_at	1.596	COL1A2	NM_000089
212489_at	1.595	COL5A1	AI983428
212091_s_at	1.927	<b>COL6A1</b>	AI141603
209156_s_at	2.391	<b>COL6A2</b>	AY029208
213622_at	1.434	COL9A2	AI733465
204724_s_at	1.6	COL9A3	NM_001853
207420_at	4.268	COLEC10	NM_006438
209335_at	1.73	DCN	BC005322
213661_at	1.516	DKFZP586H2123	AI671186
206101_at	1.554	ECM2	NM_001393
202994_s_at	1.716	FBLN1	Z95331
204359_at	1.522	FLRT2	NM_013231
209220_at	1.685	GPC3	L47125
206766_at	1.378	ITGA10	AF112345
216190_x_at	3.591	ITGB1	AA215854
204989_s_at	2.269	ITGB4	BF305661
221462_x_at	3.113	KLK15	NM_017509
202202_s_at	1.591	LAMA4	NM_002290
203417_at	1.434	MFAP2	NM_017459
203877_at	1.673	MMP11	NM_005940
201069_at	1.586	MMP2	NM_004530
205907_s_at	1.961	OMD	AI765819
202465_at	1.482	PCOLCE	NM_002593
218585_s_at	1.48	RAMP	AK001261
218452_at	1.859	SMARCAL1	NM_014140
205236_x_at	1.372	SOD3	NM_003102
208606_s_at	2.534	WNT4	NM_030761

**In bold are shown Hsa21 ECM genes.**

# NRIP1/RIP140 siRNA-mediated attenuation counteracts mitochondrial dysfunction in Down syndrome

Antonella Izzo<sup>1,†</sup>, Rosanna Manco<sup>1,†</sup>, Ferdinando Bonfiglio<sup>1,†</sup>, Gaetano Cali<sup>2</sup>, Tiziana De Cristofaro<sup>2</sup>, Simone Patergnani<sup>3</sup>, Rita Cicatiello<sup>1</sup>, Rosella Scrima<sup>4</sup>, Mariastella Zannini<sup>2</sup>, Paolo Pinton<sup>3</sup>, Anna Conti<sup>1,\*</sup> and Lucio Nitsch<sup>1</sup>

<sup>1</sup>Department of Molecular Medicine and Medical Biotechnology, University of Naples Federico II, Via Pansini 5, Naples 80131, Italy, <sup>2</sup>Institute of Experimental Endocrinology and Oncology, National Research Council, Naples 80131, Italy, <sup>3</sup>Department of Experimental and Diagnostic Medicine, University of Ferrara, Ferrara 44100, Italy and <sup>4</sup>Department of Clinical and Experimental Medicine, University of Foggia, Foggia 71100, Italy

Received February 20, 2014; Revised March 24, 2014; Accepted March 31, 2014

**Mitochondrial dysfunction, which is consistently observed in Down syndrome (DS) cells and tissues, might contribute to the severity of the DS phenotype. Our recent studies on DS fetal hearts and fibroblasts have suggested that one of the possible causes of mitochondrial dysfunction is the downregulation of peroxisome proliferator-activated receptor gamma, coactivator 1 alpha (*PGC-1α* or *PPARGC1A*)—a key modulator of mitochondrial function—and of several nuclear-encoded mitochondrial genes (NEMGs). Re-analysis of publicly available expression data related to manipulation of chromosome 21 (Hsa21) genes suggested the nuclear receptor interacting protein 1 (*NRIP1* or *RIP140*) as a good candidate Hsa21 gene for NEMG downregulation. Indeed, *NRIP1* is known to affect oxidative metabolism and mitochondrial biogenesis by negatively controlling mitochondrial pathways regulated by *PGC-1α*. To establish whether *NRIP1* overexpression in DS downregulates both *PGC-1α* and NEMGs, thereby causing mitochondrial dysfunction, we used siRNAs to decrease *NRIP1* expression in trisomic human fetal fibroblasts. Levels of *PGC-1α* and NEMGs were increased and mitochondrial function was restored, as shown by reactive oxygen species decrease, adenosine 5'-triphosphate (ATP) production and mitochondrial activity increase. These findings indicate that the Hsa21 gene *NRIP1* contributes to the mitochondrial dysfunction observed in DS. Furthermore, they suggest that the *NRIP1-PPGC-1α* axis might represent a potential therapeutic target for restoring altered mitochondrial function in DS.**

## INTRODUCTION

Data from several studies show that trisomy of chromosome 21 (TS21) affects both mitochondrial function and reactive oxygen species (ROS) production. Lower levels of the mitochondrial complexes I, III and V have been observed in the cerebellar and brain regions of subjects affected by Down syndrome (DS) (1). Moreover, reduced mitochondrial redox activity and membrane potential have been observed in DS astrocytes and neuronal cultures (2,3). Further evidence for mitochondrial dysfunction was found in the Ts1Cje mouse model for DS that shows decreased levels of ATP production (4). Similarly, fetal DS fibroblasts show both a decreased efficiency of the mitochondrial

energy production apparatus, involving adenine nucleotide translocators, ATP synthase, and adenylate kinase and a selective deficit of complex I, which might contribute to ROS overproduction by DS mitochondria. These events were correlated with changes in the cAMP/PKA signaling pathway (5,6). Similar research conducted on human primary lines of fibroblasts (HFFs) from TS21 fetuses has revealed that TS21 disrupts mitochondrial morphology, decreases oxygen consumption, increases mtCa<sup>2+</sup> load and ROS production (7). Moreover, by analyzing mitochondrial defects according to the cardiac phenotype, a more severe mitochondrial dysfunction was evidenced in cardiopathic-derived TS21 fibroblasts (7). A possible interpretation of these results is

\*To whom correspondence should be addressed. Tel: +39 0817463261; Fax: +39 0817463656; Email: anconti@unina.it

†The authors wish to be known that, in their opinion, the first three authors should be regarded as joint First Authors.

that a more pronounced pro-oxidative state might contribute to generating a more severe cardiac phenotype—a concept that might be extended to other phenotypic traits. Studies of genome-wide expression analysis in DS have demonstrated that nuclear-encoded mitochondrial genes (NEMGs) represent the main downregulated category in fetal TS21 heart samples (8). Downregulation is also manifest in DS fetal brains (9). These observations led us to hypothesize that NEMG dysregulation is likely a cause of mitochondrial dysfunction in DS (8). Among the dysregulated genes, the peroxisome proliferator-activated receptor gamma, coactivator 1 alpha (*PGC-1 $\alpha$* /*PPARGC1A*) has been found hypo-expressed at the transcriptional and protein levels in TS21 HFFs (7). *PGC-1 $\alpha$*  is indeed known to play a central role in regulating mitochondrial biogenesis and respiratory function through the interaction with transcriptional partners, such as *NRF1*, *ERR $\alpha$* , *PPARs* and *YY1* (10).

A known repressor of *PGC-1 $\alpha$*  activity is the nuclear receptor interacting protein 1 (*NRIP1*/*RIP140*) (11–13). This protein is coded by a highly conserved chromosome 21 (Hsa21) gene with consistent dosage effect in many studies on DS samples (14). *NRIP1* acts as a scaffold protein recruiting regulatory factors, such as histone deacetylases (15), COOH terminal binding protein (16) and histone methyltransferases (17), to exert its co-repressive function. Furthermore, *NRIP1* directly interacts with some nuclear receptors including *PPARs*, *ERRs* and *ERs* (18–20). More specifically, *NRIP1* negatively controls the expression and the activity of *PGC-1 $\alpha$*  as well as the expression of its targets. Indeed, in *PGC-1 $\alpha$*  null mice (21,22), as well as in knock-in *NRIP1* mice (23), NEMG expression is decreased. Likewise, *NRIP1* is always upregulated by 1.5- to 4-fold in the heart (8) and fibroblasts (7) from DS fetuses. *NRIP1* protein is also increased in the hippocampal tissue from DS subjects (24).

Thus, building upon previous research, in this study, we endeavored to provide new insights into the transcriptional changes influencing the molecular mechanisms associated with mitochondrial dysfunction in DS. In particular, we first investigated whether Hsa21 gene overexpression causes NEMG downregulation by focusing on those Hsa21 genes, transcription factors, and kinases that have the highest probability of affecting the expression of many genes. To this aim, we analyzed the public expression data related to the manipulation of Hsa21 genes to investigate their effects on NEMG downregulation. These analyses led us to the identification of *NRIP1* as a good candidate for the downregulation of mitochondria-related genes in DS.

Then, to determine whether *NRIP1* downregulation can effectively counteract mitochondrial dysfunction and some of its pathophysiological effects, we attenuated *NRIP1* expression in human fibroblasts from DS fetuses (DS-HFFs).

Understanding the molecular correlation between *NRIP1* expression levels, NEMG regulation, and mitochondrial function could lay the basis for the development of new therapeutic protocols for DS.

## RESULTS

### Analysis of public expression data suggests that *NRIP1* affects NEMG expression

Several Hsa21 genes can possibly interfere with NEMG expression. For instance, *DYRK1A* and *DSCR1*/*RCAN1* play key roles

in the calcineurin/*NFAT* pathway, which affects mitochondrial activity and morphology during heart development (25). Two more genes, *NRIP1* (23) and *GABPA*/*NRF2* (26) are also involved in mitochondrial pathways.

To identify which Hsa21 gene might possibly downregulate NEMG expression, we screened the Gene Expression Omnibus (27) repository (<http://www.ncbi.nlm.nih.gov/geo>) for gene expression data related to the modulation of Hsa21 genes. We selected the GEO GSE 19836 experiment (28), a set of data derived from a mouse embryonic stem cell (ESC) bank in which several orthologs of Hsa21 genes, with potential regulatory role, are individually overexpressed in an inducible manner. Expression data were available for 13 transcription factors (including *NRIP1*, *RCAN1* and *GABPA*), the transcriptional activator *RCAN1* and six protein kinases (including *DYRK1A*) (for details see Materials and Methods). We re-analyzed this series of data by focusing on the mitochondria-related categories and pathways dysregulated by the overexpression of each gene looking for Hsa21 genes that when overexpressed would induce NEMG downregulation. Among the 20 analyzed Hsa21 genes, only *NRIP1*, one of the seven genes that are considered ‘effective’ for the expression perturbation in the manipulated cells (28), was able to cause NEMG downregulation when overexpressed. Our analysis showed that *NRIP1* overexpression caused a significant enrichment of NEMGs among 298 downregulated genes. The ‘Mitochondrion’ was the most affected Cell Component Gene Ontology (GO) category ( $P < 0.0001$ ) (Table 1 and Supplementary Material, Fig. S1), with a cluster of 37 downregulated genes. Motif enrichment analysis, by clustering downregulated genes on the basis of their promoter regions, revealed a significant enrichment ( $P < 0.005$ ) in genes with the *ERR $\alpha$*  motif. Twenty-five downregulated genes, instead of the expected 10, showed promoter regions around the transcription start site containing the *ERR $\alpha$*  motif.

Neither *DYRK1A*, nor *RCAN1*, nor *GABPA*, all considered ‘silent’ genes (28), caused NEMG downregulation when overexpressed.

### Modulation of *NRIP1* and *PGC-1 $\alpha$* expression dysregulates the same NEMGs downregulated in DS fetal hearts

To investigate whether the sets of genes regulated by *NRIP1* and/or *PGC-1 $\alpha$*  showed any overlapping to the NEMGs downregulated in DS fetal hearts (8), we performed a meta-analysis comparing three sets of gene expression data, SET1, SET2 and SET3. SET1 included 123 genes which were both upregulated after *NRIP1* silencing and downregulated after *NRIP1* re-expression in mouse adipocytes (29). SET2 included 129 genes which were upregulated after *PGC-1 $\alpha$*  induction in SAOS2 cells (human osteoblast-like cells) (30). SET3 included the 70 genes downregulated in DS fetal heart tissues (8) belonging to the ‘mitochondrion’ GO category (Supplementary Material, Table S1). The comparison was aimed at identifying genes consistently dysregulated across these studies.

The Venn Diagram shows that NEMGs in SET3, which were downregulated in DS fetal hearts, overlap with both SET1 and SET2 (Fig. 1A). The three sets of genes overlap each other for at least 25 genes. Fifteen genes are consistently dysregulated across all three experiments (Fig. 1B). Most of these genes are included in the electron transport chain, mainly in complex I,

**Table 1.** Gene Ontology categories affected by NRIP1 overexpression in GSE 19836 series with a *P*-value < 0.05

Biological process	GO category	Genes in category	Observed	Expected	O/R ratio	<i>P</i> -value
Carboxylic acid metabolic process	GO:0019752	630	20	7.51	2.66	0.0089
Cellular carbohydrate metabolic process	GO:0044262	198	11	2.36	4.66	0.0089
Monocarboxylic acid metabolic process	GO:0032787	339	14	4.04	3.47	0.0089
Carboxylic acid catabolic process	GO:0046395	139	8	1.66	4.83	0.0100
Organic acid catabolic process	GO:0016054	139	8	1.66	4.83	0.0100
Regulation of transmembrane receptor protein serine/threonine kinase signaling pathway	GO:0090092	137	8	1.63	4.9	0.0100
Carbohydrate metabolic process	GO:0005975	527	17	6.28	2.71	0.0100
Lipid metabolic process	GO:0006629	881	23	10.5	2.19	0.0100
Oxoacid metabolic process	GO:0043436	667	20	7.95	2.52	0.0100
Organic acid metabolic process	GO:0006082	680	20	8.1	2.47	0.0100
Molecular function						
Kinase activity	GO:0016301	736	21	9.07	2.32	0.0219
Transferase activity	GO:0016740	1574	34	19.4	1.75	0.0328
Transferase activity, transferring phosphorus-containing groups	GO:0016772	857	21	10.56	1.99	0.0511
Cofactor binding	GO:0048037	244	9	3.01	2.99	0.0602
Cellular component						
Mitochondrion	GO:0005739	1480	37	17.7	2.09	0.0009
Mitochondrial envelope	GO:0005740	446	17	5.34	3.19	0.0010
Mitochondrial membrane	GO:0031966	424	16	5.07	3.15	0.0013
Organelle inner membrane	GO:0019866	330	13	3.95	3.29	0.0036
Mitochondrial part	GO:0044429	548	17	6.56	2.59	0.0043
Mitochondrial inner membrane	GO:0005743	312	12	3.73	3.22	0.0047
Organelle envelope	GO:0031967	671	18	8.03	2.24	0.0122
Envelope	GO:0031975	683	18	8.17	2.2	0.0133
Mitochondrial outer membrane	GO:0005741	111	6	1.33	4.52	0.0174
Organelle outer membrane	GO:0031968	125	6	1.5	4.01	0.0277

The 'Mitochondrion' is the category most affected by *NRIP1* upregulation (enrichment = 37 observed genes instead of 17.7 expected genes with *P* < 0.001).

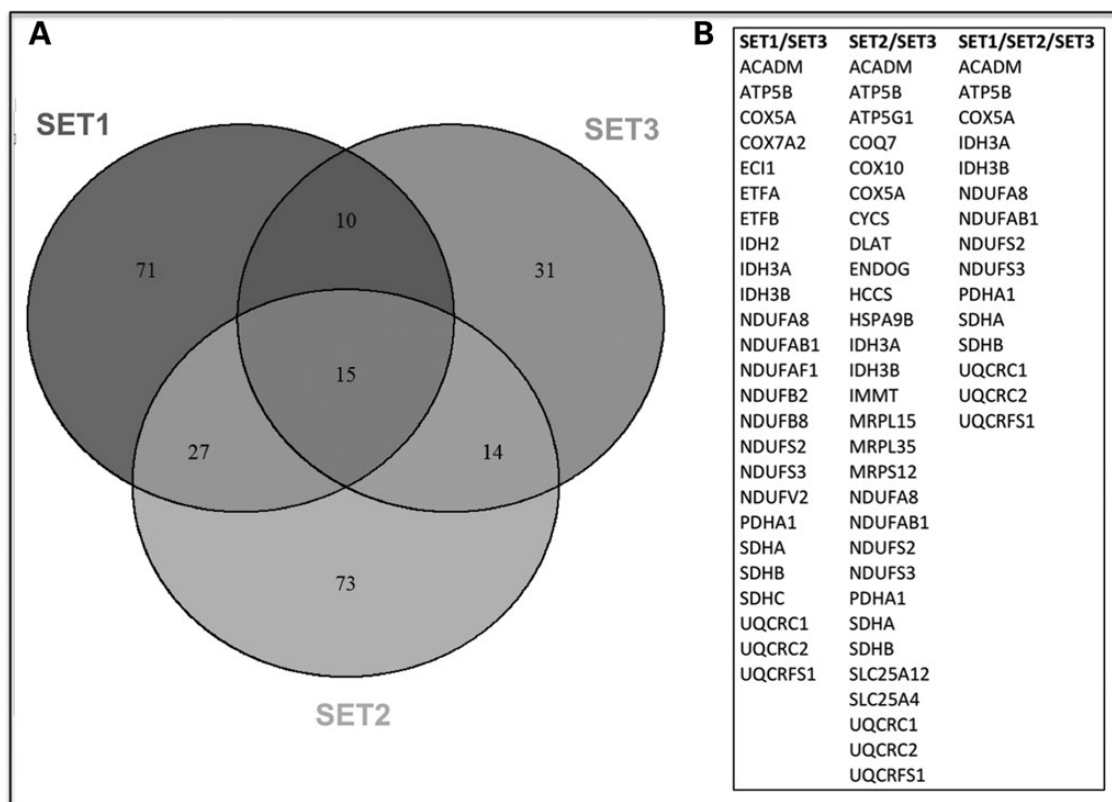


**Figure 1.** Comparison of NEMGs downregulated in DS fetal hearts with those dysregulated by *NRIP1* and/or *PGC-1α*. (A) Venn diagram showing overlapping among the three sets of data. Out of the 70 mitochondrial genes that are downregulated in DS fetal hearts (SET3) (8), 25 overlap the list of *NRIP1* regulated genes (SET1) (29) and 29 overlap the list of *PGC-1α* regulated genes (SET2) (30). (B) List of mitochondria-related genes overlapping in the three sets of data. The complete lists of genes are in Supplementary Material, Table S1.

and in oxidative phosphorylation pathways. It is also interesting to note that 42 genes overlap between the sets of genes inversely regulated by *NRIP1* and *PGC-1 $\alpha$*  (SET1 and SET2), in agreement with the antagonistic functions of the two coregulators (19).

### *NRIP1* attenuation by siRNA affects NEMG expression in DS-HFFs

We previously demonstrated that *NRIP1* is upregulated in DS-HFFs in which Hsa21 trisomy negatively regulates NEMGs and impairs mitochondrial function (7).

To test the hypothesis that *NRIP1* overexpression perturbs mitochondrial function and that this effect is associated with *PGC-1 $\alpha$*  downregulation, we performed silencing experiments of *NRIP1* gene in DS-HFFs. In brief, after re-analyzing all DS-HFF lines used for silencing experiments, we demonstrated that *NRIP1* is significantly upregulated in all trisomic samples if compared with euploid controls (Fig. 2A). Seventy-two hours after transfection of a specific SMART pool of siRNAs in DS-HFFs, an inverse correlation between *NRIP1* and *PGC-1 $\alpha$*  expression, in a siRNA dosage-dependent way, was demonstrated by qRT-PCR (Fig. 2B). By immunofluorescence analysis, we demonstrated that the NRIP1 protein localizes to the cell nucleus, as expected for a corepressor protein, both in euploid and in trisomic fibroblasts (Fig. 3). Fluorescent signal was more intense over nuclei of DS-HFFs (Fig. 3B) with respect to euploid HFFs (Fig. 3A), indicating a higher concentration of the NRIP1 protein in trisomic cells. In these cells, some fluorescent signal was also present over the cytoplasm (Fig. 3B) likely due to the overexpression of the NRIP1 protein. In DS-HFFs treated with siRNAs to attenuate *NRIP1* mRNA expression, NRIP1 fluorescent signal was significantly decreased in a siRNA dosage-dependent way (Fig. 3). Quantitative evaluation of fluorescence intensities in euploid, trisomic and siRNA transfected cells (Fig. 3F) indicated that siRNA transfection reduces NRIP1 protein levels of trisomic cells down to the range of diploid cells or even lower (Fig. 3D and E).

To determine the effects of *NRIP1* attenuation by siRNA on other mitochondria-related genes, we compared the expression of seven genes in silenced versus scrambled cells using qRT-PCR. Three genes, i.e. *COX5A*, *NDUFA1* and *NDUFS3*, were chosen from the list of 15 genes that resulted consistently dysregulated across the three sets compared in the meta-analysis (Fig. 1). The fourth gene, *NRF1*, which is downregulated in DS hearts (8) and fibroblasts (7), was chosen because of its role both as a *PGC-1 $\alpha$*  partner and as its target. Finally, three other genes, i.e. *ANT1/SLC25A4*, *ANT2/SLC25A5* and *ANT3/SLC25A6*, which are downregulated in DS fetal fibroblasts (our unpublished data), were also chosen as *PGC-1 $\alpha$*  targets (SET2, Supplementary Material, Table S1) (30). *ANT1/SLC25A4* is downregulated in SET3 and after *NRIP1* overexpression in the De Cegli's dataset (28). The expression ratio of these genes in *NRIP1*-silenced DS-HFFs versus scrambled transfected DS-HFFs demonstrated that five out of seven analyzed genes were significantly upregulated after *NRIP1* attenuation by siRNA (Fig. 4).

Furthermore, to verify the effect of *NRIP1* attenuation and consequent *PGC-1 $\alpha$*  upregulation on the mitochondrial biogenesis, we used qRT-PCR to quantify *D-LOOP* and *ACTIN* gene expression in scrambled and silenced cells, as mitochondrial

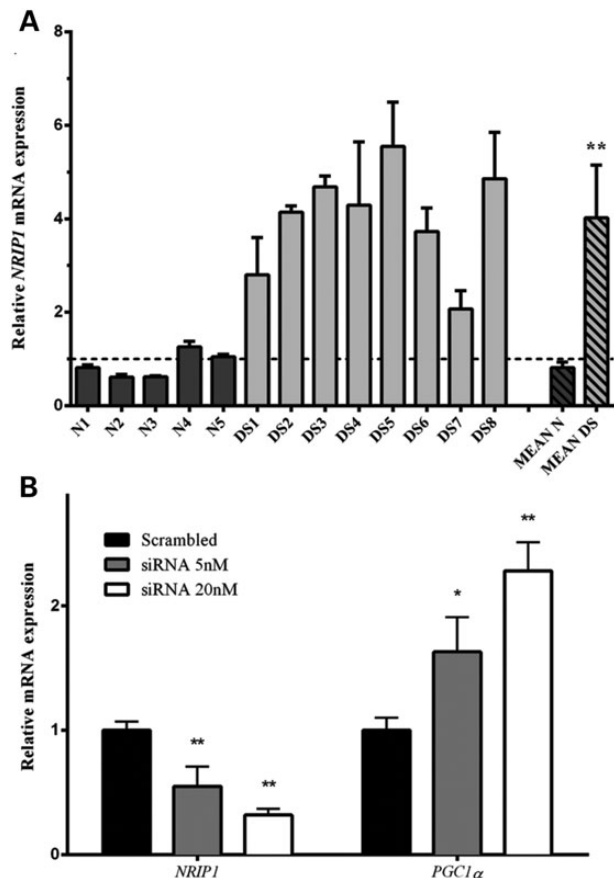


**Figure 2.** *NRIP1* modulates *PGC-1 $\alpha$*  expression in HFFs. (A) *NRIP1* mRNA expression level in euploid cells (N1-N5), and in trisomic (DS1-DS8) HFF lines used for silencing experiments. For each sample, values represent the average determination  $\pm$  SEM for three qRT-PCR experiments. A pool of euploid cells was used as a calibrator.  $**P < 10^{-4}$ . *P*-values express statistical significance for euploid versus trisomic comparisons. (B) *NRIP1* and *PGC-1 $\alpha$*  expression levels in trisomic cells transfected with a scrambled siRNA and with a *NRIP1*-specific SMART pool of siRNAs. A decrease in the *NRIP1* expression level corresponds to an increase of *PGC-1 $\alpha$*  expression level in a siRNA-dependent way. Values represent the average determination  $\pm$  SEM for eight *NRIP1*-silenced DS-HFFs carried out in triplicate.  $*P < 0.05$ ,  $**P < 0.01$ . *P*-values express statistical significance for *NRIP1*-silenced versus scrambled comparisons.

and nuclear markers, respectively. The average of the *D-LOOP/ACTIN* ratio increased by 2.5-fold in silenced trisomic cells (Fig. 5), thereby suggesting that mtDNA content does increase after *NRIP1* attenuation by siRNA and consequent *PGC-1 $\alpha$*  overexpression.

### Mitochondrial function is improved in DS-HFFs after *NRIP1* attenuation by siRNA

We verified whether *NRIP1* attenuation by siRNA, along with the consequent increases in *PGC-1 $\alpha$*  and other mitochondrial genes, might counteract the mitochondrial dysfunction in trisomic cells. For this study, intracellular ROS production, mitochondrial activity, mitochondrial calcium and ATP content were evaluated in DS-HFFs after transient *NRIP1* siRNA-mediated attenuation.

ROS production was measured by confocal microscopy imaging of cells treated with the redox-sensitive fluorescent

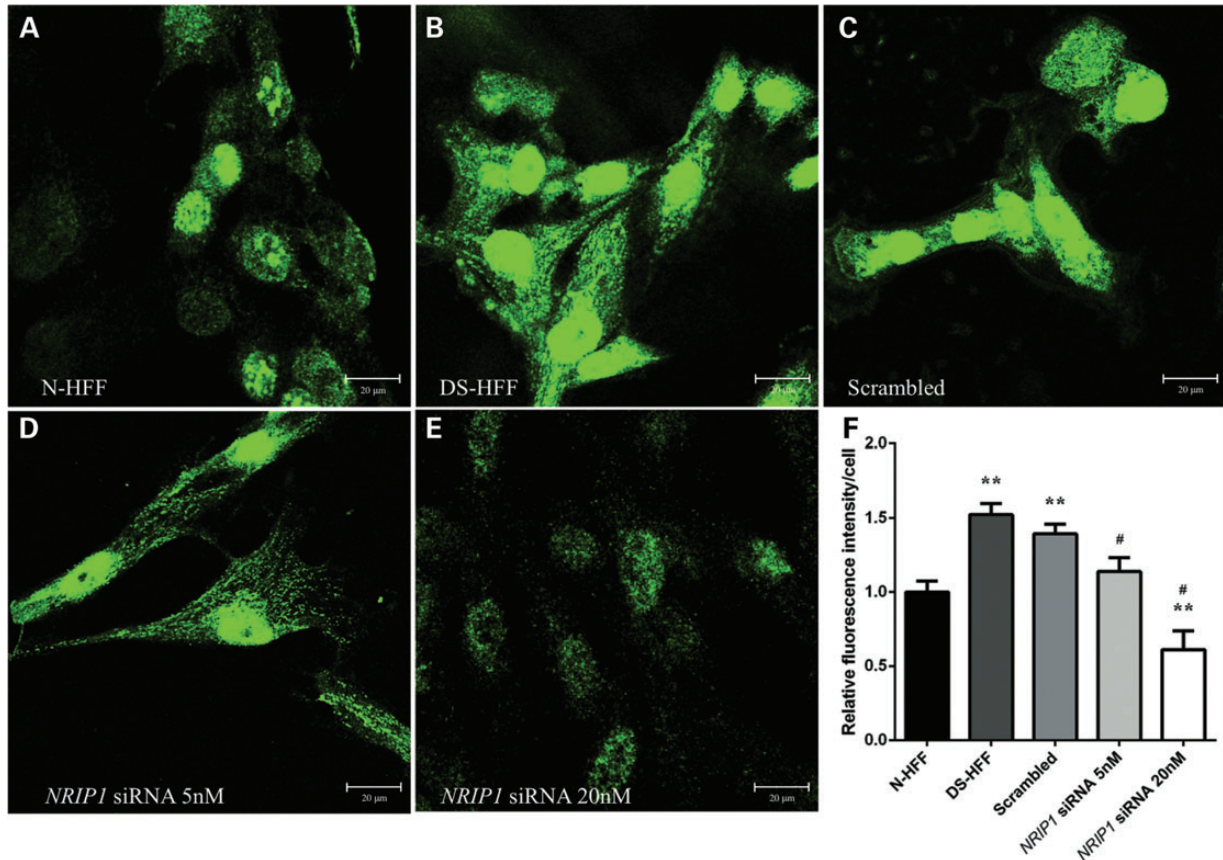


**Figure 3.** NRIP1 immunofluorescence in *NRIP1*-silenced DS-HFFs. Representative images of NRIP1 immunofluorescence analysis in (A) euploid cells, (B) trisomic cells and trisomic cells transfected (C) with a scrambled siRNA, (D) with 5 nM *NRIP1* siRNA and (E) 20 nM *NRIP1* siRNA. (F) Semi-quantitative analysis of the immunodetected signals, by the ImageJ software (means  $\pm$  SEM of three assayed samples). Fifty randomly selected, different cells for each sample/experimental condition were analyzed. A decrease of the fluorescent signal is observed in silenced versus scrambled DS-HFFs. Signal from 5 nM *NRIP1* siRNA transfected cells is comparable with euploid HFFs. Statistical significance: \*\* $P < 0.01$  for trisomic versus euploid comparisons; # $P < 0.05$  for *NRIP1*-silenced versus scrambled comparisons.

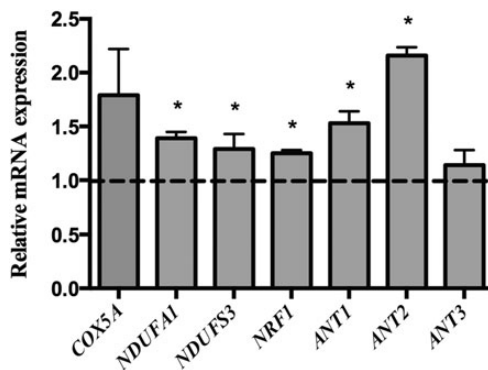


**Figure 4.** Mitochondria-related gene expression in *NRIP1*-silenced DS-HFFs. Relative mRNA expression of seven mitochondria-related genes was measured in *NRIP1*-silenced DS-HFFs versus scrambled transfected DS-HFFs. Five out of the seven genes show a significant increase in their expression level. Values represent the average determination  $\pm$  SEM for three DS-HFF samples carried out in triplicate. A pool of scrambled transfected euploid cells was used as calibrator. \* $P < 0.05$ .  $P$ -value expresses statistical significance for *NRIP1*-silenced versus scrambled comparisons.

probe dichlorofluorescein (DCF). Seventy-two hours after transfection with *NRIP1* siRNA, DCF-related fluorescence was lower with respect to scrambled DS-HFFs. Semi-quantitative analysis of fluorescent signals demonstrated that, on an average basis, the ROS-related DCF fluorescence decreased up to 50% in a siRNA dosage-dependent manner (Fig. 6).

We then established whether decreases in ROS could depend on a rescue of respiratory chain complex activities. To this aim, we incubated silenced DS-HFFs with the specific mitochondrial superoxide indicator, MitoSOX Red. This reagent is a live-cell permeant that is rapidly and selectively targeted to mitochondria. Once in the mitochondria, MitoSOX Red reagent is oxidized by superoxide and exhibits red fluorescence. In experiments performed in *NRIP1*-silenced DS-HFFs, a reduction of the MitoSOX Red signal was demonstrated thus suggesting that the decrease in ROS was partially associated with mitochondrial activity (Fig. 7).

Then, to confirm even further that *NRIP1* attenuation by siRNA improves mitochondrial function, we incubated trisomic silenced cells with the MitoTracker Red dye, a reagent that stains mitochondria in live cells and whose accumulation is dependent

upon membrane potential. A significant 50% increase of the MitoTracker Red-related fluorescence was observed in *NRIP1*-silenced cells when compared with scrambled controls, thus indicating an increase in respiratory activity (Fig. 8).

#### *NRIP1* attenuation by siRNA does not affect mitochondrial $\text{Ca}^{2+}$ homeostasis

In DS-HFFs, the mitochondrial  $\text{Ca}^{2+}$  concentration is significantly greater than that of euploid fetal fibroblasts (7). Many

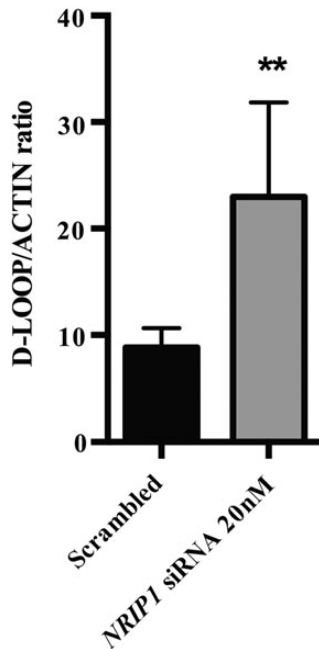


**Figure 5.** mtDNA content in *NRIP1*-silenced DS-HFFs. Ratio between the mtDNA marker *D-LOOP* and the nuclear DNA marker *ACTIN* indicates an increase after *NRIP1* attenuation by siRNA. The ratio was calculated upon normalization to a reference gene (*ABELSON*) by qRT-PCR. Values represent the average determination  $\pm$  SEM for three *NRIP1*-silenced trisomic samples carried out in triplicate. \* $P < 0.05$ .  $P$ -value expresses statistical significance for *NRIP1*-silenced versus scrambled comparisons.

extracellular stimuli exert their effect through an increase in cytosolic  $\text{Ca}^{2+}$  concentration ( $[\text{Ca}^{2+}]_c$ ) mediated by the influx of extracellular  $\text{Ca}^{2+}$  and/or the release of  $\text{Ca}^{2+}$  from intracellular stores, predominantly the endoplasmic reticulum (ER). When  $[\text{Ca}^{2+}]_c$  increases, mitochondria undergo a major rise in the matrix  $\text{Ca}^{2+}$  concentration ( $[\text{Ca}^{2+}]_m$ ). The amplitude of this rise largely exceeds that observed in the cytosol thanks to electrochemical potential across the cation-impermeant inner mitochondrial membrane that provides the driving force for mitochondrial  $\text{Ca}^{2+}$  accumulation (31).

Variations in  $[\text{Ca}^{2+}]_m$  were measured as previously described (7). In brief, DS-HFFs were transfected with a mitochondrially targeted aequorin (32) and then stimulated with histamine. This agonist elicited the production of inositol 1,4,5 trisphosphate (IP3) and the consequent release of  $\text{Ca}^{2+}$  from the ER, through the IP3 receptor.

We found no significant differences in the mitochondrial  $[\text{Ca}^{2+}]_m$  uptake in *NRIP1*-silenced DS-HFFs compared with control cells transfected with the non-targeting scrambled siRNA ( $42.0 \pm 2.6$  versus  $38.7 \pm 3.9 \mu\text{M}$ ,  $P = 0.5$ ) (Fig. 9).

#### *NRIP1* attenuation by siRNA strongly increases cellular ATP content

Levels of phosphorylated adenosine nucleotides, including the universal energy carrier ATP, define the energy state in living cells and depend mainly on mitochondrial function (33). In *NRIP1*-silenced DS-HFFs, we investigated the intramitochondrial ATP concentration ( $[\text{ATP}]_m$ ). For this purpose, we used a chimera of the ATP-sensitive photoprotein luciferase specifically targeted to mitochondria (mtLuc) to obtain a dynamic monitoring of  $[\text{ATP}]_m$ . Luciferase has been widely employed to measure ATP content both in isolated mitochondria and in intact cells; its reaction with luciferin produces a flash of yellow-green light with a peak emission at 560 nm, the intensity of which is proportional to the amount of substrates in the reaction mixture.

We found that silenced DS-HFFs showed a very strong increase (+50%,  $P = 10^{-4}$ ) in basal ATP content, calculated by the luminescence values of the plateau generated after the

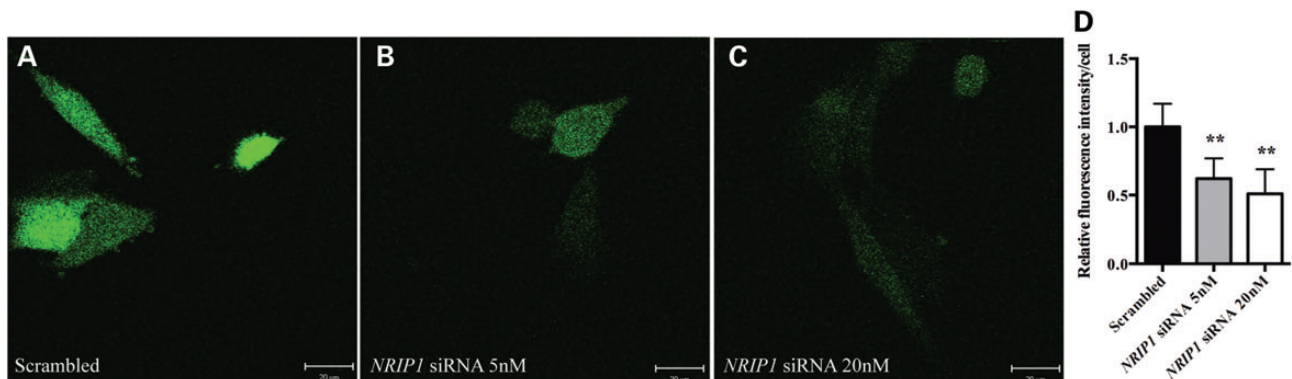


**Figure 6.** ROS decrease in *NRIP1*-silenced DS-HFFs. A confocal microscopy live cell imaging of the DCF fluorescence in transfected DS-HFFs: (A) scrambled, (B) 5 nM *NRIP1* siRNA and (C) 20 nM *NRIP1* siRNA. (D) Semi-quantitative analysis of the DCF-related fluorescence, by the ImageJ software (means  $\pm$  SEM of three assayed samples). Fifty randomly selected, different cells for each sample/experimental condition were analyzed. A significant decrease of DCF-related fluorescence is observed after *NRIP1* attenuation in a siRNA-dependent way. \*\* $P < 10^{-4}$ .  $P$ -value expresses statistical significance for *NRIP1*-silenced versus scrambled comparisons.

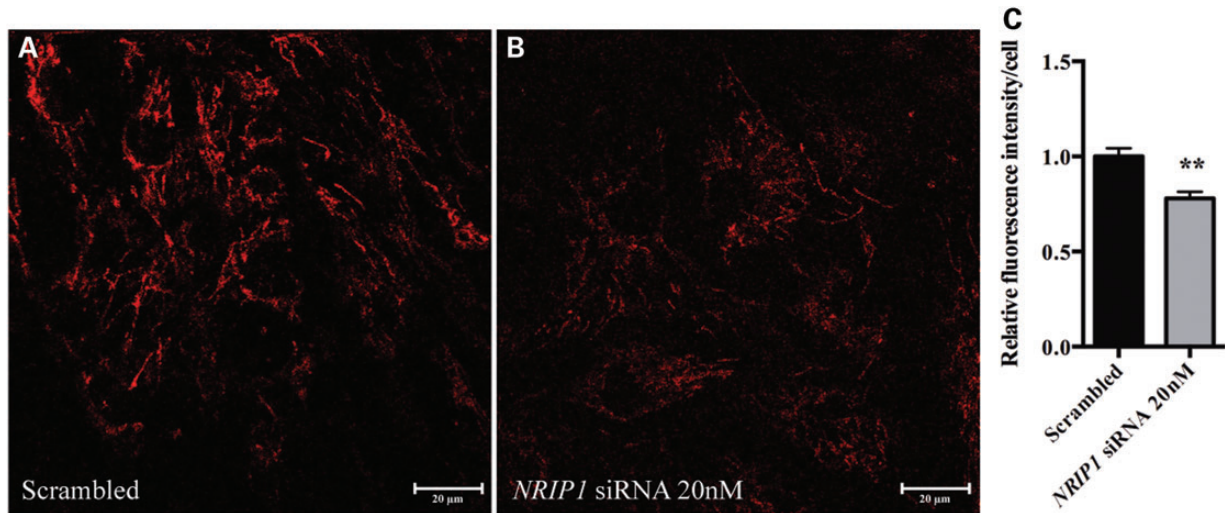


**Figure 7.** Intra-mitochondrial superoxide decrease in *NRIP1*-silenced DS-HFFs. Confocal microscopy live cell imaging of the MitoSOX Red fluorescence in transfected DS-HFFs: (A) scrambled and (B) 20 nM *NRIP1* siRNA. Note that the distribution of MitoSOX Red signal resembles the mitochondrial network. (C) Semi-quantitative analysis of the MitoSOX-related fluorescence, by the ImageJ software (means  $\pm$  SEM of three assayed samples). Fifty randomly selected, different cells for each sample/experimental condition were analyzed. A reduction of the fluorescent signal over the mitochondrial network is detected. \*\* $P < 0.01$ .  $P$ -value expresses statistical significance for *NRIP1*-silenced versus scrambled comparisons.

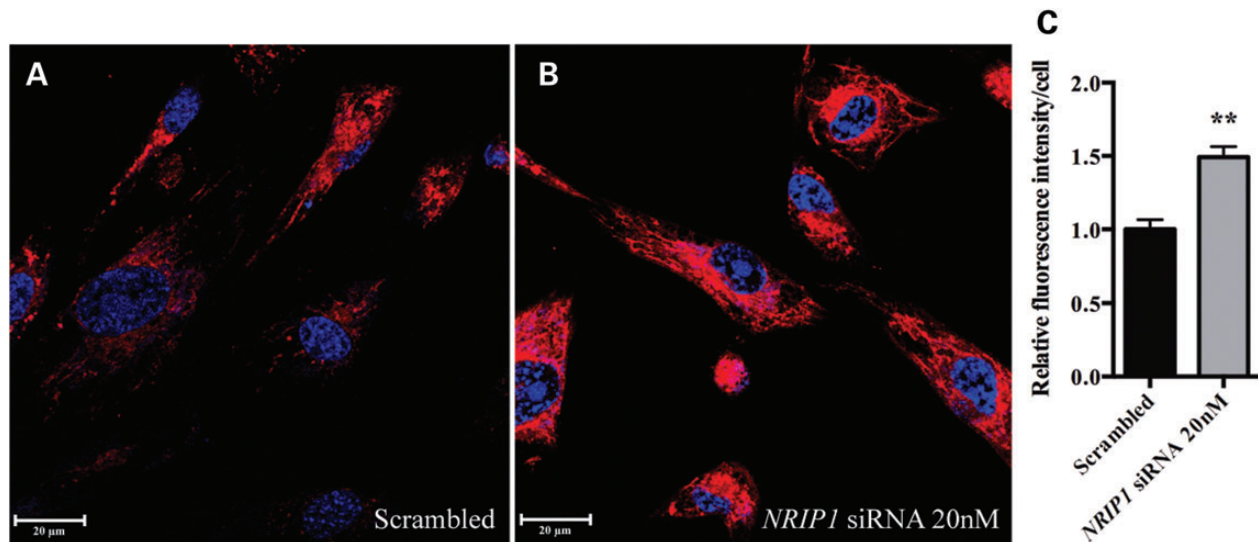


**Figure 8.** Mitochondrial activity in DS *NRIP1*-silenced DS-HFFs. Confocal microscopy live cell imaging of the Mitotracker fluorescence in transfected DS-HFFs: (A) scrambled and (B) with 20 nM *NRIP1* siRNA. (C) Semi-quantitative analysis of the Mitotracker-related fluorescence, by the ImageJ software (means  $\pm$  SEM of five assayed samples). Fifty randomly selected, different cells for each sample/experimental condition were analyzed. An increase of Mitotracker-related fluorescence is observed in *NRIP1*-silenced DS-HFFs. \*\* $P < 0.005$ .  $P$ -value expresses statistical significance for *NRIP1*-silenced versus scrambled comparisons.

addition of luciferin (Fig. 10). Since basal ATP content is highly dependent on the abundance of transfected luciferase, we determined the exact amount of the luciferase transduced under our experimental conditions through an immunoblot assay. We found that the levels of luciferase protein transduced in *NRIP1*-silenced DS-HFFs were comparable with those detected in control cells transfected with the non-targeting scrambled siRNA (Fig. 11).

In parallel, *NRIP1*-silenced cells were slightly decreased in mitochondrial ATP production 72 h after transfection. This

was calculated by subtracting the basal cellular luminescence plateau, generated after the addition of luciferin, from the luminescence values of the second plateau, generated after the addition of the  $\text{Ca}^{2+}$  mobilizing agent histamine (Fig. 10).

## DISCUSSION

This study originates from previous analyses demonstrating a global mitochondrial dysfunction in several DS models (1–4)

and a significant dysregulation of NEMGs in the heart (8), brain (9) and fibroblasts (7) from human fetuses with DS. From these studies, it emerged that genes and transcription factors responsible for the activity of respiratory complexes and mitochondrial biogenesis are globally repressed. Thus, we speculated that most of the underexpressed NEMGs might be under the same regulatory control and that this control might be affected by the trisomy of Hsa21. In the present study, we looked for a regulator of NEMGs that maps to Hsa21 and that is upregulated in DS samples, by the virtue of a gene dosage effect. To this aim, we

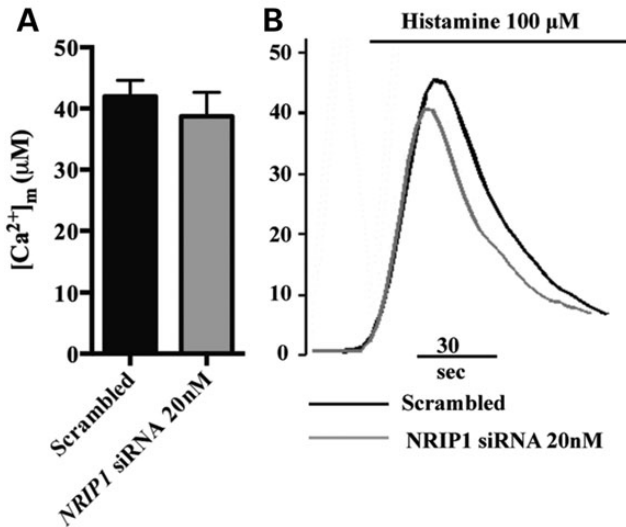


**Figure 9.** Mitochondrial calcium measurement. (A) The barplot of the  $[Ca^{2+}]_m$  in scrambled and *NRIP1* siRNA transfected DS-HFFs. The light signal was collected and calibrated into  $[Ca^{2+}]$  values, as described in Materials and Methods. Results are shown as the average of measurements from four different *NRIP1*-silenced DS-HFFs  $\pm$  SEM. (B) Effect of histamine on  $[Ca^{2+}]_m$ . The traces show the average  $[Ca^{2+}]_m$  in DS-HFFs transfected with the mitochondrially targeted aequorin. Where indicated, the cells were treated with 100  $\mu M$  histamine added to KRB. No significant variation in  $[Ca^{2+}]_m$  is observed in the two conditions.

re-evaluated the expression data from the GEO repository (<http://www.ncbi.nlm.nih.gov/geo>) by focusing on an experiment in which regulatory genes mapping to Hsa21 were individually overexpressed in mouse ESCs (28). Our analysis demonstrated that only one gene is able to cause NEMG downregulation and that no other Hsa21 tested gene exerts such an effect. This gene is *NRIP1* which encodes for a corepressor protein. Although the mean dysregulation of each NEMG elicited by *NRIP1* overexpression was not very strong, the number of affected genes was significantly enriched ( $P < 0.001$ ). The role of *NRIP1* in mitochondrial dysfunction is supported by previous findings demonstrating that both in cellular and in animal models *NRIP1* silencing upregulates the expression of genes responsible for mitochondrial biogenesis and oxidative phosphorylation, whereas *NRIP1* re-expression downregulates them (29,23). Experiments of *NRIP1* manipulation, performed in transgenic mice and human cells, have actually demonstrated that even mild variations in *NRIP1* expression can significantly affect oxidative metabolism and mitochondrial biogenesis (11,23,29,34).

We also considered the possible effects of the overexpression of other Hsa21 genes that have previously been implicated in the regulation of mitochondrial function such as *DYRK1A*, *DSCR1* and *GABPA*, but none of these genes turned out to regulate *per se* NEMG expression. *GABPA*, in particular, is a nuclear respiratory factor that would be expected to downregulate mitochondria-related genes when it is downregulated. However, *GABPA* is never downregulated in DS samples. Indeed it was normoregulated in DS fetal hearts (8), upregulated in DS fetal fibroblasts (7) and inconsistently dysregulated in Vilardell's meta-analysis (14).

On the other hand, the effect of *NRIP1* on NEMG expression could be further reinforced by another Hsa21 gene, *SUMO3*, as sumoylation modulates *NRIP1* activity (35). We thus speculate that the simultaneous upregulation of both *NRIP1* and *SUMO3* exerts a synergistic effect on mitochondrial dysfunction.

*NRIP1* is supposed to exert a repression of mitochondrial biogenesis by either interacting with nuclear receptors (19,18) or

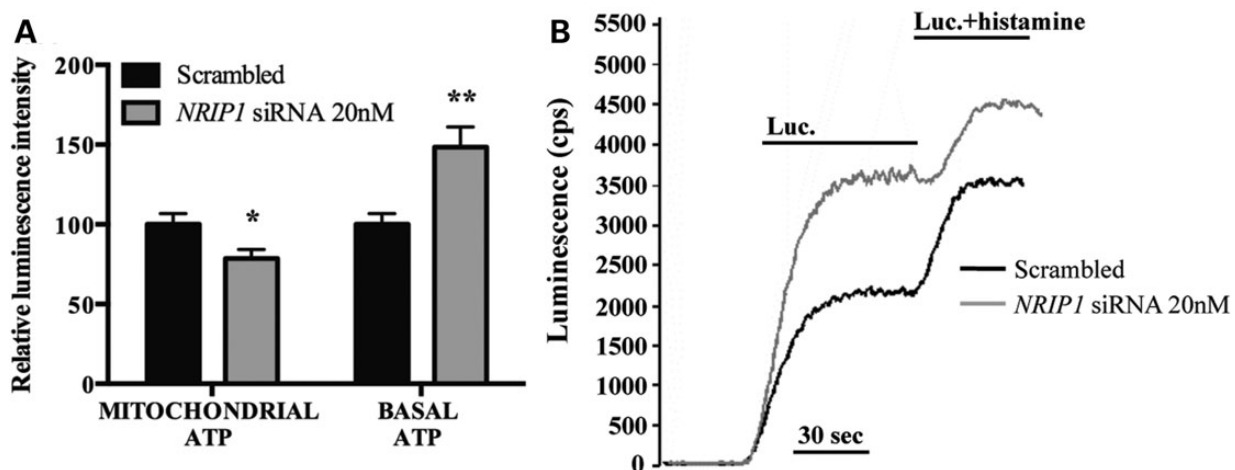


**Figure 10.** Mitochondrial ATP measurement. (A) The barplot of the mitochondrial ATP content and of the basal ATP content in scrambled and *NRIP1* siRNA-transfected DS-HFFs. (B) The traces show mitochondrial  $[ATP]_m$  changes elicited by mitochondrial  $[Ca^{2+}]$  increase in cells perfused with 100  $\mu M$  histamine as agonist. mtLuc luminescence data are expressed as a percentage of the initial value  $\pm$  SEM ( $n = 4$ ). The traces are representative of four independent experiments. \* $P = 0.05$ , \*\* $P = 10^{-4}$ .  $P$ -values express statistical significance for *NRIP1*-silenced versus scrambled comparisons.

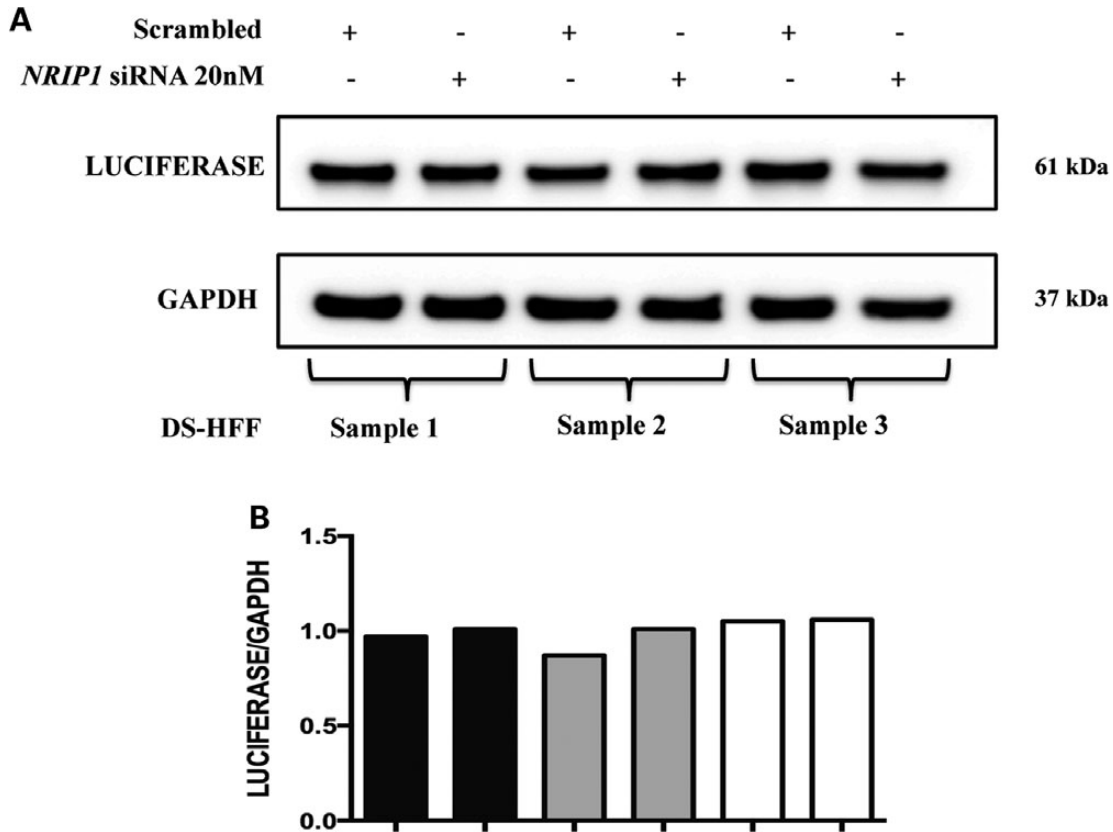


**Figure 11.** Luciferase expression following *NRIP1* attenuation by siRNA. (A) Representative immunoblot of luciferase protein in three *NRIP1*-silenced or scrambled DS-HFFs transfected with a luciferase-encoding plasmid specifically targeted to mitochondria (mtLuc) and cultured in complete medium for 72 h. (B) Quantification of luciferase accumulation by the LUCIFERASE/GAPDH ratio.

regulating *PGC-1 $\alpha$*  activity (10,12,13). *PGC-1 $\alpha$*  knockout mice show not only a decreased number of mitochondria but also a decreased respiratory capacity in skeletal muscle (21). In particular, under physiological conditions, *PGC-1 $\alpha$* , by coactivating several transcription factors, including nuclear receptors such as *PPAR $\gamma$* , *PPAR $\alpha$*  and *ERR $\alpha$* , promotes mitochondrial biogenesis and regulates mitochondrial respiratory efficiency (10,21,36). Interestingly, among the 37 NEMGs downregulated after *NRIP1* induction in the GEO GSE 19836 experiment (28), we observed an enrichment both of genes involved in *PPARs* pathways (8 genes) and of genes containing the *ERR $\alpha$*  motif in their promoter regions (25 genes) ( $P < 0.0005$ ). Notably, the known targets of *PGC-1 $\alpha$* , namely, *CIDEA* (12) and *ANT1/SLC25A4* (30), are included in the list of genes that are downregulated following *NRIP1* overexpression (28).

Moreover, to investigate whether the NEMGs repressed by *NRIP1* and induced by *PGC-1 $\alpha$*  corresponded to the NEMGs downregulated genes in DS fetal hearts (8), we performed a meta-analysis by comparing our microarray data with the results of two experiments in which the gene expression of *NRIP1* or *PGC-1 $\alpha$*  was modulated. We found that the correspondence between the three sets of genes was remarkably high, considering that they all derived from different species, tissues and experimental approaches. The high number of overlapping genes in SET1 and SET2 is in agreement with previous

research indicating an interrelationship between *PGC-1 $\alpha$*  and *NRIP1* activity on mitochondrial pathways (11).

These results, combined with the data from previous research, finally led us to verify the potential role of *NRIP1* in mitochondrial dysfunction in DS. When we transiently attenuated *NRIP1* in trisomic fibroblasts, we demonstrated an inverse correlation between *NRIP1* and *PGC-1 $\alpha$*  expression. Accordingly, we found that this attenuation induced the upregulation of five out of seven genes randomly chosen in SET3, all of which overlapped with the lists of genes regulated by *NRIP1* (SET1) and/or *PGC-1 $\alpha$*  (SET2). Moreover, *NRIP1* siRNA-mediated attenuation in DS-HFFs, and the consequent *PGC-1 $\alpha$*  and *NRF1* upregulation, elicited a significant increase in mtDNA. This result fully corroborates similar experiments performed in cardiomyocytes (11).

In the same trisomic fibroblasts, ROS production was decreased and mitochondrial activity was increased, demonstrating that the induction of NEMG expression in silenced DS-HFFs counteracts mitochondrial impairment and partially rescues mitochondrial function. However, no significant alterations of mitochondrial  $[Ca^{2+}]$  were observed after *NRIP1* attenuation by siRNA. A possible explanation to this phenomenon is either that 72 h is not a sufficient time to determine detectable differences in  $Ca^{2+}$  uptake or that many other mechanisms affect calcium uptake in TS21 cells, e.g. the trisomy of genes

involved in the calcineurin pathway (*DYRK1A* and *DSCR1*) (25). Other  $\text{Ca}^{2+}$  regulators could play a role.

Interestingly, in *NRIP1*-silenced trisomic cells, we found a significant 50% increase in the basal ATP content. These results, together with the finding that *NRIP1* attenuation by siRNA leads to an increase in the adenine nucleotide translocators *ANT1/SLC25A4* and *ANT2/SLC25A5* (Fig. 4), suggest that a more efficient exchange of ATP is induced, thus benefitting the mitochondrial activity and function of these cells, as demonstrated by the reduction in ROS production at the mitochondrial level (Fig. 7).

Supporting evidence for the opposite effects of *NRIP1* and *PGC-1 $\alpha$*  on mitochondrial function and NEMG regulation is that in neonatal rat cardiomyocytes *NRIP1* mediates an antagonistic role versus *PGC-1 $\alpha$*  in the regulation of mitochondrial energy metabolism (11). Indeed, overexpressed *NRIP1* abrogates *PGC-1 $\alpha$* -mediated induction of mitochondrial membrane potential and mitochondrial biogenesis (11). Furthermore, the *NRIP1*-dependent repression of genes involved in mitochondrial function is closely linked with post-natal impaired cardiac function as a result of reduced mitochondrial electron-transport chain activity and oxygen consumption. *NRIP1* hyperexpressing mice are indeed affected by cardiac hypertrophy (34).

*NRIP1* and *PGC-1 $\alpha$*  are also involved in glucose uptake and therefore in the physiopathology of diabetes through the regulation of the insulin sensitive glucose transporter *GLUT4* expression and its sub-cellular localization (37). These findings correlate with the fact that cardiac hypertrophy and diabetes are two important post-natal complications of DS.

Mitochondrial dysfunction might also contribute to determining DS mental retardation and other DS-associated post-natal pathologies, such as Alzheimer's disease (AD) and obesity. It is known that mitochondria also play a central role in many neurodegenerative diseases such as AD, Parkinson's disease, Huntington's disease and amyotrophic lateral sclerosis. Impaired energy metabolism, defective mitochondrial enzymatic activity, abnormal mitochondrial respiration, mutated mtDNAs and oxidative stress are all common features of these neurodegenerative conditions (38).

It is interesting to note that the bioinformatic functional analysis of the 25 genes overlapping SET1 (genes regulated by *NRIP1*) and SET3 (genes downregulated in DS fetal hearts) showed that 16 out of 25 genes characterized the mitochondrial dysfunction pathways described in neurodegenerative diseases such as AD and Parkinson's disease [KEGG Pathways <http://www.genome.jp/kegg/> (39)]. However, given that there is a high prevalence of AD in DS patients, we cannot neglect the possibility that the overexpression of the Hsa21 gene *APP* might have a main role in the development of AD in DS patients.

Taken all together our study indicates that *NRIP1* is a key gene in the regulation of the mitochondrial pathways and that it is linked to mitochondrial dysfunction in DS. Accordingly, this should be taken into account when planning therapeutic approaches aimed at improving functions and cognitive performance in DS mouse models. Many of these models are indeed inadequate since they are not trisomic for all Hsa21 genes and may also have duplications of regions non-syntenic to Hsa21. This is true, for instance, for the very popular Ts65Dn mouse that, among other Hsa21 genes, is not trisomic for either *NRIP1* or *SUMO3*. Thus, preclinical models of

Ts65Dn will be unable to address all phenotypic problems and we speculate that clinical trial oftentimes fails because the overexpression of important genes such as *NRIP1* is not taken into account.

Our results do highlight that *NRIP1* plays a relevant role in DS mitochondrial dysfunction, as evidenced by the ability of *NRIP1* inhibition to counteract mitochondrial dysfunction. However, we cannot rule out the likelihood that other genes may, in fact, be involved. A case in point is that the DS mouse model Ts1Cje manifests mitochondrial dysfunction even though it is not trisomic for either *NRIP1* or for *SUMO3*. Thus, further studies are indeed warranted to identify additional genes possibly responsible for DS mitochondrial alterations.

Finally, these results provide the basis for clinical trials aimed at restoring mitochondrial function in DS subjects to counteract specific phenotypic features such as neurodegeneration, cardiac hypertrophy, diabetes and obesity. Such therapeutic approach would be highly desirable considering that the very few therapeutic approaches undertaken so far in this direction using antioxidants and nutraceuticals have yielded either poor or discordant outcomes (40,41).

Thus, we speculate that a possible therapeutic approach in DS could be based either on *PGC-1 $\alpha$*  activators, which have been tested in other disease mouse models (42–45), or on *PPAR $\gamma$*  agonists, which attenuate mitochondrial dysfunction in AD mouse models (46–51). Such drugs are already routinely used in clinical practice for the treatment of metabolic syndromes, type 2 diabetes, and neurodegenerative diseases such as AD (52–54).

In conclusion, our study has provided further insights into the transcription factors that influence mitochondrial dysfunction in DS. Our findings could indeed pave the way for the development of new and more effective drugs capable of selectively targeting the intricate set of molecular mechanisms underlying the pathogenesis of this disease.

## MATERIALS AND METHODS

### Analysis of public expression data

A set of expression data from GSE 19836 series (28) was obtained from Gene Expression Omnibus repository GEO (<http://www.ncbi.nlm.nih.gov/geo>). This set of data was derived from the analysis of a mouse ESC bank in which 32 orthologs of human chromosome 21 genes, including transcription factors and protein kinases, were individually overexpressed in an inducible manner. A set of clones individually overexpressing 20 of the 32 genes, namely 13 transcription factors (*Aire*, *Bach1*, *Erg*, *Ets2*, *Gabpa*, *Nrip1*, *Olig1*, *Olig2*, *Pknox1*, *Runx1*, *Sim2*, *ZFP295*, *1810007M14Rik*), one transcriptional activator (*Dscr1-Rcan1*) and six protein kinases (*DYRK1A*, *SNF1LK*, *Hunk*, *Pdxk*, *Pfkl*, *Ripk4*), was transcriptionally profiled under inducing and non-inducing conditions with Affymetrix Gene Chip Mouse 430\_2. Specifically, RNAs from three induced mouse ESCs and three controls were profiled for each inducible Hsa21 gene (28). In our analysis, we used GeneSpring software vers. 11.5 Multi-Omic Analysis (Agilent technologies, Inc.) for data interpretation; however, our criteria were different from those used by the authors of the gene expression dataset, focusing on down-regulated genes. We considered genes differentially expressed with a Fold change (LogFC) >0.3 and <-0.3 with  $P < 0.05$ ,

thus producing two lists of dysregulated genes: 511 upregulated genes and 298 downregulated genes. Gene ontology (GO) functional class scoring of all the lists of significantly upregulated or downregulated genes was performed using the Web-based Gene Set Analysis Toolkit V2 (<http://bioinfo.vanderbilt.edu/webgestalt/>) (55,56). Special attention was given to mitochondria-related categories and pathways.

### Meta-analysis

We compared three sets of gene expression data from different experiments, to identify genes consistently dysregulated across the three studies. The first set, SET1, included genes dysregulated by *Nrip1* modulation in mouse adipocytes (29). The second set, SET2, included genes upregulated after *PGC-1 $\alpha$*  induction in SAOS2 cells (human osteoblast like cells) (30). The third set included mitochondria-related genes, downregulated in DS fetal heart tissue (8). The three sets were filtered according to the GO cell component category 'mitochondrion' with the above-mentioned Web-based Gene Set Analysis Toolkit V2. The resulting genes—123 genes in SET1, 129 in SET2 and 70 in SET3 (Supplementary Material, Table S1)—were intersected using the R software (<http://www.R-project.org/>). A Venn diagram was built, which shows overlapping genes across the three sets.

### Ethics statement

HFFs were obtained from the 'Telethon Bank of Fetal Biological Samples' at the University of Naples. All experimental protocols were approved by the local Institutional Ethics Committee.

### Samples

Eight skin biopsies were explanted from human fetuses with trisomy of Hsa21 (DS-HFF) after therapeutic abortion at 18–22 gestational weeks. Fibroblasts from biopsies were cultured in T25 flasks (BD Falcon) with Chang medium B + C (Irvine Scientific) supplemented with 1% penicillin/streptomycin (Gibco) at 37°C in 5% CO<sub>2</sub> atmosphere; all the analyses described throughout this study were carried out at cell culture passages 4–5.

### Transfection protocol

*NRIP1* was transiently silenced in eight DS-HFF lines using a pool of specific *NRIP1*-siRNAs (ON-TARGETplus SMART-pool, Dharmacon), with negative (ON-TARGETplus SMART-pool Non-targeting siRNAs control, Dharmacon) and positive controls (ON-TARGETplus SMARTpool, GAPDH siRNAs, Dharmacon). Interferin transfection reagent (Polyplus transfection) was used. Cells were plated on 12-well plates (50 000 cells/well) for RNA collection, on 35 mm diameter plates with 20 mm slides (Delchimica) (50 000 cells/well) for ROS production analysis and on 24-well plates (30 000 cells/well) (BD Falcon) for immunofluorescence and mitochondrial activity assays. DS-HFFs were transfected with 5 and 20 nM siRNA according to the manufacturer's protocol (Polyplus transfection). Seventy-two hours after transfection, the effects of *NRIP1* siRNA-mediated attenuation were evaluated.

### NRIP1 immunofluorescence

For the evaluation of NRIP1 protein by immunofluorescence, 30 000 cells were plated in 24-well plates on 12-mm diameter round glass coverslips. Cells were fixed in 3 : 1 methanol: acetic acid for 15 min, washed twice with PBS and then incubated twice in 0.1 M borate buffer pH 8.5 for 10 min to neutralize the pH. After two washes with PBS, the cells were incubated with DNase 1 : 10 in RDD buffer (Qiagen) at 37°C for 1 h and then treated with 2% BSA in PBS to block non-specific protein–protein interactions. The cells were then incubated with the antibody anti-NRIP1 (30  $\mu$ g/ml, ab42126 Abcam, Cambridge Science Park, Cambridge, UK) overnight at +4°C. The secondary antibody (green) was Alexa Fluor<sup>®</sup> 488 goat anti-rabbit IgG (H + L) used at a 1/200 dilution for 1 h (57). Cells were finally mounted in 50% glycerol in PBS. Immunofluorescence analysis was performed at a confocal laser scanning microscope LSM 510 (Zeiss, Gottingen, Germany) equipped with an Argon ionic laser whose  $\lambda$  was set at 488 nm, and an HeNe laser whose  $\lambda$  was set at 633 nm. Emission of fluorescence was revealed by a BP 505–530 band pass filter for Alexa Fluor 488 and by a 615 long pass filter for DRAQ5. Images were acquired at a resolution of 1024  $\times$  1024 pixels. Analysis of data was performed with the ImageJ software, version 1.37 (58). Fifty random single cells were analyzed for each imaging analysis.

### Laser scanning confocal microscopy live cell imaging of ROS production

For the evaluation of ROS production after *NRIP1* siRNA transfection, 50 000 cells were plated on 25-mm diameter round glass coverslips in an Attofluor cell chamber (Molecular Probe, Leiden, the Netherlands). Seventy-two hours later, the cells were incubated for 15 min at 37°C with 10  $\mu$ M of 2,7-dichlorofluorescein diacetate (DCF-DA) which is converted to DCF by intracellular esterases, for detection of H<sub>2</sub>O<sub>2</sub>, or with 5  $\mu$ M of MitoSOX<sup>TM</sup> Red reagent (Life Technologies, Molecular Probes), which is a live-cell permeant and is rapidly and selectively targeted to the mitochondria. Once in the mitochondria, MitoSOX<sup>TM</sup> Red reagent is oxidized by superoxide and exhibits red fluorescence. After incubation, cells were washed three times with medium without serum. To maintain the cells alive during observation and to create the proper environmental conditions, the specimen was placed in an Oko Lab (Na, Italy) Water Jacket Top Stage Incubator, kept at 37°C, under humidified condition of 5% CO<sub>2</sub> and 95% air by means of temperature controllers, gas mixers and humidifiers right on the microscope.

The analysis of immunofluorescence was performed with a confocal laser scanner microscopy Zeiss LSM 510 (Carl Zeiss, Gottingen, Germany), equipped with Argon ionic laser whose  $\lambda$  was set at 488 nm, an HeNe laser whose  $\lambda$  was set at 546 nm and an immersion oil objective 63  $\times$  /1.4f. Emission of fluorescence was revealed by BP 505–530 band pass filter for DCF and 560 Long Pass for MitoSOX Red. Images were acquired in the green or in the red channels and then saved in TIFF format to prevent the loss of information. They were acquired with a resolution of 1024  $\times$  1024 pixel with the confocal pinhole set to one Airy unit.

Analysis of data was performed with the ImageJ software, version 1.37. Fifty random single cells were analyzed for each imaging analysis.

### Mitotracker immunofluorescence

For the evaluation of mitochondrial activity, MitoTracker<sup>®</sup> Red CMXRos (Molecular Probes) was chosen. MitoTracker<sup>®</sup> probes passively diffuse across the plasma membrane and accumulate in actively respiring mitochondria. Thirty-thousand cells were plated on 24-well plates on 12 mm diameter round glass coverslips and then incubated with 150 nM of Mitotracker Red for 30 min. After incubation cells were fixed for 20 min in PBS containing 4% paraformaldehyde (Sigma) and then washed once with PBS 1×. Nuclei were stained with the DNA intercalant DRAQ5 (Bio status, Alexis Corporation). Cells were finally mounted in 50% glycerol in PBS. Immunofluorescence analysis was performed with a confocal laser scanning microscope LSM 510 (Zeiss, Gottingen, Germany). The lambda of the two HeNe lasers was set at 546 and at 633 nm. Fluorescence emission was revealed by BP 560–615 band pass filter for Mitotracker Red and by a 615-long pass filter for DRAQ5. Double staining immunofluorescence images were acquired separately in the red and infrared channels at a resolution of 1024 × 1024 pixels, with the confocal pinhole set to one Airy unit, and then saved in TIFF format. Fifty random single cells were analyzed for each imaging analysis using the ImageJ version 1.37.

### RNA extraction and quantitative real-time PCR

Total RNA from each sample was extracted using TRIzol reagent (Gibco/BRL Life Technologies, Inc., Gaithersburg, MD) and was reverse transcribed using the iScript cDNA Synthesis kit (Bio-Rad Laboratories, Inc., Hercules, CA, USA).

Real-time PCR was performed using iQ Supermix SYBR Green 2× on a Bio-Rad iCycler according to the manufacturer's protocols. PCR reactions were performed in triplicate. Primer pairs (MWG Biotech, Ebersberg, Germany) were designed using the Primer 3 software (<http://frodo.wi.mit.edu/primer3>) to obtain amplicons ranging from 100 to 150 base pairs. Expression values were normalized either versus scrambled transfected cells or versus scrambled transfected euploid cells. *ABELSON* and *GAPDH* housekeeping genes were chosen as reference genes.

### mtDNA quantification

To quantify the mtDNA content, we selected two genes: *D-LOOP* as the mitochondrial target and *ACTIN* as the nuclear target. Both targets were quantified by qRT-PCR using cDNA reverse-transcribed from RNA of three *NR1P1*-silenced trisomic samples and scrambled control. Normalization of gene expression was obtained using the *ABELSON* gene as housekeeping. The ratio between *D-LOOP* and *ACTIN* expression under each condition (*NR1P1*-silenced or scrambled trisomic cells) was calculated.

### Aequorin measurement

A chimeric aequorin targeted to the mitochondria (mtAEQmut) was used as a probe. For the experiments with mtAEQmut, cells were incubated with 5 mM coelenterazine (Fluka, 7372) for 1–2 h in DMEM supplemented with 1% FBS. A coverslip with transfected cells was placed in a perfused thermostated chamber

located in close proximity to a low-noise photomultiplier with a built-in amplifier/discriminator. All aequorin measurements were performed in KRB supplemented with 1 mM CaCl<sub>2</sub>. Agonist was added to the same medium as specified in figure legends. The experiments were terminated by lysing cells with 100 mM digitonin in a hypotonic Ca<sup>2+</sup>-containing solution (10 mM CaCl<sub>2</sub> in H<sub>2</sub>O), thus discharging the remaining aequorin pool. The output of the discriminator was captured by a Thorn EMI photon-counting board and stored in an IBM-compatible computer for further analyses. The aequorin luminescence data were calibrated offline into [Ca<sup>2+</sup>] values using a computer algorithm based on the Ca<sup>2+</sup> response curve of mutant aequorins.

### Immunoblotting

For immunoblotting, cells were scraped into ice-cold phosphate-buffered saline and lysed in a modified 10 mM Tris buffer, pH 7.4, containing 150 mM NaCl, 1% Triton X-100, 10% glycerol, 10 mM EDTA and protease inhibitor cocktail. After 30 min of incubation on ice, the lysates were cleared via centrifugation at 12 000g at 4°C for 10 min. Protein concentrations were determined by the Lowry procedure. Protein extracts (18 μg) were separated on 4–12% Bis-Tris acrylamide Gel (Life Technologies, NP0323) and electron-transferred to PVDF or nitrocellulose membrane according to standard procedures. Unspecific binding sites were saturated by incubating membranes with TBS-Tween 20 (0.05%) supplemented with 5% non-fat powdered milk for 1 h. Next, the membranes were incubated overnight with primary antibodies [GAPDH (Cell Signaling, 2118); LUCIFERASE (Invitrogen, 356700)] and the detection was assessed by appropriate HRP-labeled secondary antibodies [Santa Cruz, sc-2004 (goat anti-rabbit) and sc-2005 (goat anti-mouse)] plus a chemiluminescent substrate (Thermo Scientific, 34080). Equal loading of lanes was confirmed by incubation with an anti-GAPDH antibody.

### Luciferase measurements

Cells were seeded on glass coverslips (13 mm in diameter) for single sample luminescence measurements and allowed to grow until 50% confluence. The cells were then transfected with a cytosolic (untargeted) firefly luciferase and a mtLuc (59,60).

Cell luminescence was measured in the same purpose-built luminometer used for the aequorin measurements, constantly perfused with KRB, supplemented with 1 mM CaCl<sub>2</sub> and 20 mM luciferin. The light output of a coverslip of infected cells was in the range of 1000–10 000 counts per second (cps) versus a background <10 cps. All compounds employed in the experiments were tested for non-specific effects on the luminescence, but none was observed.

### Statistics

The ANOVA test, with a Bonferroni *post hoc* correction in case of multiple comparisons, was applied to evaluate the statistical significance of differences measured throughout the datasets presented. The threshold for statistical significance (*P*-value) was set at 0.05.

## SUPPLEMENTARY MATERIAL

Supplementary Material is available at *HMG* online.

## ACKNOWLEDGEMENTS

We thank Paola Merolla for language revision and editing.

*Conflict of Interest statement.* None declared.

## FUNDING

This work has been supported by POR Campania FSE 2007-2013, Project CREME from Campania Region to L.N.

## REFERENCES

- Kim, S.H., Vilkolinsky, R., Cairns, N., Fountoulakis, M. and Lubec, G. (2001) The reduction of NADH ubiquinone oxidoreductase 24- and 75-kDa subunits in brains of patients with Down syndrome and Alzheimer's disease. *Life Sci.*, **68**, 2741–2750.
- Busciglio, J., Pelsman, A., Wong, C., Pigino, G., Yuan, M., Mori, H. and Yankner, B.A. (2002) Altered metabolism of the amyloid beta precursor protein is associated with mitochondrial dysfunction in Down's syndrome. *Neuron*, **33**, 677–688.
- Helguera, P., Seiglie, J., Rodriguez, J., Hanna, M., Helguera, G. and Busciglio, J. (2013) Adaptive downregulation of mitochondrial function in Down syndrome. *Cell. Metab.*, **17**, 132–140.
- Shukkur, E.A., Shimohata, A., Akagi, T., Yu, W., Yamaguchi, M., Murayama, M., Chui, D., Takeuchi, T., Amano, K., Subramhanya, K.H. *et al.* (2006) Mitochondrial dysfunction and tau hyperphosphorylation in Ts1Cje, a mouse model for Down syndrome. *Hum. Mol. Genet.*, **15**, 2752–2762.
- Valenti, D., Tullio, A., Caratozzolo, M.F., Merafina, R.S., Scartezzini, P., Marra, E. and Vacca, R.A. (2010) Impairment of F1F0-ATPase, adenine nucleotide translocator and adenylate kinase causes mitochondrial energy deficit in human skin fibroblasts with chromosome 21 trisomy. *Biochem. J.*, **431**, 299–310.
- Valenti, D., Manente, G.A., Moro, L., Marra, E. and Vacca, R.A. (2011) Deficit of complex I activity in human skin fibroblasts with chromosome 21 trisomy and overproduction of reactive oxygen species by mitochondria: involvement of the cAMP/PKA signalling pathway. *Biochem. J.*, **435**, 679–688.
- Piccoli, C., Izzo, A., Scrima, R., Bonfiglio, F., Manco, R., Negri, R., Quarato, G., Cela, O., Ripoli, M., Prisco, M. *et al.* (2013) Chronic pro-oxidative state and mitochondrial dysfunctions are more pronounced in fibroblasts from Down syndrome foeti with congenital heart defects. *Hum. Mol. Genet.*, **22**, 1218–1232.
- Conti, A., Fabbrini, F., D'Agostino, P., Negri, R., Greco, D., Genesio, R., D'Armiento, M., Olla, C., Paladini, D., Zannini, M. *et al.* (2007) Altered expression of mitochondrial and extracellular matrix genes in the heart of human fetuses with chromosome 21 trisomy. *BMC Genomics*, **8**, 268.
- Mao, R., Wang, X., Spitznagel, E.L. Jr, Frelin, L.P., Ting, J.C., Ding, H., Kim, J.W., Ruczinski, I., Downey, T.J. and Pevsner, J. (2005) Primary and secondary transcriptional effects in the developing human Down syndrome brain and heart. *Genome Biol.*, **6**, R107.
- Scarpulla, R.C. (2011) Metabolic control of mitochondrial biogenesis through the PGC-1 family regulatory network. *Biochim. Biophys. Acta*, **1813**, 1269–1278.
- Chen, Y., Wang, Y., Chen, J., Chen, X., Cao, W., Chen, S., Xu, S., Huang, H. and Liu, P. (2012) Roles of transcriptional corepressor RIP140 and coactivator PGC-1alpha in energy state of chronically infarcted rat hearts and mitochondrial function of cardiomyocytes. *Mol. Cell Endocrinol.*, **362**, 11–18.
- Hallberg, M., Morganstein, D.L., Kiskinis, E., Shah, K., Kralli, A., Dilworth, S.M., White, R., Parker, M.G. and Christian, M. (2008) A functional interaction between RIP140 and PGC-1alpha regulates the expression of the lipid droplet protein CIDEA. *Mol. Cell Biol.*, **28**, 6785–6795.
- Rytinki, M.M. and Palvimo, J.J. (2009) SUMOylation attenuates the function of PGC-1alpha. *J. Biol. Chem.*, **284**, 26184–26193.
- Vilardell, M., Rasche, A., Thormann, A., Maschke-Dutz, E., Perez-Jurado, L.A., Lehrach, H. and Herwig, R. (2011) Meta-analysis of heterogeneous Down syndrome data reveals consistent genome-wide dosage effects related to neurological processes. *BMC Genomics*, **12**, 229.
- Wei, L.N., Hu, X., Chandra, D., Seto, E. and Farooqui, M. (2000) Receptor-interacting protein 140 directly recruits histone deacetylases for gene silencing. *J. Biol. Chem.*, **275**, 40782–40787.
- Vo, N., Fjeld, C. and Goodman, R.H. (2001) Acetylation of nuclear hormone receptor-interacting protein RIP140 regulates binding of the transcriptional corepressor CtBP. *Mol. Cell Biol.*, **21**, 6181–6188.
- Kiskinis, E., Hallberg, M., Christian, M., Olofsson, M., Dilworth, S.M., White, R. and Parker, M.G. (2007) RIP140 directs histone and DNA methylation to silence Ucp1 expression in white adipocytes. *Embo J.*, **26**, 4831–4840.
- Nautiyal, J., Christian, M. and Parker, M.G. (2013) Distinct functions for RIP140 in development, inflammation, and metabolism. *Trends Endocrinol. Metab.*, **24**, 451–459.
- Fritah, A., Christian, M. and Parker, M.G. (2010) The metabolic coregulator RIP140: an update. *Am. J. Physiol. Endocrinol. Metab.*, **299**, E335–E340.
- Christian, M., White, R. and Parker, M.G. (2006) Metabolic regulation by the nuclear receptor corepressor RIP140. *Trends Endocrinol. Metab.*, **17**, 243–250.
- Leone, T.C., Lehman, J.J., Finck, B.N., Schaeffer, P.J., Wende, A.R., Boudina, S., Courtois, M., Wozniak, D.F., Sambandam, N., Bernal-Mizrachi, C. *et al.* (2005) PGC-1alpha deficiency causes multi-system energy metabolic derangements: muscle dysfunction, abnormal weight control and hepatic steatosis. *PLoS Biol.*, **3**, e101.
- Mitra, R., Noguee, D.P., Zechner, J.F., Yea, K., Gierasch, C.M., Kovacs, A., Medeiros, D.M., Kelly, D.P. and Duncan, J.G. (2012) The transcriptional coactivators, PGC-1alpha and beta, cooperate to maintain cardiac mitochondrial function during the early stages of insulin resistance. *J. Mol. Cell Cardiol.*, **52**, 701–710.
- Seth, A., Steel, J.H., Nichol, D., Pocock, V., Kumaran, M.K., Fritah, A., Moberley, M., Ryder, T.A., Rowlerson, A., Scott, J. *et al.* (2007) The transcriptional corepressor RIP140 regulates oxidative metabolism in skeletal muscle. *Cell Metab.*, **6**, 236–245.
- Gardiner, K. (2006) Transcriptional dysregulation in Down syndrome: predictions for altered protein complex stoichiometries and post-translational modifications, and consequences for learning/behavior genes ELK, CREB, and the estrogen and glucocorticoid receptors. *Behav. Genet.*, **36**, 439–453.
- Arron, J.R., Winslow, M.M., Polleri, A., Chang, C.P., Wu, H., Gao, X., Neilson, J.R., Chen, L., Heit, J.J., Kim, S.K. *et al.* (2006) NFAT dysregulation by increased dosage of DSCR1 and DYRK1A on chromosome 21. *Nature*, **441**, 595–600.
- O'Leary, D.A., Pritchard, M.A., Xu, D., Kola, I., Hertzog, P.J. and Risteovski, S. (2004) Tissue-specific overexpression of the HSA21 gene GABPalpha: implications for DS. *Biochim. Biophys. Acta*, **1739**, 81–87.
- Sturgeon, X., Le, T., Ahmed, M.M. and Gardiner, K.J. (2012) Pathways to cognitive deficits in Down syndrome. *Prog. Brain Res.*, **197**, 73–100.
- De Cegli, R., Romito, A., Iacobacci, S., Mao, L., Lauria, M., Fedele, A.O., Klose, J., Borel, C., Descombes, P., Antonarakis, S.E. *et al.* (2010) A mouse embryonic stem cell bank for inducible overexpression of human chromosome 21 genes. *Genome Biol.*, **11**, R64.
- Powelka, A.M., Seth, A., Virbasius, J.V., Kiskinis, E., Nicoloso, S.M., Guilherme, A., Tang, X., Straubhaar, J., Cherniack, A.D., Parker, M.G. *et al.* (2006) Suppression of oxidative metabolism and mitochondrial biogenesis by the transcriptional corepressor RIP140 in mouse adipocytes. *J. Clin. Invest.*, **116**, 125–136.
- Schreiber, S.N., Emter, R., Hock, M.B., Knutti, D., Cardenas, J., Podvince, M., Oakeley, E.J. and Kralli, A. (2004) The estrogen-related receptor alpha (ERRalpha) functions in PPARgamma coactivator 1alpha (PGC-1alpha)-induced mitochondrial biogenesis. *Proc. Natl Acad. Sci. USA*, **101**, 6472–6477.
- Patergnani, S., Suski, J.M., Agnoletto, C., Bononi, A., Bonora, M., De Marchi, E., Giorgi, C., Marchi, S., Missiroli, S., Poletti, F. *et al.* (2011) Calcium signaling around Mitochondria Associated Membranes (MAMs). *Cell Commun. Signal*, **9**, 19.
- Bonora, M., Giorgi, C., Bononi, A., Marchi, S., Patergnani, S., Rimessi, A., Rizzuto, R. and Pinton, P. (2013) Subcellular calcium measurements in mammalian cells using jellyfish photoprotein aequorin-based probes. *Nat. Protoc.*, **8**, 2105–2118.

33. Bonora, M., Patergnani, S., Rimessi, A., De Marchi, E., Suski, J.M., Bononi, A., Giorgi, C., Marchi, S., Missiroli, S., Poletti, F. *et al.* (2012) ATP synthesis and storage. *Purinergic Signal.*, **8**, 343–357.
34. Fritah, A., Steel, J.H., Nichol, D., Parker, N., Williams, S., Price, A., Strauss, L., Ryder, T.A., Mobberley, M.A., Poutanen, M. *et al.* (2010) Elevated expression of the metabolic regulator receptor-interacting protein 140 results in cardiac hypertrophy and impaired cardiac function. *Cardiovasc. Res.*, **86**, 443–451.
35. Rytinki, M.M. and Palvimo, J.J. (2008) SUMOylation modulates the transcription repressor function of RIP140. *J. Biol. Chem.*, **283**, 11586–11595.
36. Scarpulla, R.C., Vega, R.B. and Kelly, D.P. (2012) Transcriptional integration of mitochondrial biogenesis. *Trends Endocrinol. Metab.*, **23**, 459–466.
37. Fritah, A., Steel, J.H., Parker, N., Nikolopoulou, E., Christian, M., Carling, D. and Parker, M.G. (2012) Absence of RIP140 reveals a pathway regulating glut4-dependent glucose uptake in oxidative skeletal muscle through UCP1-mediated activation of AMPK. *PLoS One*, **7**, e32520.
38. Petrozzi, L., Ricci, G., Giglioli, N.J., Siciliano, G. and Mancuso, M. (2007) Mitochondria and neurodegeneration. *Biosci. Rep.*, **27**, 87–104.
39. Kanehisa, M. and Goto, S. (2000) KEGG: kyoto encyclopedia of genes and genomes. *Nucleic Acids Res.*, **28**, 27–30.
40. de la Torre, R. and Dierssen, M. (2012) Therapeutic approaches in the improvement of cognitive performance in Down syndrome: past, present, and future. *Prog. Brain Res.*, **197**, 1–14.
41. Costa, A.C. and Scott-McKean, J.J. (2013) Prospects for improving brain function in individuals with Down syndrome. *CNS Drugs*, **27**, 679–702.
42. Rodgers, J.T., Lerin, C., Haas, W., Gygi, S.P., Spiegelman, B.M. and Puigserver, P. (2005) Nutrient control of glucose homeostasis through a complex of PGC-1 $\alpha$  and SIRT1. *Nature*, **434**, 113–118.
43. Dong, W., Gao, D. and Zhang, X. (2007) Mitochondria biogenesis induced by resveratrol against brain ischemic stroke. *Med. Hypotheses*, **69**, 700–701.
44. Lagouge, M., Argmann, C., Gerhart-Hines, Z., Meziane, H., Lerin, C., Daussin, F., Messadeq, N., Milne, J., Lambert, P., Elliott, P. *et al.* (2006) Resveratrol improves mitochondrial function and protects against metabolic disease by activating SIRT1 and PGC-1 $\alpha$ . *Cell*, **127**, 1109–1122.
45. Jager, S., Handschin, C., St-Pierre, J. and Spiegelman, B.M. (2007) AMP-activated protein kinase (AMPK) action in skeletal muscle via direct phosphorylation of PGC-1 $\alpha$ . *Proc. Natl Acad. Sci. USA*, **104**, 12017–12022.
46. Bastin, J., Aubey, F., Rotig, A., Munnich, A. and Djouadi, F. (2008) Activation of peroxisome proliferator-activated receptor pathway stimulates the mitochondrial respiratory chain and can correct deficiencies in patients' cells lacking its components. *J. Clin. Endocrinol. Metab.*, **93**, 1433–1441.
47. Nicolakakis, N., Aboukassim, T., Ongali, B., Lecrux, C., Fernandes, P., Rosa-Neto, P., Tong, X.K. and Hamel, E. (2008) Complete rescue of cerebrovascular function in aged Alzheimer's disease transgenic mice by antioxidants and pioglitazone, a peroxisome proliferator-activated receptor gamma agonist. *J. Neurosci.*, **28**, 9287–9296.
48. Escribano, L., Simon, A.M., Perez-Mediavilla, A., Salazar-Colocho, P., Del Rio, J. and Frechilla, D. (2009) Rosiglitazone reverses memory decline and hippocampal glucocorticoid receptor down-regulation in an Alzheimer's disease mouse model. *Biochem. Biophys. Res. Commun.*, **379**, 406–410.
49. Johri, A., Calingasan, N.Y., Hennessey, T.M., Sharma, A., Yang, L., Wille, E., Chandra, A. and Beal, M.F. (2012) Pharmacologic activation of mitochondrial biogenesis exerts widespread beneficial effects in a transgenic mouse model of Huntington's disease. *Hum. Mol. Genet.*, **21**, 1124–1137.
50. Sauerbeck, A., Gao, J., Readnower, R., Liu, M., Pauly, J.R., Bing, G. and Sullivan, P.G. (2011) Pioglitazone attenuates mitochondrial dysfunction, cognitive impairment, cortical tissue loss, and inflammation following traumatic brain injury. *Exp. Neurol.*, **227**, 128–135.
51. Yamaguchi, S., Li, H., Purevsuren, J., Yamada, K., Furui, M., Takahashi, T., Mushimoto, Y., Kobayashi, H., Hasegawa, Y., Taketani, T. *et al.* (2012) Bezafibrate can be a new treatment option for mitochondrial fatty acid oxidation disorders: evaluation by *in vitro* probe acylcarnitine assay. *Mol. Genet. Metab.*, **107**, 87–91.
52. Watson, G.S., Cholerton, B.A., Reger, M.A., Baker, L.D., Plymate, S.R., Athana, S., Fishel, M.A., Kulstad, J.J., Green, P.S., Cook, D.G. *et al.* (2005) Preserved cognition in patients with early Alzheimer disease and amnesic mild cognitive impairment during treatment with rosiglitazone: a preliminary study. *Am. J. Geriatr. Psychiatry*, **13**, 950–958.
53. Sato, T., Hanyu, H., Hirao, K., Kanetaka, H., Sakurai, H. and Iwamoto, T. (2011) Efficacy of PPAR-gamma agonist pioglitazone in mild Alzheimer disease. *Neurobiol. Aging*, **32**, 1626–1633.
54. Marciano, D.P., Chang, M.R., Corzo, C.A., Goswami, D., Lam, V.Q., Pascal, B.D. and Griffin, P.R. (2014) The therapeutic potential of nuclear receptor modulators for treatment of metabolic disorders: PPARgamma, RORs, and Rev-erbs. *Cell Metab.*, **19**, 193–208.
55. Zhang, B., Kirov, S. and Snoddy, J. (2005) WebGestalt: an integrated system for exploring gene sets in various biological contexts. *Nucleic Acids Res.*, **33**, W741–W748.
56. Wang, J., Duncan, D., Shi, Z. and Zhang, B. (2013) WEB-based Gene Set Analysis Toolkit (WebGestalt): update 2013. *Nucleic Acids Res.*, **41**, W77–W83.
57. Cali, G., Gentile, F., Mogavero, S., Pallante, P., Nitsch, R., Ciancia, G., Ferraro, A., Fusco, A. and Nitsch, L. (2012) CDH16/Ksp-cadherin is expressed in the developing thyroid gland and is strongly down-regulated in thyroid carcinomas. *Endocrinology*, **153**, 522–534.
58. Cali, G., Zannini, M., Rubini, P., Tacchetti, C., D'Andrea, B., Affuso, A., Wintermantel, T., Boussadia, O., Terracciano, D., Silberschmidt, D. *et al.* (2007) Conditional inactivation of the E-cadherin gene in thyroid follicular cells affects gland development but does not impair junction formation. *Endocrinology*, **148**, 2737–2746.
59. Jouaville, L.S., Pinton, P., Bastianutto, C., Rutter, G.A. and Rizzuto, R. (1999) Regulation of mitochondrial ATP synthesis by calcium: evidence for a long-term metabolic priming. *Proc. Natl Acad. Sci. USA*, **96**, 13807–13812.
60. Porcellini, A.M., Pinton, P., Ainscow, E.K., Chiesa, A., Rugolo, M., Rutter, G.A. and Rizzuto, R. (2001) Targeting of reporter molecules to mitochondria to measure calcium, ATP, and pH. *Methods Cell Biol.*, **65**, 353–380.



## Chromosomal imbalance letter

## 40 Mb duplication in chromosome band 5p13.1p15.33 with 800 kb terminal deletion in a foetus with mild phenotypic features

A. Izzo<sup>a,1</sup>, R. Genesio<sup>a,1</sup>, V. Ronga<sup>a</sup>, V. Nocera<sup>a</sup>, L. Marullo<sup>a</sup>, R. Cicatiello<sup>a</sup>, G. Sglavo<sup>b</sup>, D. Paladini<sup>b</sup>, A. Conti<sup>a,\*</sup>, L. Nitsch<sup>a</sup><sup>a</sup> Dept. of Cellular and Molecular Biology and Pathology, University of Naples "Federico II", Via S. Pansini 5, 80131 Napoli, Italy<sup>b</sup> Dept. of Obstetric, Gynaecologic and Pathophysiology of Reproduction, University of Naples "Federico II", Via S. Pansini 5, 80131 Napoli, Italy

## ARTICLE INFO

## Article history:

Received 12 July 2011

Accepted 16 December 2011

Available online 2 January 2012

## Keywords:

Array-CGH

Foetal ultrasound

General cytogenetics

Trisomy 5p

Chromosome duplication

## ABSTRACT

Large duplication of the short arm of chromosome 5 is a rare condition normally associated to severe phenotype anomalies including heart and brain malformations.

We report a prenatal case of a large 5p duplication with sub-telomeric deletion in a foetus with very mild phenotypic abnormalities. Foetal ultrasonographic examination at 22 weeks of gestation showed short femur, clubfeet, pielectasy, and facial dysmorphisms.

Chromosome investigations revealed an inverted duplication of the short arm of chromosome 5 from 5p13.1 to 5p15.33 and a 800 kb deletion at 5pter.

The absence of severe anomalies such as cardiac and cerebral defects, observed so far in all large 5p duplications, and the comparison to previous cases described both in literature and in DECIPHER database suggest that the critical region for the severe phenotype in 5p duplication syndrome might be smaller than that previously described, excluding half of the 5p13 band. This might help in prenatal genetic counselling.

© 2011 Elsevier Masson SAS. All rights reserved.

## 1. Clinical description

A 26-year-old Caucasian woman, gravida 3, para 2, at 22 weeks of gestation, was referred to our unit for prenatal diagnosis because of foetal malformations. The family history of both the mother and the father was unremarkable, and their karyotypes were normal. Foetal ultrasonographic examination showed intrauterine growth retardation, short femurs (2nd percentile), 3rd grade bilateral clubfoot, pielectasy, inter-hemispheric cyst and broad anterior fontanelle (Fig. 1A–C). Foetus biometry was as follows: biparietal diameter, 5.14 cm; occipitofrontal diameter, 6.44 cm; head circumference, 18.15; abdominal circumference, 15.87 cm; and femur length, 2.94 cm. Tridimensional sonography showed facial dysmorphisms including low-set ears, exophthalmos and a sloping forehead (Fig. 1D). The association of multiple soft markers suggested the opportunity for foetal karyotyping; therefore, cordocentesis was performed. Due to the foetal malformations and preliminary anomalous results from a BACs-on-Beads assay, the couple decided to terminate the pregnancy. An autopsy confirmed mild phenotypic

abnormalities and facial dysmorphisms. No cardiac or cerebral defects were observed.

## 2. Methods of detection

## 2.1. Cytogenetics and FISH

Chromosomal analysis was performed from foetal blood by standard G-banding technique at the 400-band level. Fluorescent in situ hybridisation (FISH) analysis was performed with the commercial probe LSI D5S23 for the cri-du-chat syndrome critical region 5p15.2 and for whole chromosome 5 (wcp5; Vysis) according to the manufacturer's protocols. The 5p15.33 region was hybridised with the Bacterial Artificial Chromosome (BAC) clone RP11-94j21. The BAC location was mapped according to the UCSC Genome Bioinformatics group (<http://genome.ucsc.edu>, GRCh37/hg19 assembly). The BAC clone was extracted using standard methods [1], labelled by random priming with CY3-dCTP and hybridised as for the LSI probe. Thirty metaphases per probe were analysed.

## 2.2. Array-CGH

The proband's DNA was isolated using MasterPure™ DNA Purification Kit (EPICENTRE Biotechnologies, USA).

\* Corresponding author. Tel.: +39 081 7463261; fax: +39 081 7463656.

E-mail address: [anconti@unina.it](mailto:anconti@unina.it) (A. Conti).<sup>1</sup> These authors contributed equally to this work.

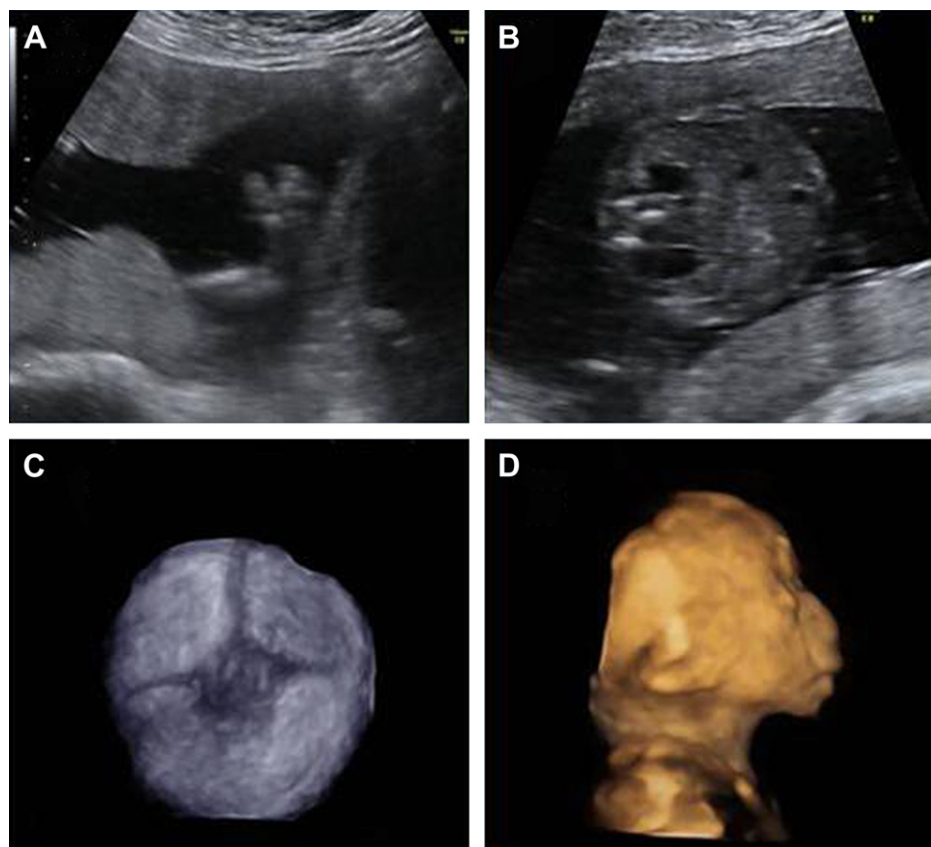


**Fig. 1.** Ultrasonographic images of the foetus showing clubfeet (A), pielectasy (B) and broad anterior fontanelle (C). Tridimensional sonography shows facial dysmorphisms such as low-set ears, exophthalmos and sloping forehead (D).

Array comparative genomic hybridisation (aCGH) was performed using the oligonucleotide-based CytoChip ISCA 4 × 44K BlueGnome (Technogenetics-Bouty, Italy) with a mean 130-kb resolution according to the manufacturer's instructions (<http://www.chitochip.com>). Fluorescent images were collected using the Perkin Elmer microarray laser scanner ScanRI. The hybridisation data were analysed by BlueFuse Multi<sup>®</sup> software V2.2 (BlueGnome, UK). The control genome was that of a standard female (Promega, USA).

### 2.3. BACs-on-Beads assay

A BACs-on-Beads<sup>™</sup> assay (BoBs, Perkin Elmer, USA), based on Luminex xMAP technology (Multi-Analyte Profiling beads), was used as the first rapid diagnostic test. Selected BAC probes are immobilised on colour-coded beads and hybridised to the proband's DNA to analyse gains and losses in targeted chromosome regions in order to detect (within 48 h) aneuploidies of chromosomes 13, 18, 21, X and Y, as well as frequently occurring microdeletion/duplication syndromes including Wolf–Hirschhorn, cri-du-chat, Williams–Beuren, Langer–Giedion, Prader–Willi, Angelman, Miller–Dieker, Smith–Magenis and DiGeorge. One male and one female control genomes were used as reference samples.

The BoBs assay was performed according to the manufacturer's instructions. Data were analysed using BoBsoft software (Perkin Elmer, USA).

### 2.4. Chromosomal anomaly

The BoBs assay revealed that the whole cri-du-chat syndrome region was duplicated (Fig. 2). Eight independent BAC probes were

included in the BoBs panel for chromosome 5p, spanning 7.7 Mb, from 5p15.2 to 5p15.33. The foetal karyotype showed additional material on the short arm of chromosome 5 (Fig. 3A). Array-CGH analysis using the oligonucleotide-based CytoChip ISCA 4 × 44K BlueGnome (Technogenetics-Bouty, Italy) with a mean 130-kb resolution, showed a de novo 40.5 Mb duplication of the 5p arm from 5p13.1 to 5p15.33 (from 943,000 to 41,584,000), with a 5pter deletion spanning approximately 870 Kb (Fig. 3B). The 5p deleted region is not represented by any BoBs probe.

### 2.5. Method of confirmation

The whole chromosome painting for chromosome 5 demonstrated that the additional material was derived from chromosome 5 only. No additional hybridisation signals were seen on other chromosomes (Fig. 3C). Dual FISH using both a cri-du-chat unique sequence mapping to the p15.2 region of chromosome 5 and the BAC clone mapping to p15.33 demonstrated that the duplication was inverted (Fig. 3D).

### 2.6. Causative of the phenotype

Parental chromosomal analysis revealed normal karyotypes without any chromosomal aberrations. These findings suggested that the abnormality detected in the foetus was de novo and causative of the phenotype.

## 3. Discussion

We have characterised the first prenatal case of inverted duplication of a large part of the chromosome 5 short arm with

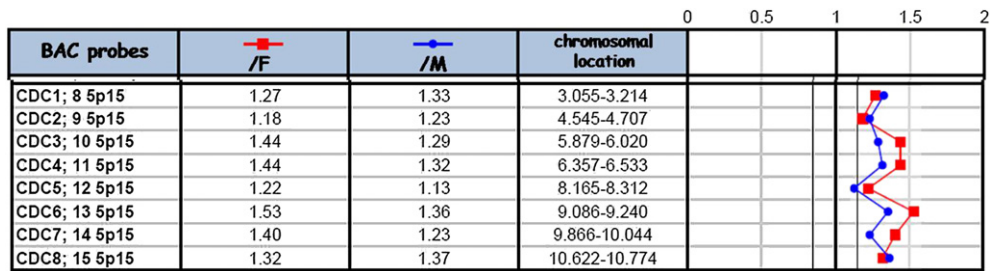


**Fig. 2.** BACs-on-Beads (BoBs) profile showing a male karyotype with duplication of BAC clones in 5p15 (cri-du-chat CDC probes 1–8). The normal ratio for BoBs probes is approximately 1.0. The normal ratio range is outlined by the vertical lines from 0.8 to 1.2. In this case, the ratios for all 5p probes higher than 1.2, compared both to normal females (red dots) and to normal males (blue dots), demonstrate a duplication of all tested 5p regions.

sub-telomeric deletion, presenting with very mild ultrasonographic anomalies. This rearrangement does not involve other chromosomes. FISH and aCGH analyses demonstrated that the duplication, which spans 40.5 Mb from 5p13.1 to 5p15.33, is inverted and includes the critical region for cri-du-chat syndrome. The terminal deletion was of approximately 870 kb.

The use of a new xMAP technology, BoBs, allowed us to detect the chromosome duplication in less than 48 h. This information

was helpful to the couple that had to decide what to do about the pregnancy. The technique is quite powerful in prenatal diagnosis because of the rapidity by which not only the most frequent aneuploidies but also frequently occurring micro-deletion/micro-duplication syndromes can be detected.

Trisomies of the short arm of chromosome 5 are uncommon abnormalities. Less than 50 subjects with complete or partial 5p duplications have been described so far. For the majority of

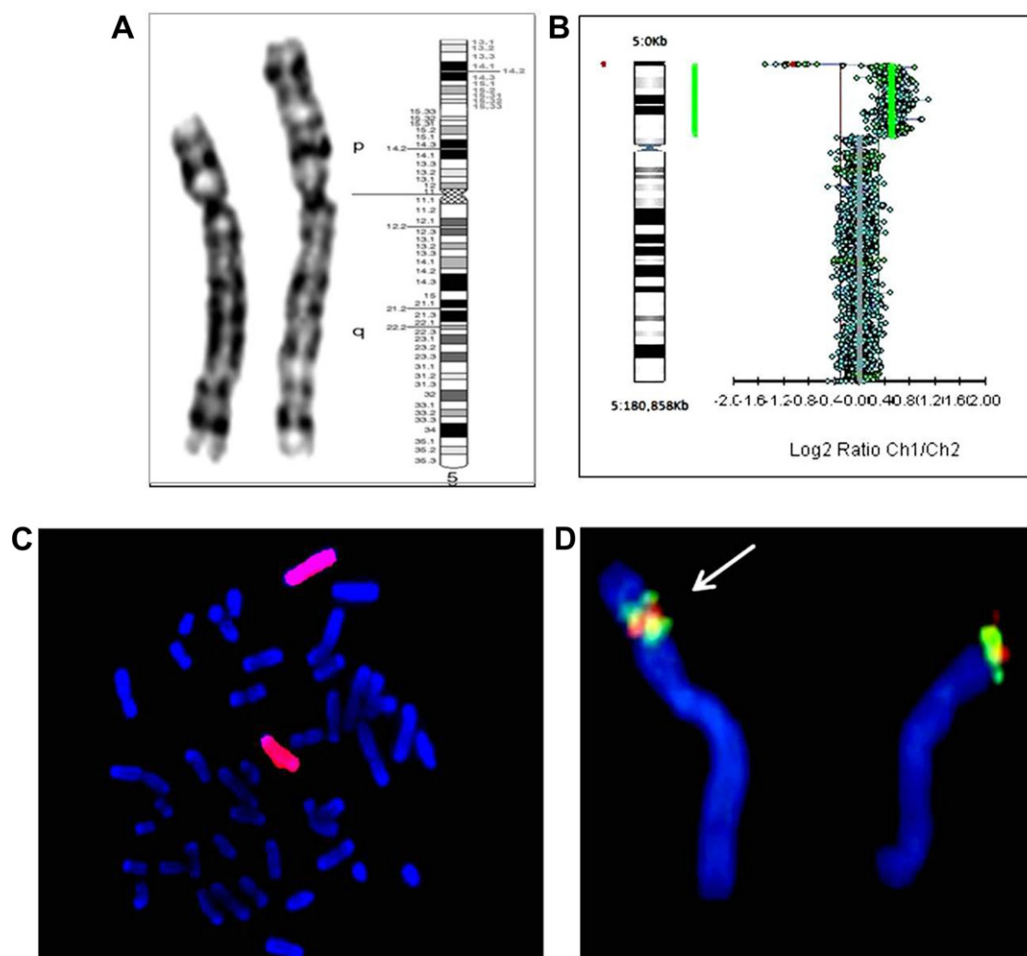


**Fig. 3.** A. G-banding karyotype and ideogram of the derived chromosome 5 from foetal lymphocytes showing the presence of additional material on the short arm of one chromosome 5. B. aCGH profile of chromosome 5 showing a de novo 40.5-Mb duplication (green line on the right side) of the 5p arm from 5p13.1 to 5p15.33 (from 943,000 to 41,584,000) and a 5pter deletion spanning approximately 870 kb (red dots on the left side). Control genome was that of a standard female (Promega, USA). C. Whole chromosome painting for chromosome 5 demonstrates that the additional material derives from chromosome 5 only. No additional hybridisation signals are seen on other chromosomes. D. Dual fluorescent in situ hybridisation, using both a cri-du-chat unique sequence (Vysis) (green signal) and the RP11-94J21 BAC clone mapping to 5p15.33 (red signal), shows two fluorescent green signals on the abnormal 5p (white arrow) with a double red signal in between, which demonstrates that the duplication is inverted.

**Table 1**  
Comparison of clinical findings among cases of partial or complete trisomy 5p.

Study	Portion of 5p duplicated	Brain abnormalities	Facial dysmorphisms	Clubfeet	Congenital heart defects	Low-set ears	Enlarged anterior fontanelle
Present study	5p13.1-p15.33	–	+	+	–	+	+
Sreekantaiah et al., 1999 [11]	5p14-p15.3	–	+	–	–	–	–
Grosso et al., 2002 [12]	5p10-pter	+	+	–	–	+	+
Cervera et al., 2005 [13]	5p13.3-p15.3	+	+	–	–	+	+
Wang et al., 2008 [14]	5p14.3-p15.31	–	+	–	–	–	–
Loscalzo et al., 2008 [3]	5p11-p13.3	+	+	–	+	+	–
Vetro et al., 2008 [4]	5p11-p14.1	+	+	+	+	+	–
Patient 4119 from DECIPHER database	5p12-p15.31	–	+	–	+	–	–
Patient 1227 from DECIPHER database	5p12-p13.2	–	+	–	+	–	–
Patient 1 from Yan et al., 2009 [6]	5p13.2	+	+	–	–	+	–
Patient 2 from Yan et al., 2009 [6]	5p13.2	–	+	–	–	+	–
Patient 3 from Yan et al., 2009 [6]	5p13.2	–	+	–	–	–	–
Patient 4 from Yan et al., 2009 [6]	5p13.2	+	+	–	–	+	–
Patient 5 from Yan et al., 2009 [6]	5p13.2	–	+	–	–	–	–

them, 5p duplications were either generated from structural chromosomal rearrangements or due to chromosome markers. Various clinical features have been associated with segmental aneuploidy on chromosome 5p [2–4]. Patients with duplications spanning from 5p13.3 to 5p15.33 show mild and relatively indistinct phenotypes, including facial dysmorphisms, clubfeet and low-set ears, while with the occurrence of complete 5p trisomy as well as duplications of the 5p10–5p13.1 segment, the anomalies are more severe, including macrocephaly, hydrocephalus, dilated cerebral ventricles, cardiac defects and other severe clinical features.

In order to establish genotype–phenotype correlations, we compared the proband's phenotype with previously reported phenotypes of inv dup 5p subjects, with or without terminal deletion (Table 1). We have excluded reciprocal translocations because the imbalance of different chromosomes could influence the phenotype. We have also excluded chromosome markers [5] because of possible epigenetic silencing of phenotypic traits.

In the present study, the proband, with 5p duplication extending from 5p13.1 to 5p15.33, shares mild phenotypic features with smaller duplications starting from 5p14. Unfortunately, some clinical features often found in these patients, such as hypotonia, speech delay and mental retardation, are not assessable in prenatal diagnosis.

Severe phenotypic signs that are associated with duplications involving chromosomal regions from the centromere to 5p13.3, such as congenital heart defects and brain abnormalities, were not observed in the present case.

The gene NIPBL, mapping to 5p13.1, was thought to be responsible for heart defects because its haploinsufficiency can cause cardiopathy in Cornelia de Lange type 1 Syndrome [6,7]. Table 1 shows that heart defects are never observed in patients with 5p duplications spanning from 5pter to the position 41,584,000 including NIPBL gene, while heart defects are present in the patient referred to as DECIPHER 1227 with a 5p duplication from the genome positions 36,240,080 to 42,862,390.

Therefore it is possible to hypothesize that NIPBL overexpression is not responsible for cardiac abnormalities and that the critical region for heart defects in the 5p13 syndrome is possibly included within the 1.3 Mb from the centromeric end of the duplication we have described and the centromeric end of the DECIPHER 1227 duplication from position 41,584,000 to 42,800,000 (Build NCBI36/hg18). Nine RefSeq genes map to this trait; only 3 of them are highly expressed in the heart tissue: SEPP1, a selenoprotein involved in extracellular antioxidant defence; GHR, the growth hormone receptor; and the OXCT1 gene, which encodes a member of 3-oxoacid CoA transferase.

Inverted duplication with terminal deletion has been hypothesised to arise by different mechanisms, all involving the formation of a dicentric chromosome that subsequently breaks during meiosis to form a monocentric duplicated and deleted chromosome.

The existence of two different couples in tandem with low-copy repeats (LCRs) spanning at least 30 kb, with similarities higher than 95% located close the breakpoint region at 5p15.33, supports the hypothesis that the mechanism of this inv dup del 5p is likely consistent with the Non-allelic Homologous Recombination model [8,9]. As suggested by Gorinati et al. [10], a paracentric micro-inversion in one parent may be present. The single copy region predicted by such a model, spanning less than 50 kb between LCRs in 5p15.33, could not be identified at the resolution of the aCGH that we used.

## References

- [1] H.C. Birnboim, A rapid alkaline extraction method for the isolation of plasmid DNA, *Methods Enzymol.* 100 (1983) 243–255.
- [2] G.V. Velagaleti, D.L. Morgan, V.S. Tonk, Trisomy 5p. A case report and review, *Ann. Genet.* 43 (2000) 143–145.
- [3] M.L. Loscalzo, T.A. Becker, M. Sutcliffe, A patient with an interstitial duplication of chromosome 5p11-p13.3 further confirming a critical region for 5p duplication syndrome, *Eur. J. Med. Genet.* 51 (2008) 54–60.
- [4] A. Vetro, A. Iasci, B. Dal Bello, E. Rossi, J. Messa, L. Montanari, S. Cesari, O. Zuffardi, A prenatal case of duplication with terminal deletion of 5p not identified by conventional cytogenetics, *Prenat. Diagn.* 28 (2008) 1171–1173.
- [5] F. Sheth, J. Andrieux, E. Ewers, N. Kosyakova, A. Weise, H. Sheth, S.P. Romana, M. LeLor'h, B. Delobel, O. Theisen, T. Liehr, S. Nampoothiri, J. Sheth, Characterization of sSMC by FISH and molecular techniques, *Eur. J. Med. Genet.* 54 (2011) 247–255.
- [6] J. Yan, F. Zhang, E. Brundage, A. Scheuerle, B. Lanpher, R.P. Erickson, Z. Powis, H.B. Robinson, P.L. Trapane, D. Stachiw-Hietpas, K.M. Keppler-Noreuil, S.R. Lalani, T. Sahoo, A.C. Chinault, A. Patel, S.W. Cheung, J.R. Lupski, Genomic duplication resulting in increased copy number of genes encoding the sister chromatid cohesion complex conveys clinical consequences distinct from Cornelia de Lange, *J. Med. Genet.* 46 (2009) 626–634.
- [7] K. Oexle, M. Hempel, A. Jauch, T. Meitinger, N. Rivera-Brugues, S. Stengel-Rutkowski, T. Strom, 3.7 Mb tandem microduplication in chromosome 5p13.1-p13.2 associated with developmental delay, macrocephaly, obesity, and lymphedema. Further characterization of the dup(5p13) syndrome, *Eur. J. Med. Genet.* 54 (2011) 225–230.
- [8] L.R. Rowe, J.Y. Lee, L. Rector, E.B. Kaminsky, A.R. Brothman, C.L. Martin, S.T. South, U-type exchange is the most frequent mechanism for inverted duplication with terminal deletion rearrangements, *J. Med. Genet.* 46 (2009) 694–702.
- [9] O. Zuffardi, M. Bonaglia, R. Ciccone, R. Giorda, Inverted duplications deletions: underdiagnosed rearrangements?? *Clin. Genet.* 75 (2009) 505–513.
- [10] M. Gorinati, D. Caufin, A. Minelli, L. Memo, G. Gaspario, A. Dodero, Inv dup (8) (p21.1–22.1): further case report and a new hypothesis on the origin of the chromosome abnormality, *Clin. Genet.* 39 (1991) 55–59.
- [11] C. Sreekantaiah, D. Kronn, R.C. Marinescu, B. Goldin, J. Overhauser, Characterization of a complex chromosomal rearrangement in a patient with a typical catlike cry and no other clinical findings of cri-du-chat syndrome, *Am. J. Med. Genet.* 86 (1999) 264–268.

- [12] S. Grosso, M. Cioni, G. Garibaldi, L. Pucci, P. Galluzzi, R. Canapicchi, G. Morgese, P. Balestri, De novo complete trisomy 5p: clinical and neuroradiological findings, *Am. J. Med. Genet.* 112 (2002) 56–60.
- [13] M. Cervera, S. Sanchez, B. Molina, M.A. Alcantara, V. Del Castillo, A. Carnevale, A. Gonzalez-del Angel, Trisomy of the short arm of chromosome 5 due to a de novo inversion and duplication (5)(p15.3 p13.3), *Am. J. Med. Genet. A* 136A (2005) 381–385.
- [14] J.C. Wang, B.P. Coe, B. Lomax, P.M. MacLeod, M.I. Parslow, J.E. Schein, W.L. Lam, P. Eydoux, Inverted duplication with terminal deletion of 5p and no cat-like cry, *Am. J. Med. Genet. A* 146A (2008) 1173–1179.